

Activity Report 2020

INDEX

1. INTRODUCTION	3
2. ITER PROJECT	5
2.1. ACTIVITY FOR THE DEVELOPMENT OF NEUTRAL BEAM INJECTORS FOR ITER	5
2.1.1. <i>PRIMA and host activities</i>	6
2.1.2. <i>SPIDER</i>	12
2.1.3. <i>MITICA</i>	33
2.1.4. <i>ITER Neutral Beam Injector Physics</i>	44
2.1.5. <i>Vacuum high voltage holding modeling and experiments</i>	51
2.2. ITER NBI PHYSICS ACTIVITIES AND ACCOMPANYING PROGRAM	61
2.2.1. <i>Introduction</i>	61
2.2.2. <i>NIO1 Experiment</i>	62
2.2.3. <i>NBI Complex system and controllability</i>	68
2.2.4. <i>Alternative ion Sources</i>	69
2.3. ITER DIAGNOSTICS.....	70
2.3.1. <i>Development of Software Algorithms for ITER Magnetics Diagnostic</i>	70
3. RFX FUSION SCIENCE AND TECHNOLOGY: RFX-MOD2 AND PLASMA PHYSICS	72
3.1. INTRODUCTION	72
3.2. IMPLEMENTATION OF THE MACHINE TOROIDAL ASSEMBLY MODIFICATIONS	72
3.2.1. <i>Vacuum Tight Support Structure (VTSS)</i>	72
3.2.2. <i>Passive Stabilizing Shell (PSS)</i>	74
3.2.3. <i>First Wall</i>	77
3.2.4. <i>Development of components made by additive manufacturing</i>	77
3.3. REVAMPING OF EXPERIMENTAL PLANTS AND AUXILIARY SYSTEMS	78
3.4. DESIGN AND INSTALLATION OF DIAGNOSTIC SYSTEMS FOR RFX-MOD2	79
3.4.1. <i>Internal Sensors/Systems</i>	79
3.4.2. <i>Diagnostics developments</i>	83
3.5. PREPARATION FOR RFX-MOD2 EXPERIMENTS	88
3.5.1. <i>Changes and new algorithms for magnetic data analysis</i>	88
3.5.2. <i>Analysis and documentation of the RFX-mod 2 magnetic control system</i>	88
3.5.3. <i>Characterization of reconnection processes</i>	89
3.5.4. <i>Relation between density limit and Hartman number</i>	89

3.5.5.	<i>Collaboration with RELAX on relaxed states</i>	90
3.5.6.	<i>RFX-mod2 tokamak: DEMO-like shaped operations</i>	91
3.5.7.	<i>RFX-mod tokamak: negative triangularity preliminary equilibrium analysis</i>	91
3.6.	RFX THEORY AND MODELLING ACTIVITIES	92
3.6.1.	<i>3D nonlinear visco-resistive MHD modelling</i>	92
3.6.2.	<i>Lagrangian Coherent Structures</i>	94
3.6.3.	<i>Use of machine learning tools in transport studies</i>	95
3.6.4.	<i>Wave-particle energy transfer studies with Hamiltonian approach</i>	95
3.6.5.	<i>Excitation of Alfvén eigenmodes by magnetic reconnection</i>	96
3.6.6.	<i>Simulation of disruption mitigation by shattered pellet injection</i>	96
3.7.	STUDIES ON RFP MACHINE AS NEUTRON SOURCE AND POWER GENERATION	96
4.	EUROFUSION PROGRAMME	97
4.1.	ITER PHYSICS WORK PACKAGES	97
4.1.1.	<i>Introduction</i>	97
4.1.2.	<i>MST1</i>	98
4.1.3.	<i>JET1</i>	104
4.1.4.	<i>DTT</i>	110
4.1.5.	<i>WPSA</i>	120
4.1.6.	<i>WPS1</i>	123
4.1.7.	<i>WPISA</i>	125
4.1.8.	<i>Further collaborations. Plasma equilibrium and 3D em code integration</i>	125
4.2.	PPPT PROJECTS	125
4.2.1.	<i>WPHCD – Heating and Current Drive systems</i>	125
4.2.2.	<i>WPFTV - Tritium, Fuelling and Vacuum Pumping Systems</i>	127
4.2.3.	<i>WPBoP - Balance of Plant</i>	127
4.2.4.	<i>WPMAG – Magnet System: Quench Protection Circuit Studies</i>	130
4.3.	SOCIO ECONOMIC STUDIES (SES) AND DEMO	130
4.3.1.	<i>Fusion power plant assessment studies</i>	130
4.3.2.	<i>The role of fusion in long term energy scenarios</i>	130
4.4.	EDUCATION AND TRAINING	132
4.5.	COMMUNICATION AND OUTREACH	133
5.	BROADER APPROACH	134
5.1.	CONTRIBUTION TO THE JT-60SA POWER SUPPLY COMBINATION TESTS	134
5.2.	POWER SUPPLIES FOR IN-VESSEL SECTOR COILS FOR RWM CONTROL	134
6.	INDUSTRIAL AND NON-FUSION RELATED COLLABORATIONS	135
6.1.	DESIGN OF VACUUM INTERRUPTERS WITH THE VOLTAGE HOLDING PREDICTION MODEL (VHPM)	135
6.2.	BIOMEDICAL PLASMA APPLICATIONS	136
7.	PUBLICATIONS	138

1. Introduction

This Report describes the activities and the results obtained in the year 2020, developed along the guidelines of the 2020 Activity Programme approved by the Consorzio RFX partners meeting held on 29 November 2019.

The activities in 2020 year have been strongly affected by the COVID-19 pandemic. The first initial impact of the pandemic is dated on January 30th. From the middle of February more and more restrictions on the activities have been implemented up to March 9th when a strict lockdown has been imposed by the government and all the on-site activities have been closed for 6 weeks up to end of April. In the same time teleworking has been implemented for almost all of the staff. On May 4th the on-site activities were allowed to be restored with very strict sanitary procedures to avoid the diffusion of the infection. Such procedures are still in place.

The activities entailing just computational studies and analyses were only slightly affected, since, from the very start of the lockdown, all of the personnel was on-line connected to the Consorzio RFX network thanks to the work of the information technology department. On the other hand all of the construction, assembly, commissioning and experimental activities have been somewhat hindered. Overall, the on-site activities suffered a delay of the order of 6 months.

After the restart of on-site activities on May 4th the teleworking remains the preferable way to work for all the activities that do not require the physical on-site presence. The percentage of staff working on Consorzio RFX premises starting from March 9th is shown in Fig. 1.1.

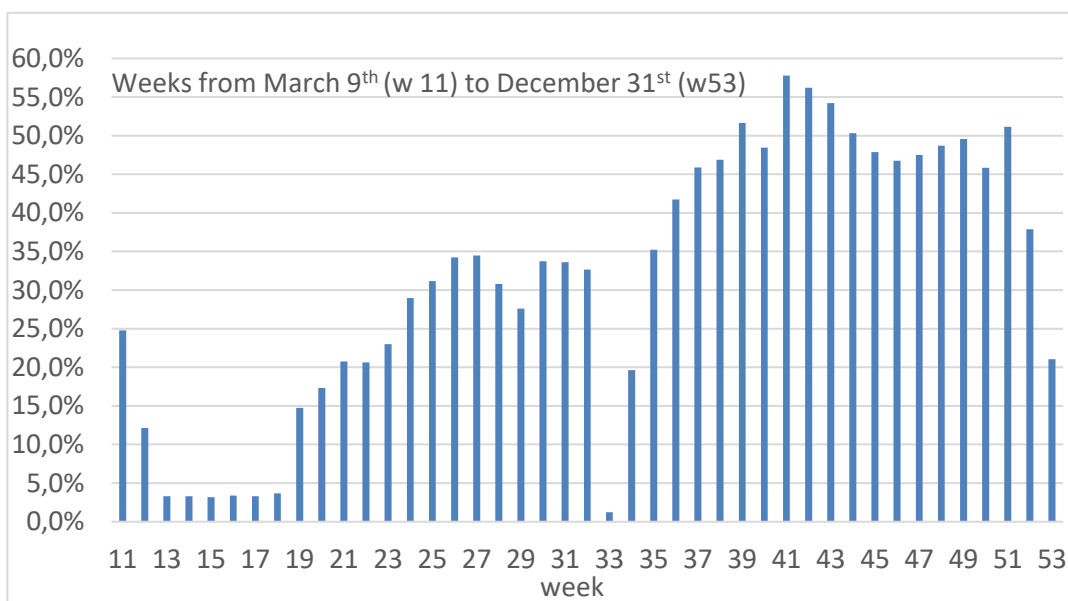


Fig. 1.1 Staff working on-site starting from the lockdown date (March 9th) in percentage.

The detail of the impact on the different part of the 2020 programme due to the pandemic is detailed in the report.

The pandemic has affected also the scientific events, the public outreach and communication activities organized by Consorzio RFX. The conferences and workshops have been moved to 2021 starting from next summer, whereas the public outreach and communications activities have been moved to the web, social and video conferences platforms.

The same situation affected also the National, European and International scientific events that have been moved or to 2021 or to video conferences platforms.

The re-schedule of many scientific events has affected the overall scientific production of Consorzio RFX; but, since most of the papers connected with the participation to Conferences and Workshops held in the year are usually published on the following year, a significant negative impact is expected also in 2021.

This highlighted in Fig. 1.2: the number of Conference papers in 2020 has been much lower than in previous year, violating the systematic trend, that sees a higher number of papers in even years (mainly due to the biennial SOFT Conference). Conversely, the number of journal papers in 2020 has not been so badly affected.

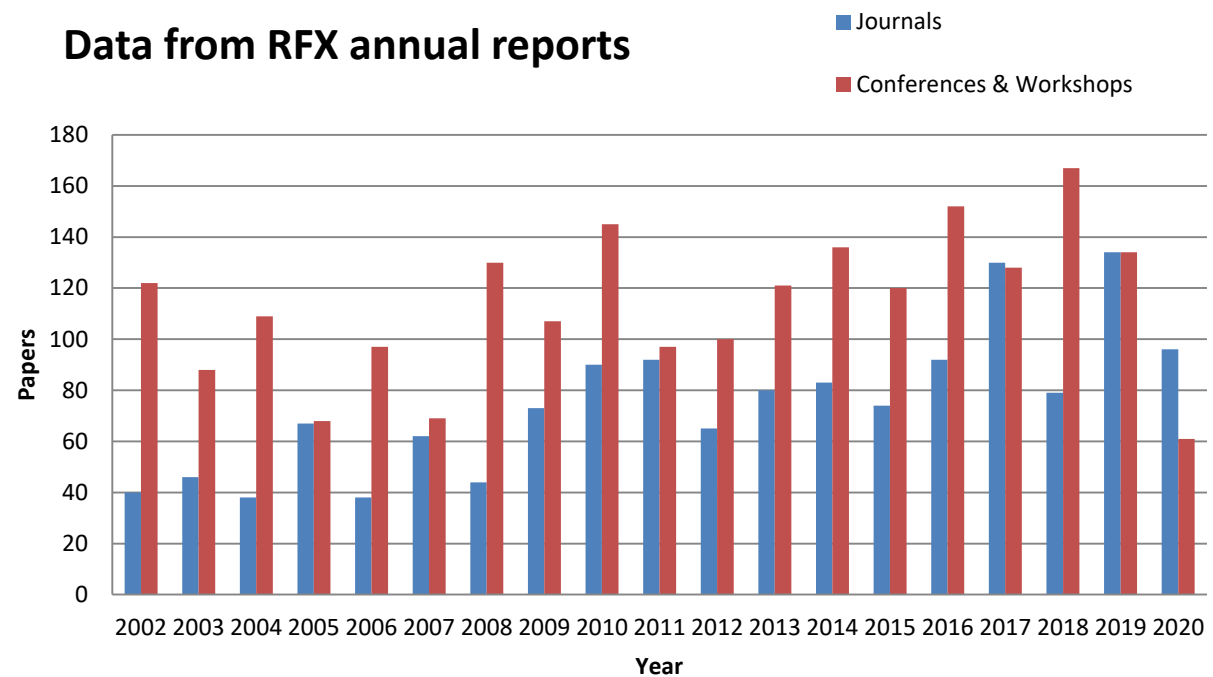


Fig. 1.2 Total number of Journal and Conference papers per year by Consorzio RFX. The effect of Covid-19 can be seen in particular for the 2020 Conference papers. (last red bar)

2. ITER Project

2.1. Activity for the development of Neutral Beam Injectors for ITER

In 2020 the new Agreement between IO and Consorzio RFX was applied for the first time; as a consequence, various organizational and coordination activities were carried out. They included: completion and commissioning of the new organization, development of the resource plan made available by both Consorzio RFX and EUROfusion, coordination with the responsible officers of Framework Contracts for the procurement of MITICA components and plants under the responsibility of F4E, preparation of NBTF Project Plan and Quality Plan, etc. The recruitment of people supported by EUROfusion was a long process. The first researcher, out of the 14 supported by EUROfusion, began to collaborate in January, the last one (14th) in early November. Of course, this resulted in organizational difficulties due to the unavailability of resources which were originally planned.

During Q1 the problem of COVID-19 emerged which strongly influenced the on-site activities. The experimental activities on SPIDER were first slowed down and then completely stopped for some weeks; similarly for the MITICA on-site activities. All other activities were carried out by teleworking. At the beginning of May, SPIDER on-site activities resumed, initially at a reduced pace and subsequently at full capacity. In June the experimental activity resumed with extended shifts and this continued till the end of the year. It was alternated with short shutdowns for inspection, modification and repair that became necessary. Similarly, in MITICA the construction site activities resumed in May and returned to full capacity, even while respecting the health restrictions imposed by Covid-19. In particular, the installation, commissioning and acceptance tests of plants procured by F4E continued regularly. In order to continue MITICA power system integration activities, the presence of experts from QST and Hitachi is required. As, due to the restrictions on travel related to Covid-19, this was not possible, an organization that allows the remote supervision of the on-site activities pertaining to them was agreed and set up. In September, the completion activities of the JADA liability plants resumed with the new organization. In parallel, the preparation of test plans for integrated 100kV tests continued with the collaboration of IO, QST and NBTF Team. These tests were carried out in October, followed by the preparation of the Acceleration Grid Power Supply (AGPS) integrated power tests that will be performed at the beginning of 2021.

As for modelling, activities progressed regularly, as they could be performed without any major restrictions even in teleworking, more details can be found in Section 2.1.4.

The SPIDER experiment activity was reduced compared to what was planned at the beginning of the year for two reasons: limitations to on-site activities due to the lockdown; frequent failures and malfunctions of the experimental plants that required additional shutdowns not originally foreseen. All this called for a 9 month postponement of the long shutdown, in which the source will be significantly modified. Nevertheless, a lot of useful information was collected, fundamental for the design of the changes that will be implemented during the long shutdown. Details on results, issues and improvements can be found in Section 2.1.2.

In addition to the changes that directly concern the Beam Source, two other important improvements are foreseen on SPIDER: the enhancement of the SPIDER vacuum pumping system; the replacement of RF oscillators with RF solid state amplifiers (this regards both SPIDER and MITICA experiments). These two changes are very significant, both from a technical and economic point of view, and have an impact on the planning of the two experiments. Much effort was devoted in 2020 in order to develop the technical proposals and related strategic plans to be submitted to the NBTF SC for approval. Details about the two improvements are reported in Section 2.1.2.11 and 2.1.2.12, respectively.

Finally, it is expected that at the end of the power integrated tests and before the installation of the in-vessel components, MITICA will be used to perform HV holding tests in vacuum and at low gas pressure, similar to that expected during MITICA operation. To do this, electrostatic mock-ups must be installed inside the vacuum vessel in place of the source, as well as dedicated auxiliary pumping systems and dedicated diagnostics. In 2020, a lot of work was dedicated to agree with IO and QST the strategy to be implemented, and to design of the necessary components, as reported in more detail in Section 2.1.5.

2.1.1. *PRIMA and host activities*

2.1.1.1. *Building and auxiliaries*

In 2020 the last activities related to buildings were completed. They concerned three MITICA systems:

- completion of concrete shield door of MITICA bio-shield including auxiliaries and safety interlocks;
- installation and commissioning of the fire extinguish systems of 1 MV insulating transformer;
- installation and commissioning of the rotating platform for Beam Source (BS) and Beam Source Vessel (BSV) Rear Lid removal

Finally, the integration and interface management work continued also in 2020 to ensure the coherent integration of the experimental devices by monitoring the construction activities and the full 3D CAD model of the facility.

2.1.1.2. Cooling Plant

After completion of hydraulic installation works for MITICA Plant Unit, the plant commissioning and Overall Site Acceptance Tests, done in 2019, had identified some non-conformities and a number of issues to be solved. This led to further effort in Q1/2020, both on the Supplier and NBTF Team sides, to solve some hydraulic issues (new pressurizing systems for PC01, PC08 and PC09) and to perform several sensors/control system adjustments.

Continuous activities have been carried out in 2020 by NBTF Team to support, verify and witness the supplier's activities, commissioning and Overall Site Acceptance Tests on-site. A huge effort was given for the follow-up of activities on electrical and I&C control systems.

Technical documents, procedures and schedule for Overall Acceptance Tests of MITICA and Shared Plant Units were reviewed and discussed among the Supplier, NBTF Team and F4E, aiming to complete all the tests and the Acceptance Data Package (ADP) within Q2/2020, always guaranteeing the availability of SPIDER Cooling Plant when needed for experimental sessions.

Closure of the contract and transfer of Plant ownership to IO occurred in Q2/2020.

During 2020 the Cooling Plant Unit for SPIDER allowed the execution of SPIDER operations when required during 2020. To be noted that during 2020 the SPIDER cooling plant was mostly used in local or manual mode, waiting for the final integrated commissioning with CODAS, which was finally completed in Q4/2020.

The team of engineers and technicians was well trained for plant operations, tuning and maintenance. Continuous presence and follow-up during SPIDER operations was guaranteed, with a particular effort for managing issues as the failure of a pump occurred in 2020 and managing of water resistivity degradation using the off-line Chemical Control System. Overall views of Cooling Plant equipment inside Building 2 are shown in Fig. 2.1. Pictures of hydraulic pipes installed on the back wall of SPIDER Neutron Shield and inside the MITICA Neutron Shield are shown in Fig. 2.2.

A specific project was launched in 2020 aiming to identify the reasons for the fast degradation of water electrical resistivity during SPIDER operations and the way for solving the issue. This problem was causing delays and problems during operations, due to the need for a quite frequent water change in the Primary Circuit PC01 for SPIDER Power Supply.



Fig. 2.1 Left: Overall view of the equipment of SPIDER, MITICA and Shared Plant Units inside Building 2; Right: View of pumps of secondary and tertiary circuits in Building 2 at level -4.0 m



Fig. 2.2 Left: Overall view of SPIDER distribution circuits on the back wall of SPIDER Neutron Shield; Right: Overall view of Primary Circuits pipes inside MITICA Neutron Shield

The following activities were carried out in 2020:

- Literature investigation about corrosion phenomena of different materials in presence of high purity water (W-I water resistivity 5.0 - 10 M Ω cm at 25 °C);
- Collection of requirements and main characteristics of SPIDER cooling plant primary circuits and water purification and storage system;
- Realization of a tool to retrieve the data recorded during the experimental campaign;
- Collection of measurements acquired during the first phase of SPIDER and Cooling Plant operations to highlight the issue: operational periods, water refilling, water resistivity degradation, temperature, flow rate etc.

Some preliminary estimates were carried out on the basis of collected information and first cross checking with experimental measurements are on-going.

Some experimental measurements of water conductivity increase during SPIDER operations are shown in Fig. 2.3.

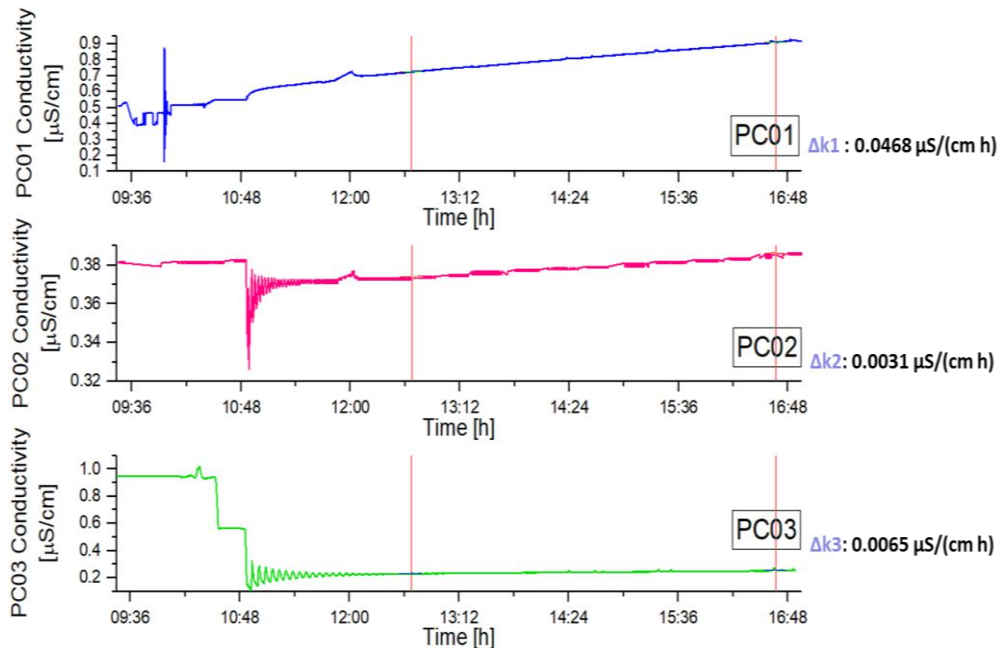


Fig. 2.3 Measurements of water conductivity increase during SPIDER operations

The next activities scheduled in 2021 foresee some dedicated measurement campaigns and/or acquisition during SPIDER operations, aiming to measure further water chemical characteristics and finally to identify the causes of water degradation and a problem solving strategy.

2.1.1.3. Vacuum, gas injection and gas storage for SPIDER and MITICA

The SPIDER Gas and Vacuum plant System (GVS) plant was routinely used and maintained for SPIDER operations in 2020.

Preparation and follow-up of maintenance contracts with several companies were carried out in 2020.

Two activities improving the performance of the SPIDER GVS have been carried out. The first one concerns the control optimization of the BS gas injection obtained by acting on the PID of the pressure control valve which allowed to minimize the oscillation of gas pressure injected in Beam Source. The second activity concerns a significant modification of the partial regeneration of the cryopumps required to perform the experimental operation using Caesium. In fact the partial regeneration allows to evaporate only the light trapped gases (as Hydrogen or Deuterium) while keeping a vessel pressure lower than $1 \cdot 10^{-4}$ mbar.

All the on-site activities in 2020 were strongly affected by the sanitary restrictions due to the Covid-19 pandemic and availability of Supplier's personnel.

The following main activities were performed for MITICA GVS in 2020:

- Installation of gas pipes, vacuum components and vacuum sensors.
- Successful execution of electrical, pressure and leak tests.
- Testing of all the sequences of gas injection using the HMI interface.

The preliminary inspection for the ATEX and EMC certification has been performed, putting in evidence some non-conformities to be solved before the official inspection. The relevant activities were completed.

The installation activities of MITICA GVS were finally concluded in Q4 2020.

The remaining activities for MITICA GVS in 2021 are, commissioning, execution of SATs, the ATEX, PED inspections and EMC tests, training of NBTF personnel, completion, review and approval of the Acceptance Data Package, closure of the contract.

Pictures of SPIDER and MITICA pumping units connected to the vessels are shown in Fig. 2.4.

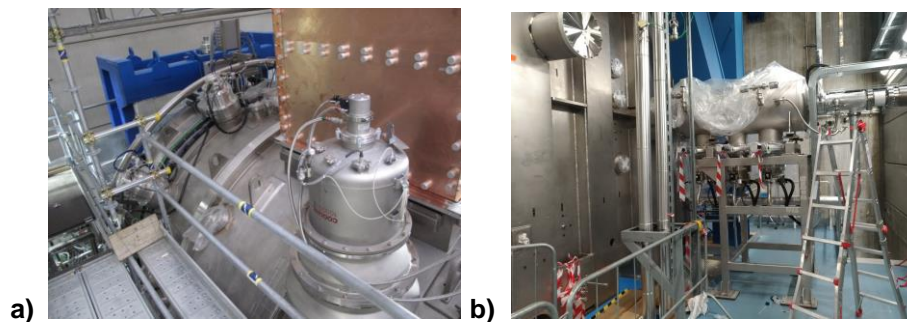


Fig. 2.4 Views of GVS pumping units installed on SPIDER Vacuum Vessel (a) and beside the MITICA Beam Source Vessel (b)

Engineers and technicians of NBTF Team were deeply involved in the technical follow-up during 2020: participation to periodic technical meetings, controls and solving of problems due to integration issues, review of documents submitted in F4E-IDM, preparation of maintenance contracts (with several companies), continuous presence and follow-up during the SPIDER operational period.

2.1.1.4. Host activities

The NBTF Team managed and executed the SPIDER experiments; all activities on SPIDER plant systems in order to guarantee the correct maintenance, to address troubleshooting and to solve minor and major faults; activities necessary during numerous shutdowns including apertures and closures of the SPIDER vacuum vessel.

Resources were spent for construction supervision and coordination, mainly concerning the installation and integration of of MITICA components and plant systems. In particular,

integration management activities were needed for the installation of the MITICA Beam Line Vessel, the AGPS Dummy Load and the Short Circuiting Device, the Cryoplant, the MITICA GVS and the MITICA Cooling Plant.

The NBTF metrology team continued the site and components survey activities, where and when necessary. In particular, metrology activities were fundamental during the installation phase of the MITICA Beam Line Vessel (BLV) and during the installation of the MITICA Rotating Platform.

The NBTF-site management, with reference to “Titolo IV of D.Lgs. 81/08” (Health and Safety on-site), whose structure had been set up through the Implementation Agreement, continued in 2020: the Responsible of Works and the Safety Coordinator continuously monitored and periodically reported the state of the site.

With the support of the Coordinator of the Directors of Works (namely CDL) the time schedule for MITICA on-site activities was prepared and discussed among NBTF Team, IO and all involved Domestic Agencies during the year. Furthermore, as a coordination method, weekly Site Progress Coordination Meetings (SPCMs) have been held, and the minutes distributed. The MITICA time schedule has been managed by preparing, discussing and verifying weekly the activity plan with a visibility of one week, 3 weeks and 3 months.

On a weekly basis, a Safety Coordination Meeting among the CSE, the RSPP of Consorzio RFX and the Site Manager was held to discuss and manage the interferential risks between the yard activities (managed by the CSE) and the activities performed by Consorzio RFX, such as for example the SPIDER operation and the maintenance contracts, but not only.

General follow up activities were performed for all the companies working on-site and all the companies working under “Balance of Plant” procurements. Further activities were devoted to the follow-up of companies involved into the three signed Framework Contracts (CODAS-Interlock-Safety, Diagnostics, Assembly).

In 2020 the Transfer of Responsibility for Use to Consorzio RFX of some plants, such as MITICA Cooling system, MITICA Vacuum Vessel and MITICA GRPS, was obtained. allowed the prosecution on the integration activities without any interruption.

The management of safety and the organization of personnel works on roster for the commissioning (SPIDER and MITICA) and experimental activities (SPIDER) prosecuted during the whole year.

Futhermore the NBTF Team guaranteed a continuous support in the management of the insulating SF6 Gas in order to fill and empty HV components for the HV acceptance test, also managing a contract of assistance with an external company expert in this kind of activities.

In particular, Consorzio RFX accepted the responsibility of the MITICA HV power tests, from the safety point of view, through the appointment of the Responsible for the Test and the emergency coordinator and squads.

Finally, in compliance with the duties provided for in the new agreement, the NBTF Team guaranteed logistical support to all scientists coming from other European laboratories with the contribution of EUROfusion.

2.1.2. SPIDER

2.1.2.1. SPIDER experiments: main results and issues

In 2020 two types of operations were conducted with SPIDER: the former was devoted to the spatial characterisation of the plasma in different operational conditions; the latter was devoted to the verification that SPIDER plants satisfy the requirements for operation during Caesium evaporation. During the latter campaign, some experiments were devoted to investigating the beam features. Most of the topics discussed in this section are described in ¹. The activities performed with SPIDER in 2021 are shown in the graph in Fig. 2.5 and are described in the following sections.

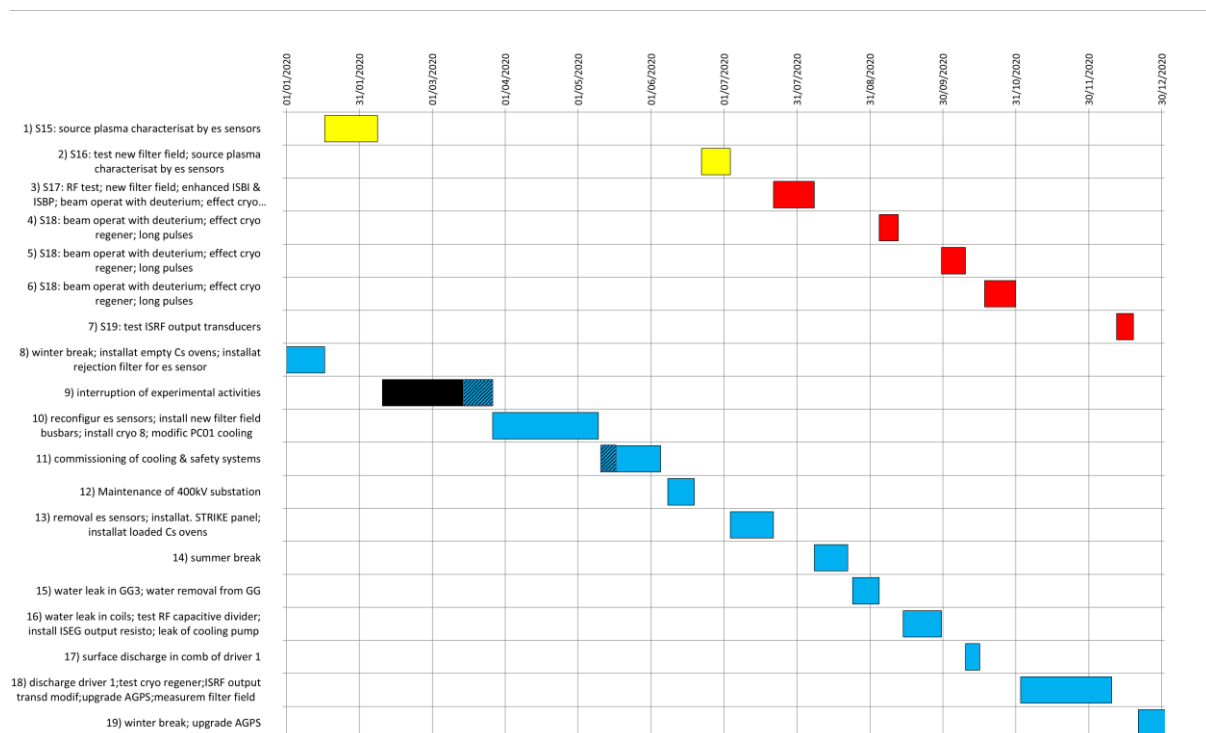


Fig. 2.5 Spider activity schedule: in yellow and red experimental campaigns, in blue the shutdown phases

¹ V. Toigo et al., On the road to ITER NBIs: SPIDER improvement after first operation and MITICA construction progress, submitted to Fusion Engineering and Design

2.1.2.2. Plasma characterisation

Campaigns S15 and S16 in 2020 were devoted to the characterisation of the plasma particularly in the new configuration of the magnetic filter field.

As mentioned in the 2019 report, the magnetic field configuration originally designed and implemented by CRFX in SPIDER had to be modified to improve the plasma generation in the RF drivers. In 2020 the design of the new configuration was completed, also with the help of dedicated numerical simulations (see Section 2.1.4.3) and it was implemented, which entailed adding some busbars on the rear side of the source. The resulting setup allows a broad margin of variation of the field inside the drivers, while keeping it almost unchanged close to the PG. Preliminary results on the first configuration tested in SPIDER showed a considerable improvement²: in Fig. 2.6 it is shown that, during the entire range of the filter field current 0-5kA, the plasma is not quenched. However, a non-ideal operation of the bottom drivers is still found.

After the setup in 2019, the system of movable electrostatic probes accessing the ion source from the accelerator side was installed in SPIDER (see Fig. 2.7a). A very accurate alignment technique and specific in-vacuum movement procedures were developed to this end; particular care was paid in the installation of RF chokes in vacuum, after the initial tests. The electrical connections from the high-voltage deck and the power supplies was modified by connecting to ground each acceleration grid up to the Plasma Grid (PG), thus allowing a safe access to the movable metallic structures from the accelerator apertures. Processing of the current-voltage characteristics was performed automatically during the operation, fitting the

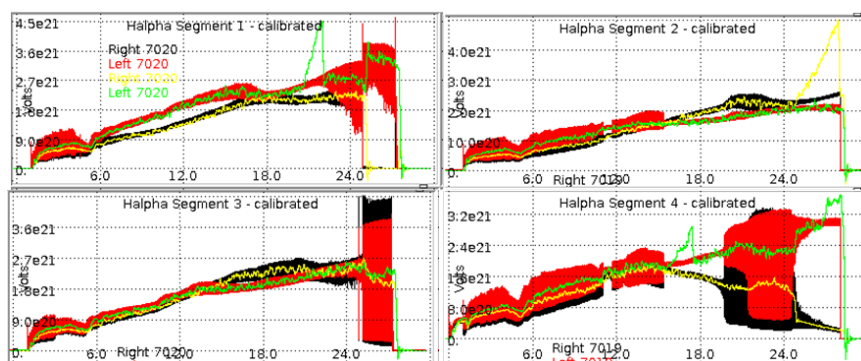


Fig. 2.6 Plasma light in the 8 RF drivers obtained in two separate pulses where the plasma grid current was ramped from 0 to 5 kA. RF1 and RF4 (left) and RF2 and RF3 (right) are activated together during the two pulses. Black lines correspond to right drivers, red lines to left drivers.

² N. Marconato et al., Synthesis of an optimized and flexible configuration for the magnetic filter in the SPIDER experiment, submitted to Fusion Engineering and Design

characteristics and providing plasma parameters at a few time intervals; this allowed to evaluate the obtained results before executing the following plasma pulse.

The plasma parameters were obtained at many positions, for several configurations of the ion source and with various control parameters. The dedicated experimental setup comprised 8 RF-compensated single electrostatic probes, one floating double probe, one 4-pin Mach probe to study drifts in the expansion region, and a couple of retarding field energy analysers, dedicated to the characterization of the positive ion distribution function at the Plasma Grid. In particular, the ion source was operated with a single pair of drivers to obtain clean current-voltage characteristics, while avoiding beating. The isotope effect was also studied by operating in Deuterium and in Hydrogen with varying filter field strength, as shown in Fig. 2.7b. One example showing the influence of pressure on the plasma parameters inside the drivers is shown in Fig. 2.8.

The operation with multiple generators was investigated to characterize the spectrogram of the characteristic frequencies, either in terms of ion saturation current or of floating potential, confirming the results of the plasma light signal. With the old filter field topology in Hydrogen, a steady plasma was found with the simultaneous operation of RF generators 3 and 4 (the two central pairs of drivers) up to 1kA of filter field current (about 1.5 mT); for a higher filter field strength, the fluctuation made the current-voltage characteristics unusable for the standard analysis. The simultaneous use of all four generators made the characteristics unusable even at 1kA.

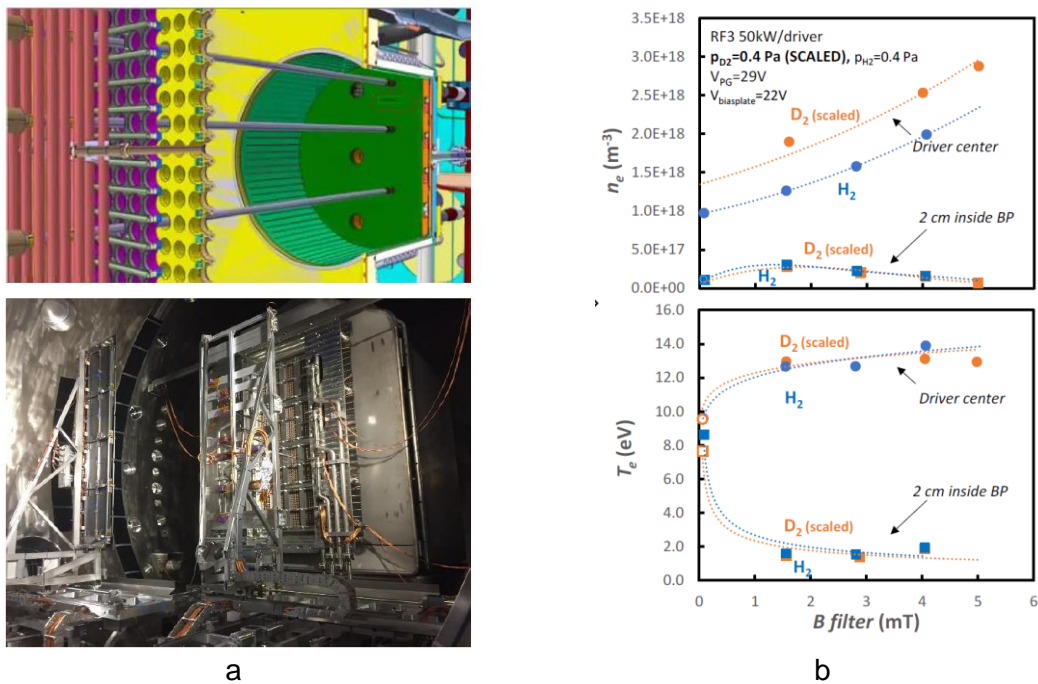


Fig. 2.7 a) top: arrangement of the sensors inside the plasma chamber; a) bottom: view of the supporting system; b) dependence of electron density and the electron temperature on the magnetic filter field for Hydrogen and Deuterium discharges.

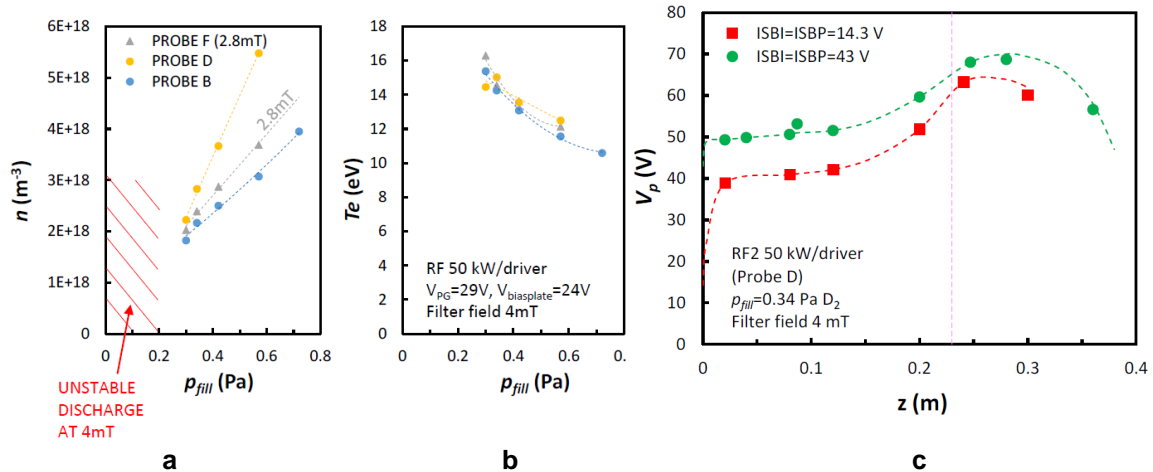


Fig. 2.8 Electron density (a) and temperature (b) as a function of the operating pressure in different positions inside the plasma chamber; (c): profile of the plasma potential for different voltages applied to plasma grid and bias plate.

The analysis of the single Langmuir probe characteristics provided the full axial profiles of plasma density, electron temperature and plasma potential from the Plasma Grid to the backplate of the drivers. Profiles were obtained for different values of filling pressure, filter field strength, RF power, voltages applied to Plasma Grid and bias plate; one example is shown in in Fig. 2.8 c , showing the difference between measured potentials for two different values of bias. The radial non-uniformities inside one driver were also obtained (by inserting three probes within the same driver).

The measurements provided essential data to clarify the role of the filter field in SPIDER, quantifying the electron temperature decrease with the increase of filter field strength, and the consequent density increase within the drivers. It also provided a reference measurement for the optical emission spectroscopy and for the RF power coupling. Finally, the different behaviour between the four pairs of drivers was quantified, highlighting the different response to pressure and filter field, and the peculiar behaviour of the electron temperature at the bottom pair of drivers.

2.1.2.3. Compliance of SPIDER plants with requirements of Caesium operation

In July 2020, experiments resumed, including campaigns S17 and S18, devoted to assessing the compliance of SPIDER plants with the requirements of the campaign with Caesium injection. These essentially correspond to the following types of operational conditions:

- operation with Plasma Grid at $\geq 140\text{C}$ and source walls at $\geq 35\text{C}$, for Caesium distribution inside the ion source
- frequent pulses ($\sim 30\text{s}$ plasma with 1/6-1/10 duty cycle) at low RF power (25-30kW/driver), for *Caesation* of the ion source

- pulses with normal frequency (20-60s plasma with 1/10-1/20 duty cycle) at maximum RF power ($\sim 50\text{kW}/\text{driver}$), for qualification of *Caesation*
- long pulses ($\sim 500\text{s}$) at maximum RF power ($\sim 50\text{kW}/\text{driver}$), for qualification of resilience of *Caesation*.

Correspondingly, the possibility for SPIDER plants to attain the following conditions was experimentally demonstrated:

- operation up to Plasma Grid temperature of 110C ; source walls at room temperature
- frequent pulses (30s plasma every 100s) at low RF power (240kW, 4 RF generators)
- long pulses: 660s with 240kW, 4 RF generators; 300s with 320kW, 4 RF generators; 880s with 180kW, 3 RF generators.

However a part of the assessments needs to be repeated, since some problems emerged (see section Experimental Issues, 2.1.2.5).

As for the characterisation of the beam in SPIDER³, the effect of the modified filter field and of the larger available range for the bias voltages was verified in the SPIDER beam operation. In particular, the co-extracted electron current was reduced effectively without depleting the negative ion current (see Fig. 2.9).

The beamlet ellipticity (difference between vertical and horizontal size of the beamlets) was found to be reduced with respect to the 2019 campaign, probably thanks to the new Plasma Grid mask, which is thicker and thus less prone to deformation than the earlier one. Deuterium

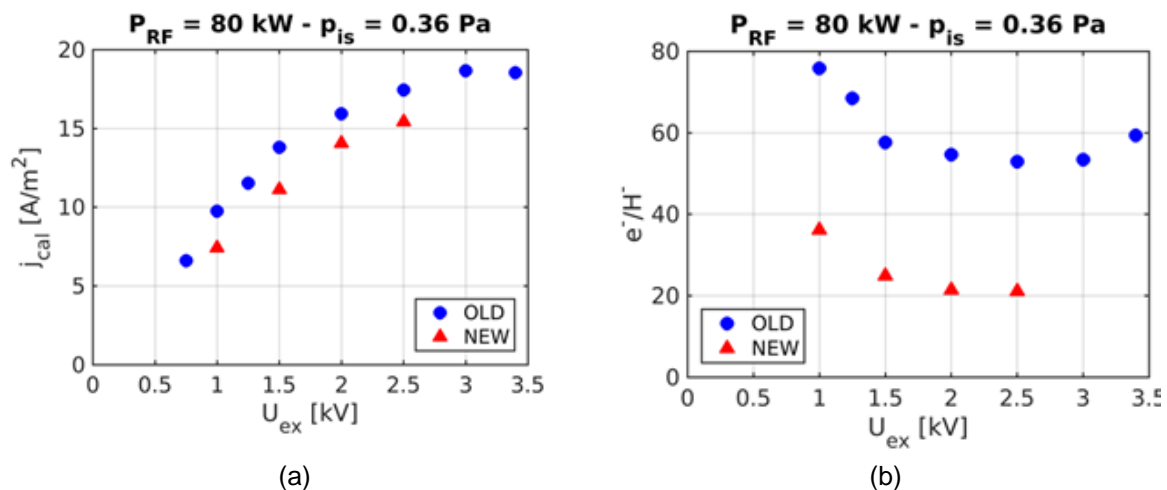


Fig. 2.9 Dependence of accelerated current density (a) and electron-to-ion ratio (b) on the extraction voltage in the previous and in the present setup. $P_{RF} = 80 \text{ kW/gen}$, $P_{is} = 0.36 \text{ Pa}$. For previous configuration: $I_{filter} = 1500 \text{ A}$, $IBP = 0 \text{ A}$, $IPG = 0 \text{ A}$, pulse #6229-30-31-31. For present configuration: $I_{filter} = 1300 \text{ A}$, $IBP = 100 \text{ A}$, $IPG = 100 \text{ A}$, pulse #7427..

³ A. Pimazzoni et al., Reduction of co-extracted electrons and beam inhomogeneity in the large negative ion source SPIDER, submitted to Fusion Engineering and Design

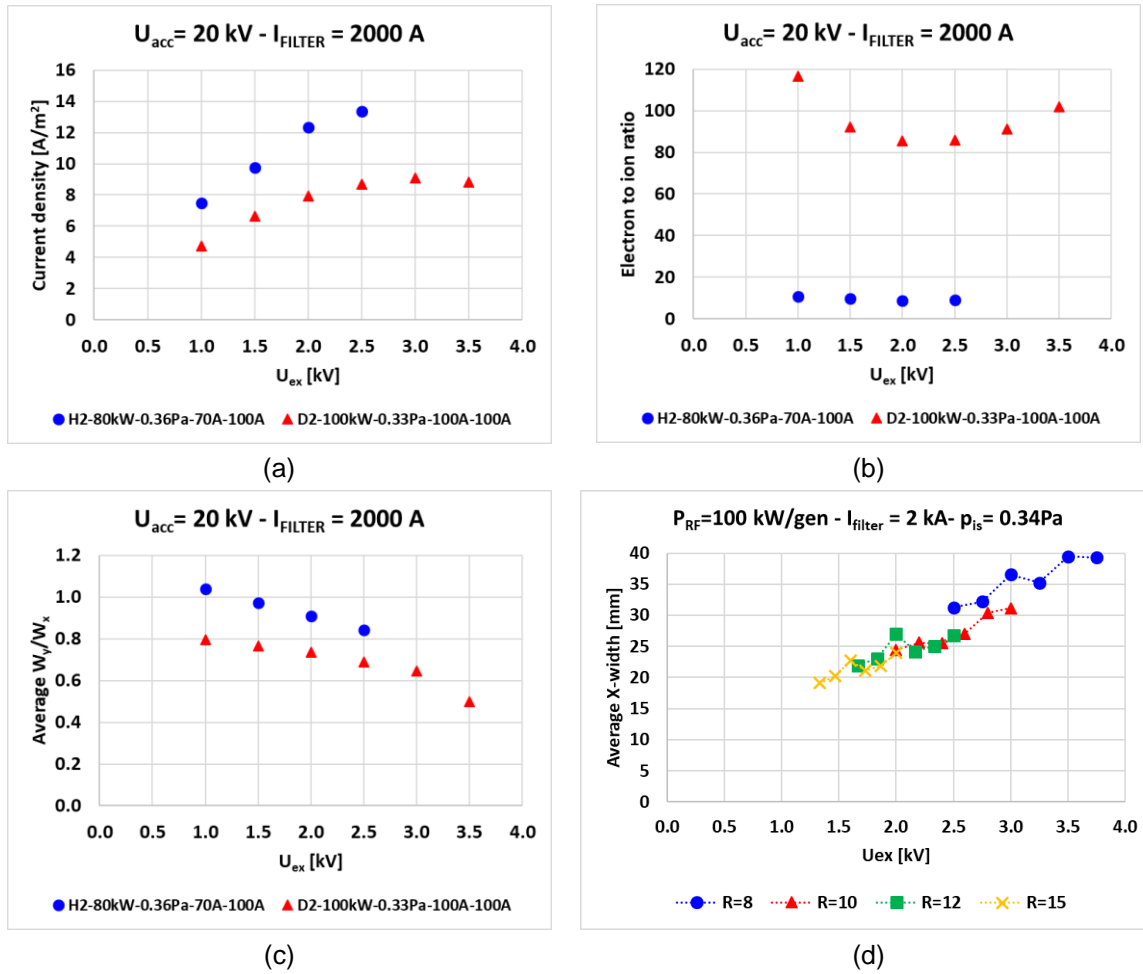


Fig. 2.10 (a-b-c) Extraction voltage scan with H- and D- beams. (a) Accelerated current density; (b) electron to ion ratio; (c) Beamlet ellipticity. (d) Extraction voltage scans in D2, with different U_{acc}/U_{ex} ratios.

beams were also accelerated, finding a much larger electron-to-ion current ratio (Fig. 2.10b) and a more pronounced beam ellipticity than with Hydrogen (see panel c of the Fig. 2.10). A comparison between H^- and D^- beams, with similar source parameters, is given in Fig. 2.18. Optics scan in Deuterium (see panel d of Fig. 2.10) show that the best optics is found at minimal extraction voltages, suggesting a very low D^- production.

From the beam footprint onto STRIKE it was possible to derive a vertical profile of the beam intensity. Such a profile is found to exhibit peaks corresponding to the RF driver centres. The corresponding inhomogeneity increases with the filter field and the extraction voltage, while it is lowered by increasing the source pressure. An example of the profile is given in Fig. 2.11..

Optical emission spectroscopy in the SPIDER source shows that the plasma fills the whole plasma chamber, despite the spatial localisation of the RF drivers, even when operating single RF generators. Vertical and horizontal profiles of the emitted light were measured, showing an increase of the brilliance with respect to the RF power and a decrease with the magnetic filter field (see Fig. 2.12)⁴. Moreover, the extraction region seems to be more affected than the driver region by the filter field.

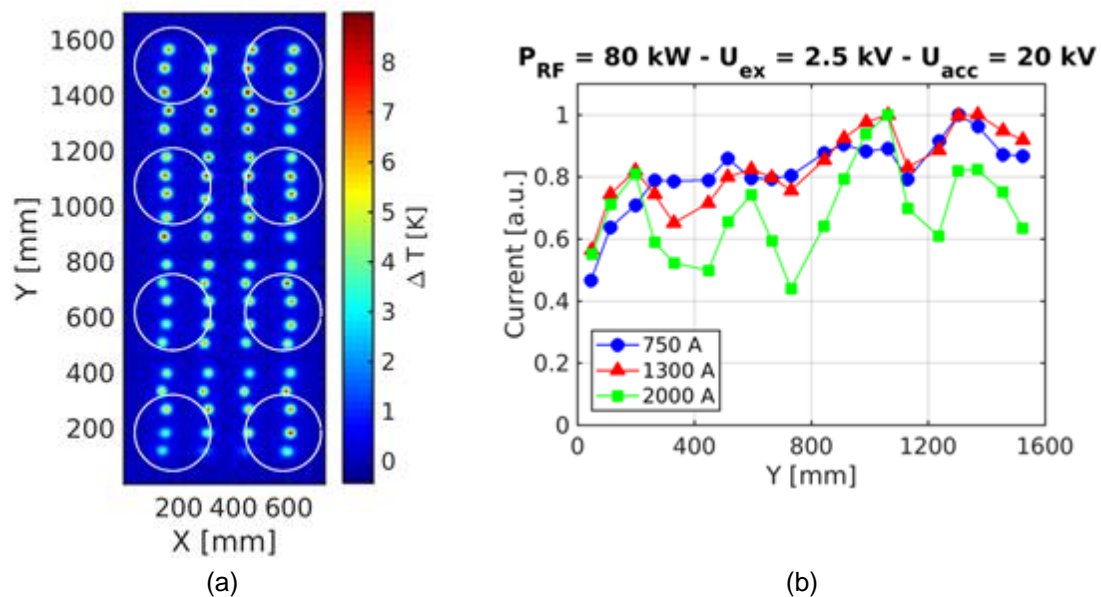


Fig. 2.11 (a) Temperature increase measured on STRIKE. Image is taken 5 seconds after the beam start. (b) Effect of filter current on the beam vertical profile. PRF = 80 kW/generator, $P_{is}=0.36$ Pa, $U_{ex}=2.5$ kV, $U_{acc}=20$ kV.

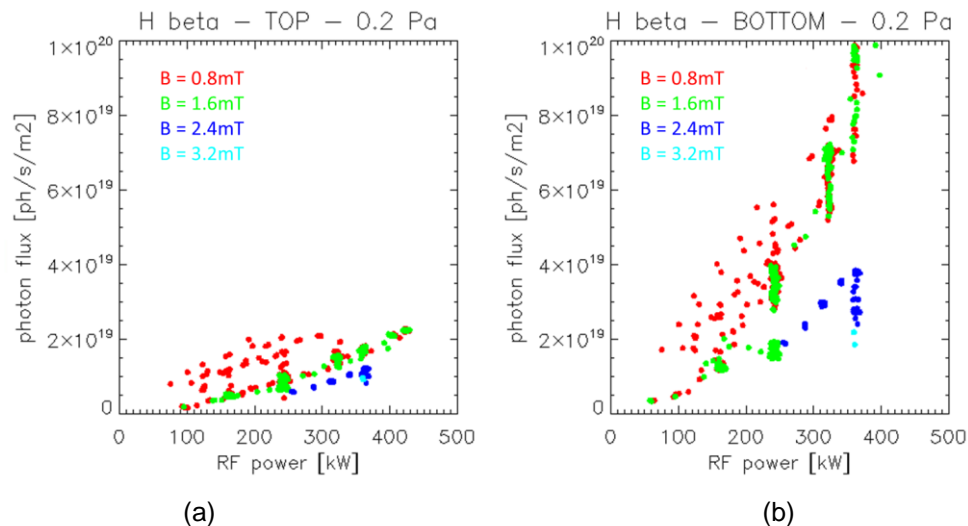


Fig. 2.12 Electron density (a) and temperature (b) as functions of the filling pressure in hydrogen in different vertical positions inside the expansion region; measurements from the top segment are missing.

⁴ B. Zaniol et al., Rev. Sci. Instrum. **91** (2020) 013103

2.1.2.4. Test of modified RF circuits

The Capacitive Voltage Divider (CVD) at the output of the Ion Source RF Oscillators (ISRF-OSCs) allows the circulation of common mode current in plants and diagnostic systems. The CVD measurement is used both for overvoltage protection and power estimation, used in feedback by the RF oscillators.

A solution to reduce the common mode current was identified in the connection of the CVD, properly modified, to the primary side of the output transformer of the RF generators, so that only the stray capacitance between the windings is in the loop for the common mode current.

The solution was tested locally on ISRF-OSC n.2 generator without plasma and remotely with plasma in order to verify the reduction of the common mode currents and the correct operation of the oscillators. After encouraging results (reduction of the common mode current by about 87%; correct operation of the oscillator) the modification was repeated on ISRF-OSC 4 with similar results and in the near future it will be tested on the remaining oscillators.

2.1.2.5. Experimental issues

As mentioned in 2019 report, a Plasma Grid *mask* had to be introduced, to prevent pressure inside the vessel from reaching during operation values not manageable by the current vacuum pumping system, resulting in RF discharges on the back side of the source. The *mask* is exposed to the plasma and only weakly thermally connected to the Plasma Grid, so that its temperature can rise during the plasma pulse, well above the Plasma Grid temperature. Thermal analyses, together with monitoring of the mask with an infrared camera, which was previously calibrated with respect to temporary thermocouples attached to the mask, allowed to trim pulse length and to prevent overheating of the Pyrex pushers, that keep the mask in position, by the heat coming from the mask itself. Experiments have shown that around 400C thermal radiation becomes effective in dissipating the heat and the *mask* temperature stabilises with Hydrogen. Operating in Deuterium, 400s pulses seem to be acceptable with respect to the Pyrex operating temperature, if the magnetic filter field is strong enough to reduce the plasma density in front of the Plasma Grid and thus the thermal load onto the mask. Again in relation to the extracted particles, a specific assessment was carried out also on co-extracted electrons, which are deflected onto the extraction grid, where they deposit their kinetic energy. As electrons tend to focus when magnetically deflected, an indication of the possible localised overheating due to the energy flux associated to electrons can be obtained from the electrical power on the extraction grid power supply by numerically simulating the particle trajectories. So an interlock could be set up to stop SPIDER operation when the electrical power at the extraction grid power supply exceeds 40kW, a value defined to allow for a factor 2 asymmetry of the local electron energy flux with respect to the average. This limit

takes into account the reduction of the extracted particles by the temporary presence of the mask.

Another limit on the beam power was defined and set up to control the heat impinging on the grounded grid, mostly due to secondary electrons, particularly because the bottom segment has not yet actively cooled since the start of SPIDER operations, due to a leak identified at the end of assembly. This turns into a limit on the beam duration: direct measurement by thermocouple of the grounded grid temperature was adopted to check the amount of secondary particles and, in case, adjust the operational limit.

During the operations in 2020, some issues had to be addressed:

- water leak from segment 3 of the grounded grid
- release of water during plasma discharges
- water leak in one of the cooling pumps
- voltage holding problem in the RF circuit of generator 3
- surface discharge in the coil support for RF driver 1

All the above issues resulted in stopping the experiments for a total of several weeks

2.1.2.6. SPIDER Beam Source improvements

SPIDER has been in use since June 2018. During this period experimental activities have been alternated with short shutdowns, necessary to carry out improvements and repairs. Indeed, upgrades and modifications were implemented also in 2020, in order to cope with some topics:

- issues identified during installation, preventing full exploitation;
- refurbishment of damaged parts;
- revision of specific sub-systems preventing increase of performances;
- multiple actions to address RF drive discharges.

The following activities were carried out on the SPIDER BS during 2020:

- Several inspections to verify the status of the BS, identify possible damages and marks of arc discharges.
- Replacement of the mask installed downstream of the *Plasma Grid* (PG), leaving only 80 apertures open out of 1280, to limit the gas pressure increase during SPIDER pulses and to prevent RF driven electrical discharges on the back side of the source. The mask was replaced with a thicker one, still in Molybdenum, held in place by pirex® supports instead of peek®. The new supports should withstand higher heat loads to allow higher performance of the source, which entails higher power loads on the supports.

- A new PG bus bar routing for enhanced filter field configuration, in particular inside the drivers, has been installed and has been used in the latest experimental campaigns, confirming the expected beneficial effect.
- The cooling circuit feeding the PG mounting flange has been re-routed, now sharing the same inlet of *Extraction Grid* (EG), and *Grounded Grid* (GG) mounting flanges, hence minimizing difference of temperature and possible thermal deformations inducing stress on insulators linking such parts.
- Disconnection of the GG inlet/outlet from the cooling plant, excluding all the segments after the leak on the GG segment 3, in addition to the original leaky GG segment 4 segment.
- Replacement of a driver comb “burnt” by local discharges.
- Long-lead procurements of damaged parts (GG3 segment and hydraulic bushing, after careful assessment of possible causes and options for improvements.

Pictures of SPIDER BS while applying some changes during 2020 shutdowns are shown in Fig. 2.13 , Fig. 2.14 and Fig. 2.15.



Fig. 2.13 Installation of the new PG bus bars

The tests and relevant activities carried out on the BS also during 2020 required a huge amount of resources (engineers and technicians) competent on vacuum and hydraulic technologies, electrical insulation in air and in vacuum, radio frequency circuits, diagnostics, metrology and magnetic measurements. During the period of SPIDER operations a big effort was still kept to investigate the issue of electrical discharges during pulses, both inside the BS

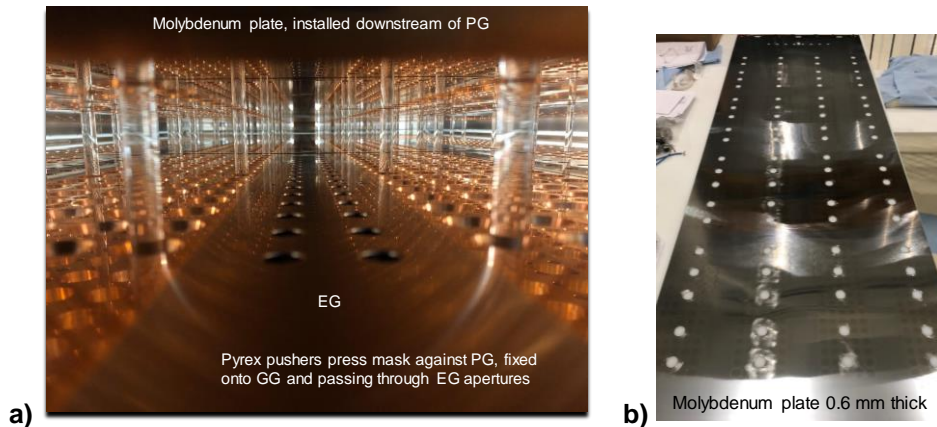


Fig. 2.14 a) New Pyrex® pushers pressing the mask against Plasma Grid, acting from Grounded Grid side; b) The new mask molybdenum plate 0.6mm thick

and towards the vacuum vessel. During short shutdowns, several inspections and minor modifications were carried out, involving a high number of people.

In view of the revision of the RF driver configuration, expected during the long shutdown starting in 2021, the longest lead procurement has already been completed with the delivery of quartz driver cases to replace current alumina ones, with also dimensional modifications in order to minimize the electric field in the most critical areas close to the RF coil.

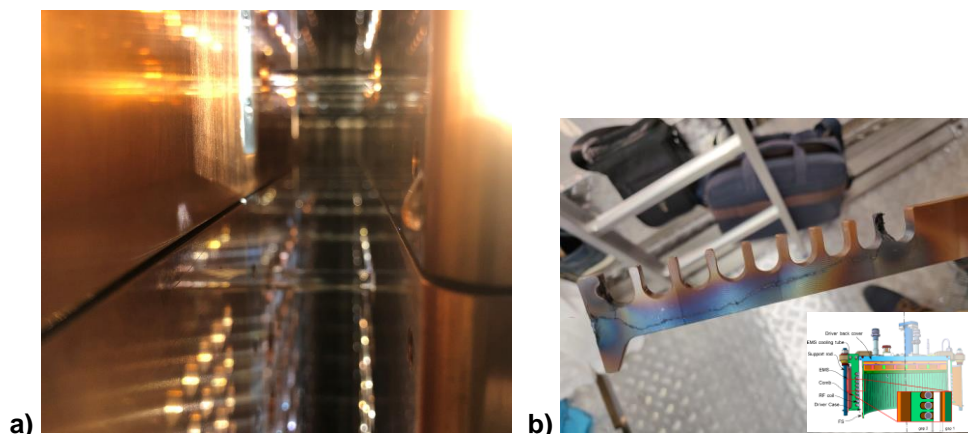


Fig. 2.15 a) Leak close to the edge of the GG3 segment; b) Damaged driver comb

2.1.2.7. Caesium system

During 2020 functional tests of the SPIDER Cs oven #3 were carried out, and results compared to the other ovens (see Fig. 2.16).

The preliminary results highlight that the Oven #3 has a proper behaviour: it is repeatable and in good agreement with Oven #1 and Oven #2 previously tested, especially related to the oven *Surface Ionization Detector* (SID), which allowed to estimate the Cs emission rate.

The activities for Cs Oven system integration in SPIDER significantly progressed in 2020 and are almost completed: cabinets have been prepared, including electronic boards managing the oven subsystems. Preparation of software for control and data acquisition has progressed, taking into account that during the first phase of Cs usage in SPIDER some additional flexibility will be necessary to address the reference procedures identified in CATS⁵. Particular attention has been devoted to the definition of cabinet & hardware protection from disturbances and overvoltages, together with strategies for maximum safe exploitation of the oven features, in terms of control, data acquisition and parameter range, on the basis of the campaigns carried out in CATS on oven prototype and series systems. In order to obtain relevant information on such aspects, empty ovens were installed inside SPIDER to carry out a preliminary verification of interfaces and signal disturbances.

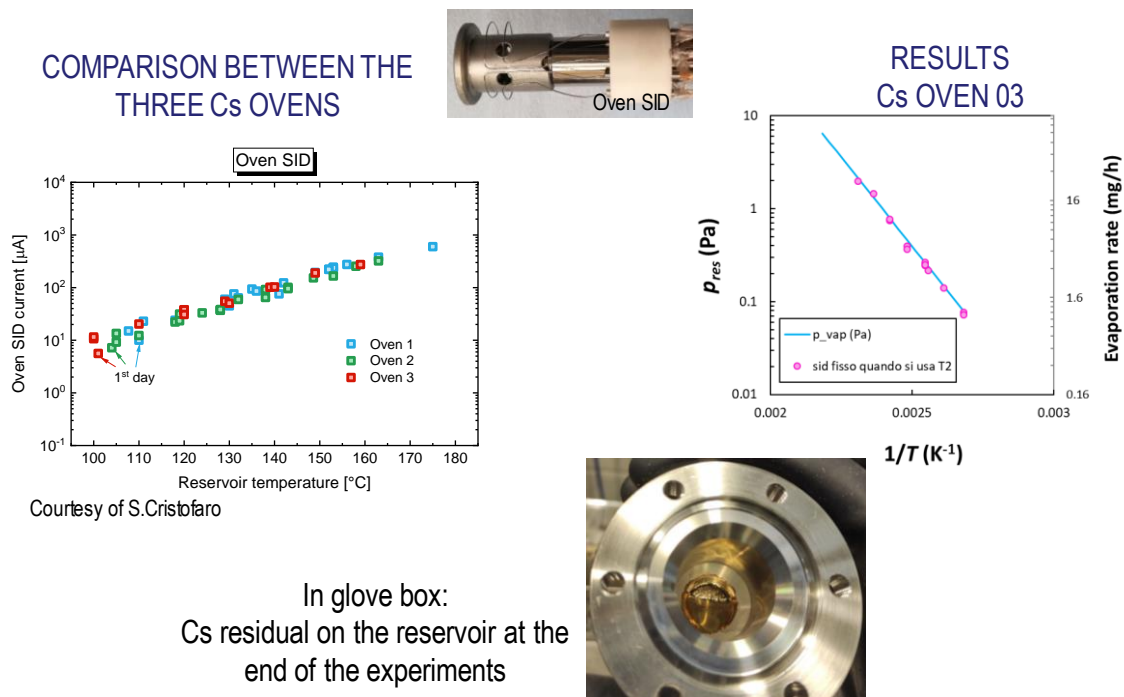


Fig. 2.16 Results of the test on Cs oven #3

⁵ CAesium ovens Test Stand (CATS)

At the beginning of 2021, after a few weeks of operation, SPIDER will begin a short shutdown during which the Vessel will be opened, the ovens loaded with Caesium and then the experiment activity will restart.

2.1.2.8. SPIDER Power Supplies improvements

The SPIDER Power Supplies (PS) include the Ion Source Power Supply (ISEPS), hosted in a Faraday cage - called HVD (High Voltage Deck) , air insulated versus ground for -100 kV and the Acceleration Grid Power Supply (AGPS). A Transmission Line connects the HVD to the BS through the HV Bushing installed on the Vacuum Vessel. The AGPS has been procured by INDA, while all the other PS and auxiliary plants necessary to operate SPIDER have been procured by F4E.

In 2020 the SPIDER PS has been extensively used during the experimental sessions. Improvements and optimization have been done in ISEPS in view of the Caesium operation. The SPIDER AGPS is being modifiede to operate with acceleration voltage up to 100kV.

Ion Source and Extraction Power Supply (ISEPS) system

ISEPS is in operation since 2017. In 2020 ISEPS has been extensively used in experimental campaigns, with the aim of extending the pulse duration, enhancing the reliability of the RF system and achievieng the performance needed for the Caesium operation. After the lockdown period due to the coronavirus, the work concentrated on the support of the experimental campaign and on the modifications needed to limit the RF conducted disturbance coupling. To extend the pulse capability, the Ion Source Extraction Grid (ISEG) power supply output filter has been further improved to be able to dissipate the power due to the above mentioned coupling in Caesium-like pulses. Moreover, output filter resistors of some power supplies have been tested in long pulses to check their readiness for Caesium operation. EMI

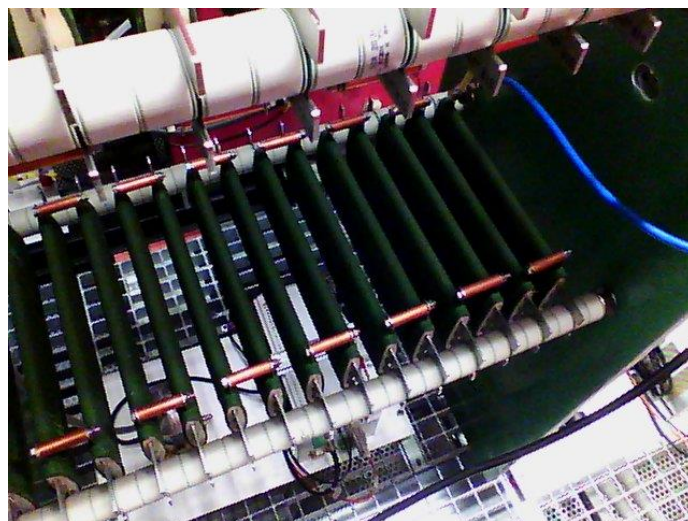


Fig. 2.17 New configuration of the ISEG filter.

filters have been placed on some power supply current measurement data links to improve common mode disturbance rejection. In Fig. 2.17, the new configuration of the ISEG filter is shown. The new resistor nominal ratings are as follow: 32 base resistors 5,6 ohm each, for a total resistance of 44.8 Ohm; installed power is 16kW while nominal energy is 800 kJ.

The resistor has been tested to check its capability to sustain the thermal load expected during a high power SPIDER pulse. An infrared thermocamera has been used to detect the temperature of the different elements; the test showed that the new installation was able to cope with the expected load. Fig. 2.18 shows an image of the thermocamera.

The studies to get rid of the RF coupling in ISEPS progressed and finally, after evaluating the feasibility of different options and search the market for viable solutions, it has been decided



Fig. 2.19 View of CVD installation in RF Generator #3.

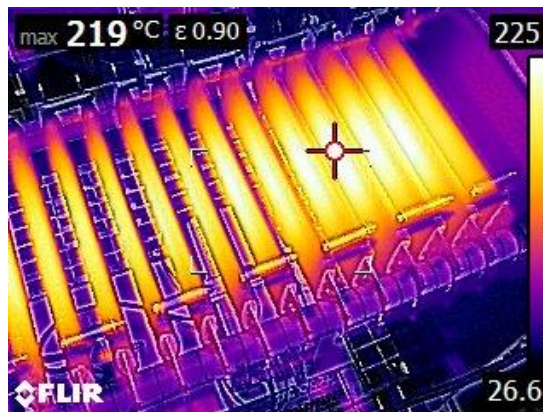


Fig. 2.18 Infrared thermo-camera image of the new ISEG filter resistor during thermal tests.

to implement a modified connection for the Capacitive Voltage Divider (CVD), see Fig. 2.19. The CVD is used by the RF oscillators to get the output voltage measurement, which is used for feedback control, power computation and protection. In the original configuration, the CVDs (one for each generator) were placed at the secondary side of the RF transformer; the central point of the CVD was connected to the HVD and this was the main coupling path of the RF common mode disturbance. The new idea is to move the CVDs at the primary side of the transformer. A great amount of work has been performed to understand the feasibility of this modification and the impact on the overall RF system, including control. Some adaptations have been necessary with ad hoc developments of electronic boards to compensate for the different phase displacement of the measurement. Tests have been done to ensure that the different working conditions of the capacitors. In late 2020 the CVD connections have been modified and the first tests on SPIDER have been performed with very positive results and great reduction of the common mode current.

Acceleration Grid Power Supply (AGPS) system

In 2019 the AGPS system was integrated in the control system and then extensively used for SPIDER operations to extract and accelerate the beams. At the moment the system is certified to operate at reduced voltage, up to 30 kV. In 2020, after the break of the on-site activities due to the pandemic restrictions, discussions for the definition of the modification extend the certification beyond 30 kV and up to 100 kV have resumed. The new disconnecter and earthing switch and the new 100kV cable have been delivered during summer. The replacement of the disconnecter and earthing switch took place in November and December 2020, while the lay down of the 100kV cable is foreseen in early 2021.

2.1.2.9. SPIDER & MITICA diagnostics

All remaining SPIDER diagnostic have been procured in 2020 within F4E contract OFC-531-02. The full instrumented calorimeter STRIKE, now with both panels installed, cavity ring down spectroscopy (CRDS), the neutron diagnostic and the visible beam tomography system have all been commissioned and have entered into operation. They complete the suite of diagnostics initially conceived to assist operation and characterize the source plasma and the beam. The source plasma is now studied with optical emission spectroscopy, over a large number of lines of sight which cover the source extension and allow to study, assisted by a collisional radiative model, asymmetries and time evolution of plasma parameters (electron density and temperature and atomic species populations) from the detected spectrum of atomic and molecular lines.⁶ Faster signals on selected spectral lines, detected with

⁶ B.Zaniol et al., Rev. Sci. Instrum. 91, 013103 (2020)

photodiodes and a photomultiplier measure fast dynamics up to 1 MHz. Electrostatic probes installed on the bias plate and Plasma Grid measure electron temperature and density in that region. A specific campaign with insertable probes was conducted to map the full 3D profile inside the source. The new entry CRDS is routinely operational, with a sufficiently stable cavity alignment, and has been able to measure negative ion densities with an accuracy of about 10^{15} m^{-3} , which allows enough sensitivity to estimate the low density of a non-caesiated plasma⁷, see Fig. 2.20.

The beam is well diagnosed by STRIKE^{8,9}, (see Fig. 2.21) beam emission spectroscopy (BES) and visible beam tomography¹⁰.

New diagnostics, not financed by the F4E contract but from the IO activity program, as only recently conceived and developed, are gradually entering into operation for specific studies.

An Allison emittance scanner recently installed, remotely controlled to scan a small area at the exit of the accelerator, has just started to measure the phase-space distribution of three isolated beamlets.¹¹ A beam current monitor has been designed and installed on the exit face of the grounded grid to measure the single beamlet current with an Hall sensor, to be compared with calorimetric estimates on STRIKE, and the frequency spectrum of this current with current transformers to study the harmonics in the beam current due to the RF generators.

To prepare for the imminent campaign with Caesium evaporation, the laser absorption spectroscopy diagnostics, fully tested previously on the Caesium test bed, is now installed on

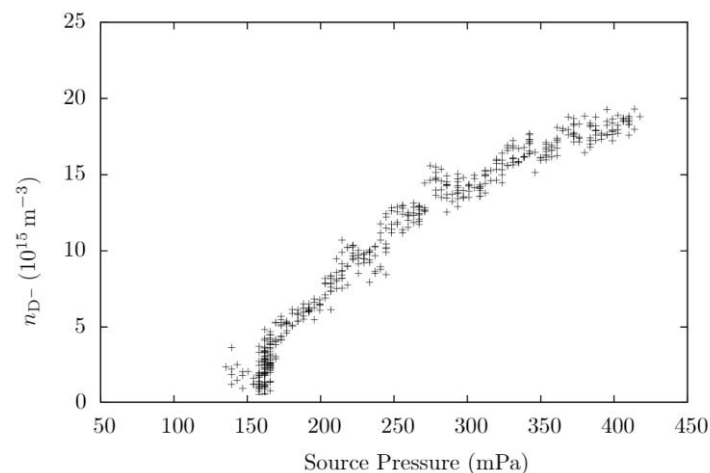


Fig. 2.20 D- density measured as function of source pressure. The plasma was sustained by 4x60 kW. IPG filter current was 750 A.

⁷ M.Barbisan et al., Review of Scientific Instruments, submitted

⁸ A.Pimazzoni et al., Rev. Sci. Instrum. 91, 033301 (2020)

⁹ A.Pimazzoni et al., Fusion Engineering and Design, submitted

¹⁰ M. Ugoletti et al, Fusion Engineering and Design, submitted

¹¹ C.Poggi et al., Fusion Engineering and Design, submitted

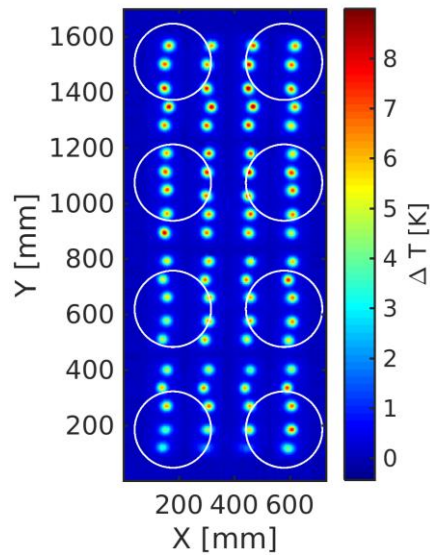


Fig. 2.21 Temperature increase measured on STRIKE. Pulse #7427: PRF = 80 kW/generator, $P_{is}=0.36\text{Pa}$, $I_{filter}=1300\text{A}$, $U_{ex}=2\text{ kV}$, $U_{acc}=20\text{ kV}$, image is taken 5 seconds after the beam start.

SPIDER, ready to measure the atomic Caesium density both during and outside plasma shots. In addition a new temperature programmed desorption (TPD) diagnostic has been developed and installed to enable in-situ measurements of the desorption rate of various Cs-composites formed at surfaces inside the source and the amount of Cs deposited at a specific location inside the ion source.

Preparation of the diagnostics for MITICA has started within the F4E-OFC-531 contract. MIC thermocouples to be installed on the grounded grid of MITICA beam source have been procured and delivered. A set of fibre sensors based on Bragg gratings to measure temperature, strain and acceleration on the beam line components (BLC) has been procured. Prototypes of the electrostatic sensors, also to be installed on the BLC, have been manufactured and tender for the procurement of the full series has been launched.¹²

2.1.2.10. SPIDER I&C integration and commissioning

On the front of Instrumentation and Control (I&C), 2020 activity was focused on SPIDER operation and completion of SPIDER integrated commissioning.

SPIDER operation has required a constant support for I&C to progressively improve its quality and performance and increase the control systems usability and reliability. In detail: i) Fine-tuning the performance of data retrieval and visualization from the short-term data storage, ii) Effective integration of diagnostics (e.g. electrostatic probes), iii) development of new

¹² S.Spagnolo et al., Fusion Engineering and Design, submitted

diagnostic systems, such as the movable electrostatic probes, iv) maintenance of Central Interlock System, required many efforts.

As for SPIDER integrated commissioning, two campaigns were prepared: the first one for the integrated tests of SPIDER/PRIMA cooling system with SPIDER CODAS and Central Interlock System, the second one to test the coordinated operation of SPIDER CODAS, Central Interlock and Safety Systems. Both campaigns were held in 2020, highlighting a list of issues related to the integrated operation of the systems. While it was possible to complete a significant part of the former, the latter will be completed during an additional session in 2021.

Moreover, the new developments listed below were implemented:

- SPIDER long pulses with repeated beam generation;
- Long-term archiving of post-elaborated data;
- Real-time processing and visualization of SPIDER heat fluxes;
- Improvements of CODAS HMI and development of SPIDER overall HMI panel;
- Integration with CODAS of Cavity Ring-down Spectroscopy;
- Integration with CODAS of SPIDER Caesium Ovens;
- Implementation of data acquisition for new diagnostic systems, such as insertable electrostatic probes and emittance scanner;
- Debug and upgrade of WebScope for browser data display;
- Support to development of SPIDER Tomography.

2.1.2.11. SPIDER vacuum enhancement

The need to enhance the SPIDER vacuum pumping capability was highlighted ever since the first stages of the SPIDER experiments, when unexpected RF driven discharges occurred on the rear side of the source, depending on the local value of pressure.

In particular, the increased required pumping depends on three main aspects: the measured higher conductance of the beam source (against the one calculated with reference to the initial design of the source), the presence of RF-induced breakdowns on the rear side of the beam source at high pressure in the vessel (greater than 40mPa) and the increased working pressure in the source ($\geq 0.3\text{Pa}$). All these aspects, which are linked, require the installation of an additional pumping system to be operated in parallel to the existing one.

Three possible options were investigated: commercial cryopumps, custom cryopump and non-evaporable getters (NEG). Quite soon the solution including commercial cryopump was

discarded for logistic reasons, as too many additional units were needed, incompatible with available space and interface with the vessel, see Fig. 2.22.

In depth study of the two leading solutions was carried out, including numerical analyses,

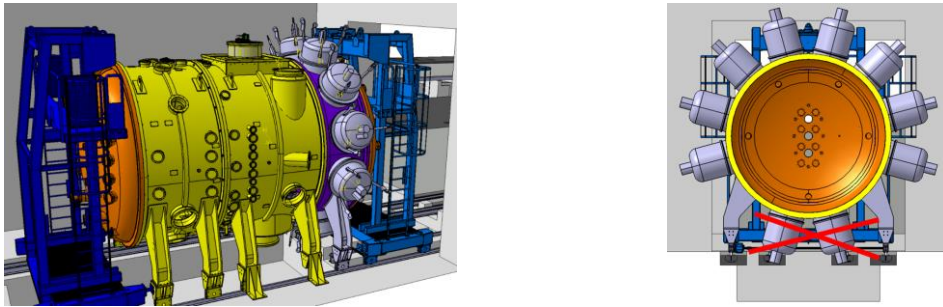


Fig. 2.22 Option based on commercial cryopumps

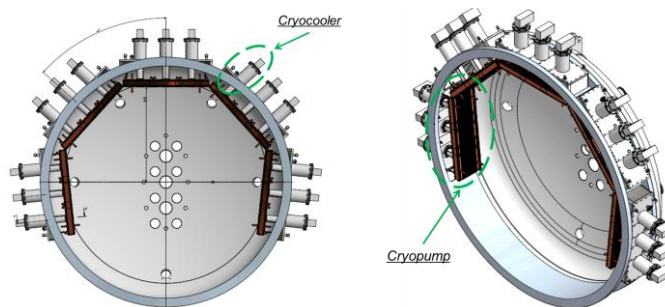


Fig. 2.23 Option based on custom cryo-condensation panels

market survey, preliminary design and experimental tests for NEG.

For the custom cryopumps, a contact with colleagues from Budker Institute of Nuclear Physics was developed, discussing in detail the possible implementation: the proposal is based on the newly developed custom cryo-condensation panels, which are of smaller dimensions than those proposed for SPIDER. Contrarily to the assumptions considered for the first preliminary design (based on TCV pumping system), it seems that a liquid N₂ system to cool the first stage of the proposed cryopumps is necessary; furthermore, no charcoal is foreseen for the H₂/D₂ pumping panel (2nd stage). A new dedicated cryoplant would be needed, including 15 cryo-coolers and 15 cryo-compressors, to be hosted inside SPIDER bio-shield (Fig. 2.23).

As for NEG pumps (Fig. 2.24), some potential issues on their performance and characteristics (for example, their behaviour in the presence of water or water vapour; the pumping performance in “not clean” vacuum conditions; the regeneration time) have been investigated and addressed through the execution of tests performed by the Company also in SPIDER. The most important result is that NEG pumps can be operated at room temperature in not

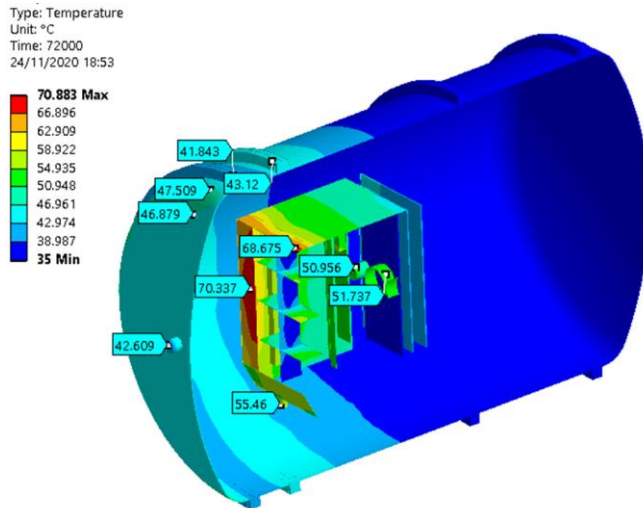


Fig. 2.25 Thermal simulation of regeneration conditions with NEG pumps

clean conditions (as presently in SPIDER): this is because the H₂ pumping speed is not largely affected by the pumping of other gases (O₂ and N₂ mainly). This also led to eliminate the

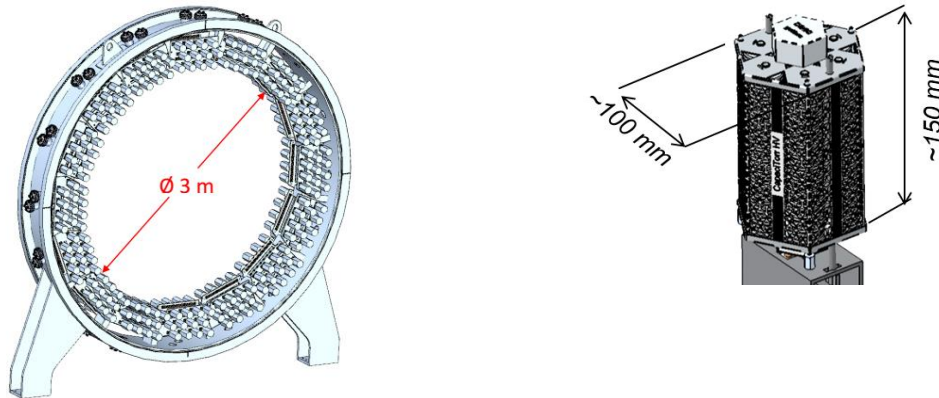


Fig. 2.24 Option based on NEG pumps

issue concerning the water dissociation at high temperature (550°C) in the NEG cartridge due to a possible leakage of the cooling circuit. It was therefore confirmed that NEG technology is a viable solution.

In-vacuum additional thermal shields are necessary to prevent the excessive heating both of the vessel and of the Beam Source parts, see Fig. 2.25. This component can be integrated with the electrostatic shield. A dedicated cooling system for the thermal shields is necessary, in order to prevent the overheating of the vessel O-rings and Beam Source components. Numerical simulations are contributing to identify the proper design solution.

Moreover, it is useful to speed up the cooling down of the pump after the regeneration. Indeed, a sudden large intake of air in the vessel while NEG pumps are at high T for regeneration could be detrimental for their performances, hence it has to be avoided.

A new vessel module 0.6 m long is necessary to host the new pumps, for both solutions.

The studies for the comparison was completed and a Preliminary Design Review held with a panel of experts of IO and Consorzio RFX. A full description of both the solutions was given, including functional aspects, integration implications and cost estimation, highlighting an edge towards NEG pumps. This document has just been submitted to the NBTF Scientific Committee, which will have to take the final decision by early January 2021.

2.1.2.12. RF Solid state generators

Since the beginning of the experiments in SPIDER, the operation of the RF oscillators has been hindered by some important limitations:

- The appearance of the so called “frequency flips”, an instability preventing the achievement of the matching conditions (bad matching) and producing strong limitations of the performances in terms of power delivered to the source
- The presence of high voltage inside the oscillators, requiring frequent conditioning for high voltage vacuum components (tetrodes, capacitors) and maintenance
- The coupling of the drivers combined with oscillator operation, resulting in cross-talking among generators and producing intermodulation effects in the plasma

Since the start of the procurement contract for the Ion Source and Extraction Power Supplies (ISEPS) for SPIDER, MITICA and ITER, quite significant experience has been gained; more recently the expertise grew, in the NBTF facility, with SPIDER campaigns exploiting the free-tetrode based RF oscillators. Moreover, recently, IPP Garching dismissed the oscillators in favor of RF amplifiers based on solid state components, with very positive improvements in BATMAN and ELISE. Thanks to that experience, a sound experimental basis is now available to assess how the two technologies (tetrodes oscillators and solid state amplifiers) compare in terms of robustness, availability and general behaviour, when applied to the production of the plasma required for the generation of negative ions for NBIs. The results of the assessment led to the conclusion that a change from the current tetrode oscillator scheme to solid state amplifiers is needed in order to achieve the required performance in the ITER ion sources

In 2020, a feasibility study activity started to replace the existing RF generators, based on tetrode oscillators, with solid state switching amplifier. A work with ITER was done to identify the framework for the implementation of the modification, considering also that the SPIDER ISEPS procurement under F4E is still ongoing for the ITER units. On the technical side, the NBTF team worked together with the Supplier of ISEPS to identify the critical aspects of the design, the impact on existing plants, the integration in the existing facilities, and, finally, to prepare a technical specification for the procurement, whose contract is to start in early 2021.

An overall strategic plan that includes technical, economic and timing assessments has been developed and submitted to the NBTF SC for approval. At the beginning of December, the SC approved the roadmap, thus giving the green light to proceed with its implementation.

The procurement contract will be signed in Q1 2021, then NBTF will proceed with the development and construction of the solid state amplifiers and their installation on both SPIDER and MITICA, after removing the RF oscillators. The completion of the activities on SPIDER are expected by the first half of 2022 in time for restarting the experiments after the long shutdown.

2.1.3. **MITICA**

2.1.3.1. **MITICA Vacuum Vessel**

After Beam Line Vessel delivery in December 2019, the remaining activities carried out for MITICA VV in 2020 were the completion of BLV installation inside MITICA Neutron Shield, the welding between BLV and BSV, the execution of final SATs after welding, completion, review and approval of the Acceptance Data Package.

All the foreseen tests on-site, mainly positioning metrology tests and vacuum leak tests, were properly performed with successful results.

The activities were performed on-site with a minimum stop of about two months due to Covid-19 pandemic. The good organization of works by the Supplier and the effective collaboration with NBTF Team allowed to conclude all the activities without impacting the start of successive activities planned by MITICA overall schedule.

The Closure Meeting of the contract was held on 3rd July 2020.

Some pictures of MITICA VV installation are shown in Fig. 2.26.

The NBTF Team carried out the following activities in 2020:

- Follow-up of procurement contract OPE-520 MITICA VV;
- Participation to several meetings, both technical and managerial;
- Technical support both to F4E and the Supplier during the procurement contract, in particular for vacuum tests and metrology campaign execution;
- Witnessing and direct support during the tests on-site;
- Review of technical documents submitted by the Supplier.

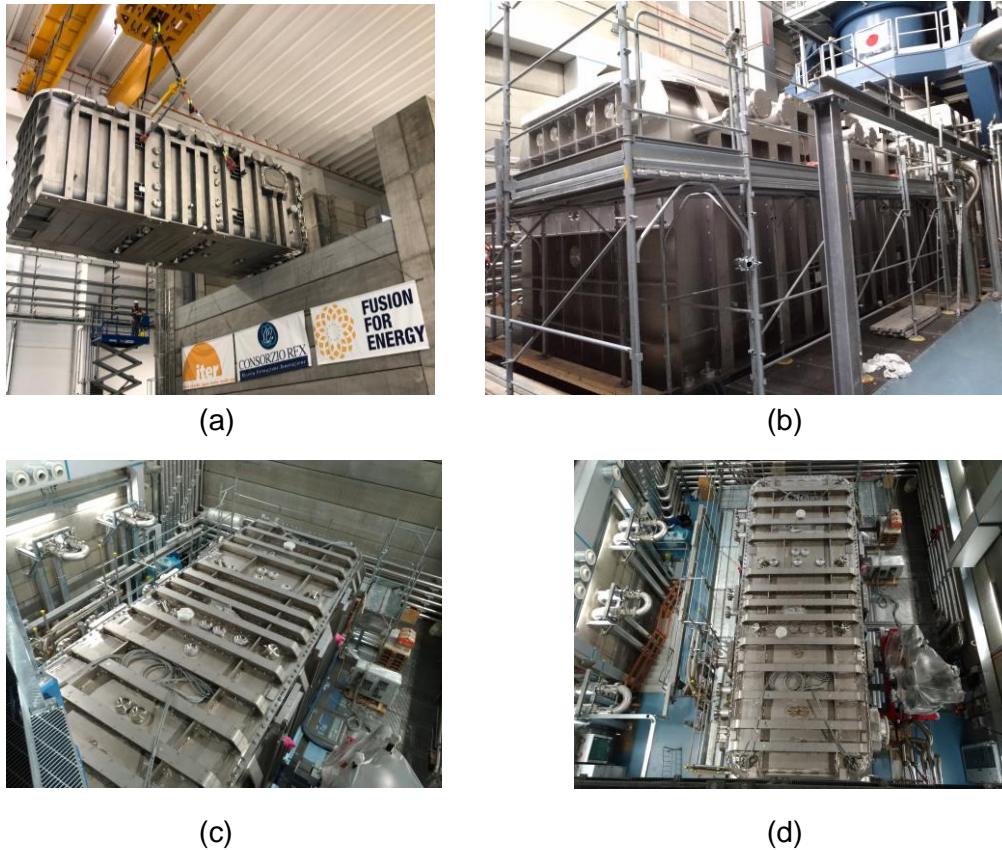


Fig. 2.26 MITICA BLV on-site installation (a) and views of the complete MITICA VV as installed inside the Neutron Shield (b,c,d)

2.1.3.2. MITICA Beam Source

The main in-vessel components of MITICA Injector are shown in Fig. 2.27. All these components are actually full size prototypes of the ones to be manufactured and installed on the ITER Heating Neutral Beam Injectors. Procurements for manufacturing and tests of all these components are on-going.

The MITICA Beam Source is the key component for Negative Ion Beam generation and acceleration. The negative ion beam will be generated and extracted by a RF plasma source operating at an applied electric potential of about -1 MV. Five acceleration grids (AG1, AG2, AG3, AG4, GG) at intermediate electric potential increasing by 200 kV steps, are located downstream the RF source, thus constituting a 5-stage electrostatic accelerator (Fig. 2.28).

The MITICA BS procurement contract progressed in 2020 with engineering activities performed in parallel with construction of prototypes or first series production parts, both at Supplier's and sub-suppliers' workshops. Obviously, the spread of the COVID pandemic affected the activities to some extent.

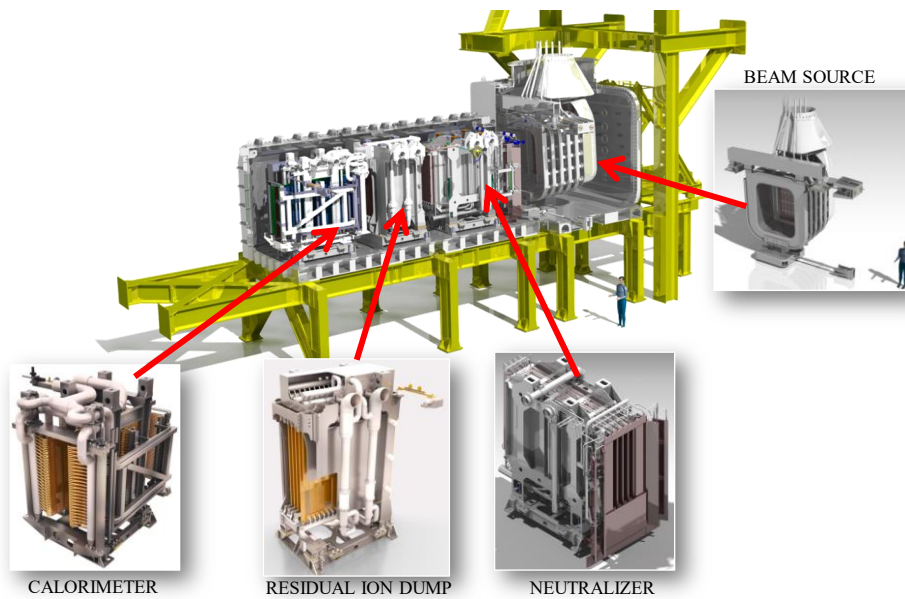


Fig. 2.27 CAD section view of the MITICA Injector with Beam Source and Beam Line Components

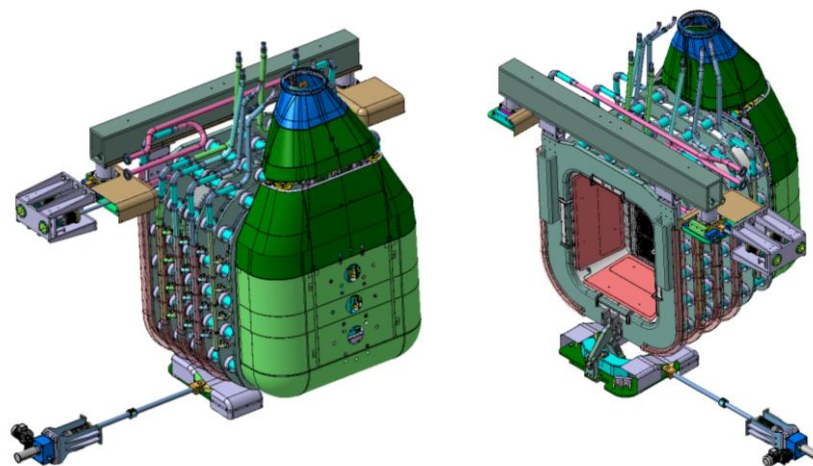


Fig. 2.28 CAD views of the MITICA Beam Source

The equipment for accelerator assembly/test and a prototype of a complete AG4 stage were manufactured and tested; first Acceleration Grid segments were manufactured and partially tested at sub-supplier's workshop. Some tests on prototypes were carried out in Q1 2020 with witnessing by NBTf Team personnel.

Several manufacturing processes were developed and qualified at different workshops of Supplier and sub-suppliers.

The activities were executed in 2020 in parallel at many premises spread all over Europe.



Fig. 2.29 Pictures of BS Acceleration stage assembly and other prototypes manufacturing

The first prototypes of MITICA BS Post Insulators were delivered to RFX in March 2020 in order to perform the electrical insulation tests at HVPTF and HVSGTF in Padova. The tests up to 200 kV were carried out with positive results.

First two series Post Insulators (samples of PIs to be installed between GG and AG4) were delivered to RFX in order to be electrically tested. The tests are on-going and will be completed in January 2021.

The main activities performed by the NBTF Team were:

- Participation to meetings and technical support during the procurement contract;
- Review of outstanding documents for MRR (revised technical notes, CAD models and drawings);
- Assessment and feedback to Non-Conformities and Technical Queries by the Supplier;
- Analyses and verifications for alternative design for the SCLW water manifolds;
- Execution of numerical simulations to assess queries on Electron Dump and SCLW water tank and PDPQ thermal behaviour during heat treatment;
- Preparation of procedure for GG thermocouples installation;
- Electrical tests on ceramic breaks insulators to be performed at RFX premises have been agreed and relevant documentation prepared for offer submission.

Fig. 2.29 shows some pictures of the BS acceleration stage under assembly at supplier's workshop and other prototypes under manufacturing, while Fig. 2.30 shows a extractor insulator under electrical test in HVSGTF.



Fig. 2.30 Pictures of an extractor insulator under electrical test in HVSGTF

2.1.3.3. MITICA Beam Line Components

Three Beam Line Components (BLCs) are foreseen downstream the Beam Source, as shown in the Fig. 2.27. The negative ion beam generated by the Beam Source at 1 MeV, after passing through a gas cell Neutraliser and an Electrostatic Residual Ion Dump (RID), shall produce a ~17 MW D0 or H0 neutral beam focused onto a target Calorimeter for a duration up to 3600s.

A two stages contract was launched in 2018 for BLCs procurement: Stage 1 for baseline review, Stage 2 for MITICA BLCs procurement. After completion of Stage 1 the BLCs procurement contract was awarded to the Spanish company AVS–Tecnalia in December 2019 and the procurement activities started in January 2020.

The engineering phase was performed by the supplier in 2020, preparing the main documents and drawings for manufacturing of prototypes and series parts. The main sub-suppliers were identified and first manufacturing process qualification started. The assembly sequence and handling-assembling tools were deeply discussed for the main assemblies of the beamline components, with reviews of some supplier proposals.

Electrical tests on ceramic breaks and electrical standoff insulators to be performed on RFX testbed have been agreed and relevant documentation prepared for offer submission.

The review of prototypes drawings has been completed and the approval of certificates for procurement of prototype materials has been completed.

Manufacturing, Assembly and intermediate Testing Plan (MAT) including welding aspects have been reviewed. MRR drawings including manufacturing features/steps and metrology topics have been submitted and commented by F4E/RFX.

The main NBTF Team activities carried out during 2020 were:

- Follow-up of procurement contract OMF-795 MITICA BLCs;

- Participation to meetings and technical support during the procurement contract;
- Review of technical documents submitted by the supplier.

2.1.3.4. MITICA Cryogenic Pumps

Two large Cryogenic Pumps will be installed inside the MITICA Beam Line Vessel to guarantee proper vacuum conditions inside the vessel during MITICA operation (see Fig. 2.31).

The Cryopumps are based on adsorption pumping by charcoal coated cryopanel (CPs), 8 m long, 2.8 m high and 0.45 m deep, operated between 4.5 K and 400 K. These cryopanel are surrounded by a Thermal Radiation Shield (TRS) operated between 80 K and 400 K. The CPs will be at the lower temperatures during normal operations, while 100 K or 400 K will be achieved during periodic pump regenerations necessary to remove from the CPs the adsorbed gas (H₂ or D₂). The pumping speed estimated for the two pumps operating in parallel are 5000 m³/s for H₂ and 3800 m³/s for D₂.

The complex procurement of Cryopumps is subdivided into three lots, corresponding to specific knowledge and expertise of different suppliers: Lot 1 for support frame and assembly, Lot 2 for expansion profiles and Lot 3 for charcoal coating of pumping surfaces.

The contract for procurement was awarded in 2018 and the procurement activities are on-going. During 2020 technical follow-up was carried out by NBTF Team to support F4E during the procurement phases. In particular material purchase and specific manufacturing processes and prototypes for qualification were thoroughly discussed.

Some technical issues regarding the qualification of hydroforming process for Cryopanel, charcoal coating and surface finishing created some problems and delays on procurement.

As regards Lot 1 (Support Frame manufacturing and assembly) F4E is going on with negotiations with the supplier SDMS, in order to solve the still open contractual issues. However, some technical meetings continue, as does the supplier's work on some documents.

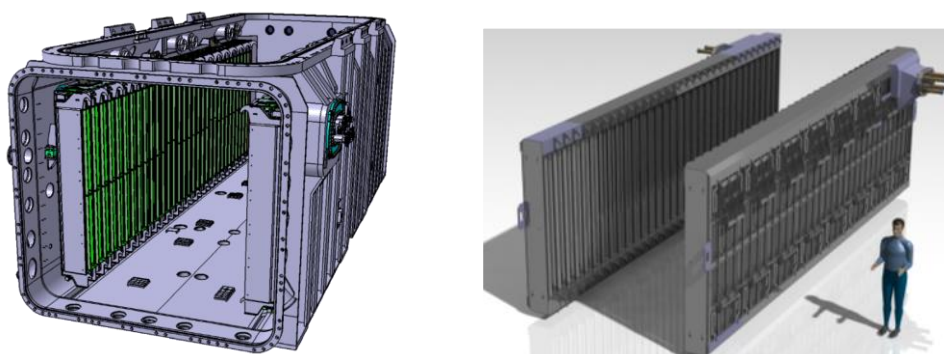


Fig. 2.31 CAD Views of MITICA Cryogenic Pumps

With regard to Lot 2 (Expansion profiles manufacturing) the supplier Ravanat is ending with the supply of dummy panels and latest Cryosorption Pumping panels to SDMS. Then formally the contract with Ravanat will end at the beginning of next year when the Thermal Radiation Shield panels will be shipped to SDMS.

Lot 3 (Charcoal coating of pumping surfaces) continued in 2020: the supplier SDMS is doing the sandblasting of the panels and is about to start with the charcoal coating, after completion of qualification of the process.

Some pictures showing the manufactured expansion profiles are shown in Fig. 2.32.

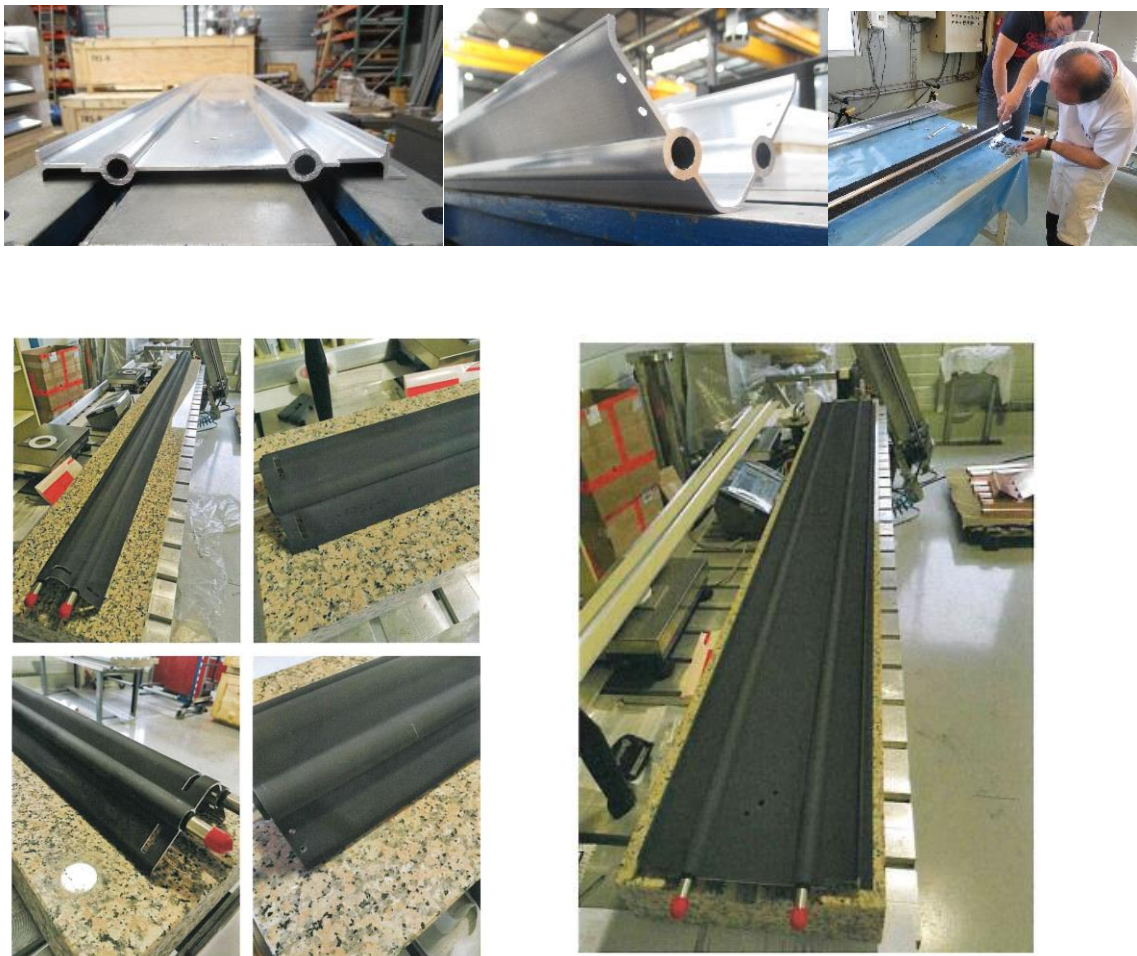


Fig. 2.32 Pictures of extruded aluminium profiles and expansion profiles manufactured for MITICA Cryopumps

2.1.3.5. Cryogenic Plant

The MITICA Cryogenic Plant is designed to produce supercritical Helium (ScHe) at 4.6K and gaseous Helium (GHe) at 81K and to feed these cryogenic fluids respectively to the cryosorption panel (CP) and to the thermal radiation shield (TRS) assemblies of the cryopumps. The expected heat loads to be removed in pulse-on scenario are 800 W on CP

and 17.4 kW on TRS assembly. The same plant shall also manage the regeneration of Cryopumps at different temperatures.

The procurement contract for MITICA Cryogenic Plant was launched in September 2016 and the supplier is ALAT (Air Liquide Advanced Technologies).

All the equipment, components, warm lines and cryo lines, sensors, electrical boards and cabling were delivered and installed in 2019. After commissioning of the plant performed in 2019 some issues were identified regarding the actual performance as compared with the contractual ones.

Some works were carried out on-site in 2020 to solve the issues. As final outcome the overall cooling power of the plant is now sufficient, however problems with stability of parameters and detected parasitic heat loads make the overall acceptance tests impossible. Further investigation by the supplier ALAT identified some potential source of instabilities/heat load in the installed heaters in the Cryogenic Plant lines.

So some further changes shall be applied to the plant to finally achieve the expected results in terms of performance and regular operations. These are planned during the next year 2021.

NBTF personnel training was carried out in 2020 involving two engineers and two technicians of NBTF Team.

Completion of Site Acceptance Tests and closure of contract is now foreseen in Q2 2021.

The main NBTF Team activities in 2020 were:

- Follow-up of procurement contract OPE-307 MITICA Cryogenic Plant.
- Technical support during the procurement contract.
- Discussions about organization of on-site activities.

Review of electrical documentation received from Supplier.

Picture of Cryogenic Plant installation are shown in Fig. 2.33.

2.1.3.6. MITICA Power Supply system

In 2020, the activity on the MITICA Power Supplies focused on the: preparation and realization of integration tests between CODAS, AGPS-CS and the HV components procured by JADA, and on the installation and site commissioning of the MITICA ISEPS.

MITICA ISEPS

The procurment of the MITICA ISEPS has been completed in 2020 with the installation of the equipment in HVD1 and the site commissioning and acceptance tests. The system is now

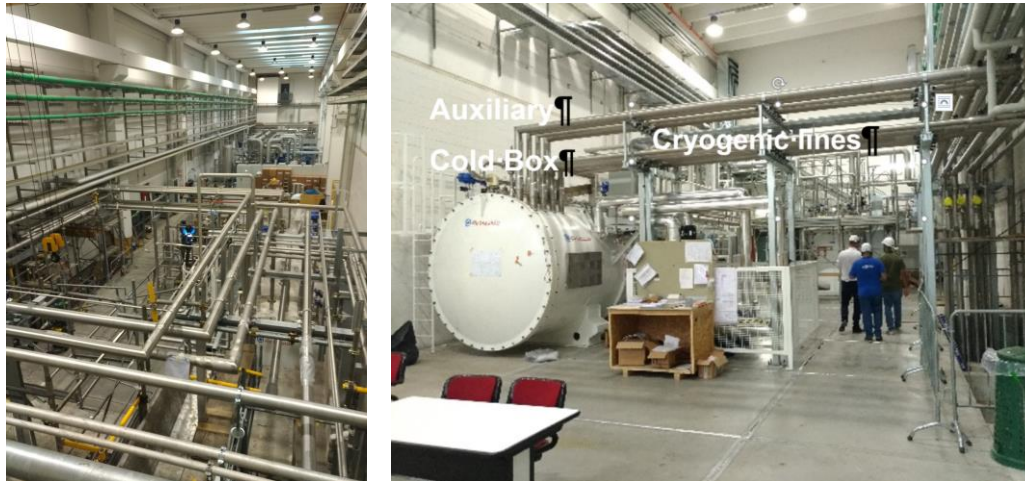


Fig. 2.33 Pictures of MITICA Cryogenic Plant components and piping inside Building 2

ready to be integrated in the MITICA power supply system under CODAS. In late 2020, the system has been provisionally transferred for use to Consorzio RFX; this was necessary because the Core Snubber Bias Power Supply is needed to perform the AGPS integration tests. Moreover, the energization of the 1MV Insulating transformer has been anticipated with respect to the original schedule for the same reason.

MITICA AGPS-CS

In early 2020, the AGPS Ringing Filters installed in 2019 have been commissioned, showing their beneficial effects in reducing the voltage oscillations at the primary side of the DCG transformers as expected. The setup of the voltage measurements at the filter interface is shown in Fig. 2.34. A comparison of the voltage obtained for the same modulation index of the inverters with and without in Fig. 2.35 shows that the filter is very effective.

Concerning the integration between CODAS and AGPS-CS, the activity has been completed in January 2020, just before the lockdown. A pulse on the Dummy Load installed in Building 3 has been achieved using miniCODAS with the AGPS-CS control in remote.

MITICA AGPS power integrated tests



Fig. 2.34 Setup of the line to line voltage measurement at the ringing filter connection.

In the plan presented in the Activity plan 2019, the MITICA power supply power integrated tests were to be performed under CODAS control in 2020. These important tests should allow to verify and to demonstrate the correct operation of the AGPS system including the verification of full performance (1MV, 60MW for 2 seconds) on the Dummy Load (DL). Moreover, the correct sequence management, i.e. fast shutdown and automatic restart of the AGPS, in case of grid breakdown simulated by means of a power device, the Short Circuit Device (SCD) installed inside the VV, should also be performed.

At the beginning of 2020, the preparatory activities for the power tests were carried out. In particular:

- the installation of the 1MV, 50MW dummy load, see Fig. 2.36, a resistive dummy load about 12 m high and cooled in natural air
- the removal of the TPS, used for the insulation tests of the high voltage components and no longer necessary

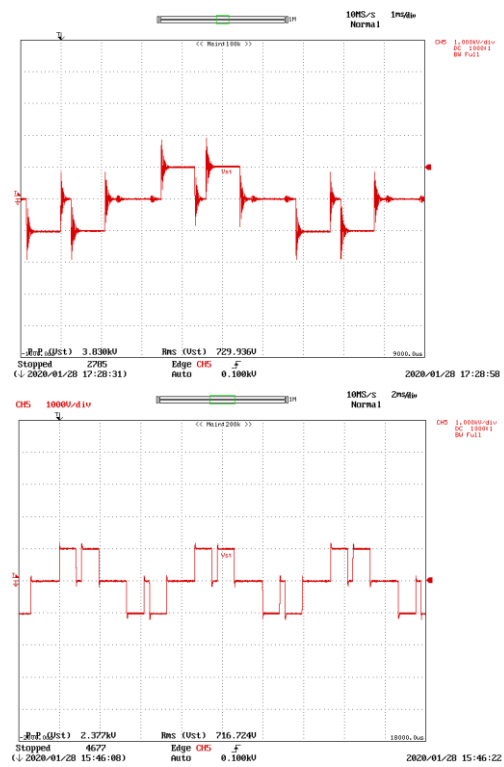


Fig. 2.35 Line-to-line voltage at the DCG primary side without (above) and with ringing filter connected.



Fig. 2.36 AGPS 1MV, 50MW Dummy Load

- the installation of the SCD inside the BSV in place of the source, see Fig. 2.37, complete with pneumatic controls to simulate the break down between the grids.

Unfortunately, due to the Covid-19 restrictions, the AGPS power integrated tests, foreseen to start in Q2 2020, have been postponed to late 2020, after having set up an organization that allowed to proceed with the activities under the responsibility of the Japanese DA even without their physical presence on-site.

The first part of the integration tests with the High Voltage components took place in October, with the so-called “AGPS integration tests at 100kV in air”. These tests were aimed at checking for the at low voltage the operation of each AGPS stage individually, in order to ensure and confirm the integrated operation of the power supply. Each stage was connected to the Dummy Load in Building 8 through the HV Deck1. The tests were successful. In Fig. 2.38, miniCODAS operator and power supplies expert are setting up a pulse and discussing the results. The tests were followed-up

remotely from Japan by QST colleagues, not allowed to come to the NBTF site due to the pandemic restrictions. Fig. 2.39 shows some results of the tests: the oscilloscope reports voltage and currents of the stage under test. In late 2020 the system was ready to perform the final integration tests in nominal configuration up to 1MV and complete the power integrated



Fig. 2.37 AGPS Short Circuiting Device (SCD) installed inside BSV

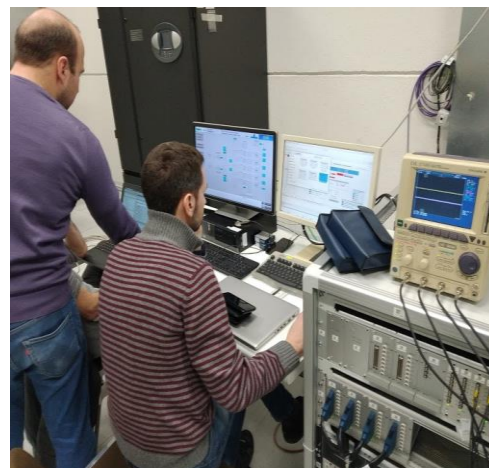


Fig. 2.38 MITICA operators during AGPS integration tests.

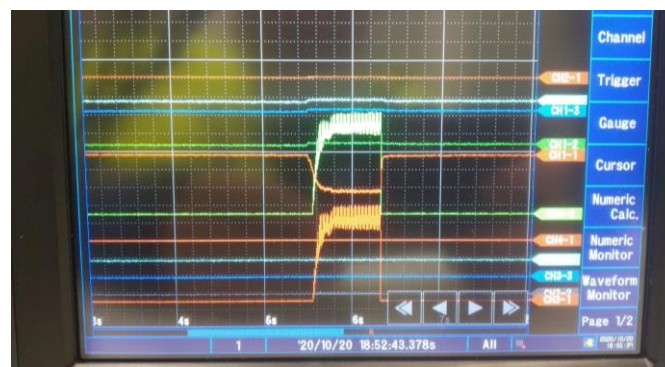


Fig. 2.39 Some results of the first AGPS integration tests at low voltage.

tests also acceptance tests for the Japanese procurement. Discussion on test details has started and a test procedure has been shared with all involved partners. These tests will begin in January 2021 to be concluded in March.

2.1.3.7. MITICA I&C

The integrated commissioning of MITICA AGPS with miniCODAS and miniInterlock progressed. The interface with the AGPS plant unit was completely tested and the whole pulse sequence was executed in remote control mode and Beam-on Global Operating State. Data acquisition was tested and improvements were applied, especially to the AGPS distributed data acquisition based on optical links carrying digitalized measurements. The MITICA CODAS human machine interface of ISEPS was developed and successfully tested during ISEPS SAT.

With reference to the central I&C interface with MITICA plant systems, activities were carried out for the follow-up of the MITICA cooling and gas & vacuum systems and for the implementation of the relevant MITICA CODAS interfaces. The CODAS human machine interface of the MITICA cooling was developed and tested and the self-description data (SDD) of the interface process variables for the MITICA gas&vacuum was completed.

2.1.4. ITER Neutral Beam Injector Physics

Several numerical models were developed or verified in 2020 to support the operation of Negative Ion Beams. They are described in the following sections.

2.1.4.1. Development of numerical models to support Caesium operation

Collisional-radiative model

In view of the Caesium operation of SPIDER, the development of a collisional-radiative (CR) model was started, dedicated to the Caesium atom in a Hydrogen plasma. The use of a Cs CR model allows to use the optical emission spectroscopy to quantify the line-averaged density of Cs neutrals at different positions, despite the large variations in the electron temperature in the strongly heterogeneous plasma of the negative ion source. The model is based on the works published by IPP Munich and IIT Roorkee, who previously developed CR models dedicated to Caesium; at the present state of development, the presence of Cs⁺ recombination is being included. A very preliminary application to the spectra obtained in NIO1 during the recent Cs operation is presented in Fig. 2.40: the contribution of all Cs emission lines related to de-excitation from the 6p, 7p, and 7d levels, presented with yellow points, are used to estimate the density of ground state Cs atoms, which are orders of magnitude higher. For electron temperatures above 3eV, the density of excited levels saturates and therefore there is no difference between the CR results (blue and green squares in Fig. 2.40). The Cs⁺

recombination via three-body recombination and Hydrogen negative ion neutralization was not included in this calculation and will be included in the next year. It is planned to use the CR model to prepare a dataset of results, to be used during the SPIDER campaign to provide a real-time estimation of the Cs density during plasma discharges; ideally, this analysis can be applied to both the driver region and the extraction region.

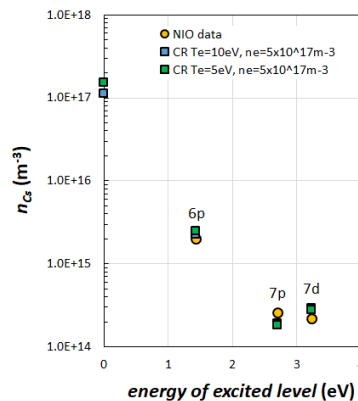


Fig. 2.40 Density of caesium excited levels in NIO1.

Caesium transport model

A 3D model for Caesium transport in a plasma discharge is being developed to support the Cs operations in SPIDER. The use of such codes to investigate Cs dynamics in negative ion sources was proposed by IPP Munich and was applied to the IPP prototype sources to support the *Caesation* procedure. The numerical code being developed is based on ray-tracing simulations of Cs and Cs⁺ in electrostatic and magnetostatic fields, to determine the mutual exchange of Cs particles between each pair of surface elements. A matrix of exchange coefficients is created in this way. A set of linear exchange equations exploits the matrix of exchange coefficients to calculate, in a transient simulation including the expected duty cycles of plasma discharges, the Cs transport, from the Cs ovens towards the Plasma Grid (the converter surface) from the initial emission. At the present state, the physics of Cs evaporation, sputtering and sticking is being included in the exchange equation, also considering the minor presence of oxygen and water in the background atmosphere, which is expected to passivate the Cs layer (during the nights and the weekends). Given the lack of reference data concerning these processes, experimental activities (for instance based on Temperature Programmed Desorption applied to Cs adsorption in the presence of Cs-gettering gases) are planned to support the modelling activities.

2.1.4.2. Model of RF inductive coupling with plasma

In the cylindrical RF drivers, an azimuthal RF electric field is created by the concatenated magnetic induction produced by the RF currents in the external coil. When a plasma is ignited, layers of azimuthal currents are produced, which contribute to the magnetic induction and are limited in depth inside the plasma cylinder (skin depth). An axisymmetrical numerical model was developed to describe the induced fields, and the power density developed by ohmic heating that sustain the discharge. A phasor notation was employed to describe the azimuthal electric fields, the induced currents (via a conductivity of the plasma in complex notation) and the delivered power, under the assumption of a radial profile of plasma density. At reasonably high plasma densities, the numerical complexity of these calculations increases due to the thin skin-depth that pushes the induced electric fields to the plasma edge, and small cell sizes are required. An example of this effect is shown in frame a of Fig. 2.41. At present, the development focuses on the inclusion of passive structures in the model, as it is expected that the presence of metal parts deforms the induced fields (see an example in Fig. 2.41 (b)); it will be important also to model the presence of a sliced Faraday shield (which is discontinuous along the azimuthal direction). This electromagnetic module will be coupled to plasma simulations (either fluid or PIC models) to obtain self-consistency of power density and radial number density profiles. A further development would be to include stochastic heating.

2.1.4.3. Simulation of electron trajectories

Numerical models have been developed and implemented to simulate trajectories of particles in the magnetic field of the negative ion source SPIDER. The aim of this work was to support the choice of the optimal magnetic configuration of the filter field. It was motivated by the lack of the proper computational tools and the necessity to develop suitable models. The assessment of the SPIDER filter field has been tackled with different levels of complexity.

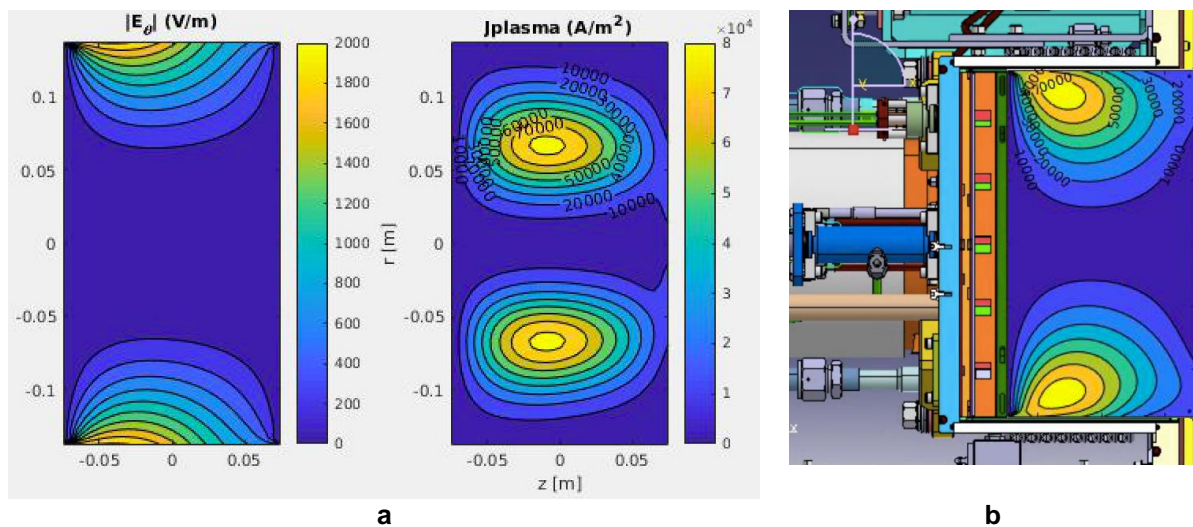


Fig. 2.41 Density of caesium excited levels.

The simplest approach was based on the analysis of the magnetic field lines and its connections to the different geometrical parts of the driver. Next, the guiding centre approximation (GCA) was applied to investigate the trajectories of the particles in the driver. However, the simulations showed that GCA is marginally applicable for electrons and completely not valid for ions.

In order to investigate the particle motion in the driver it was necessary to develop full particle trajectory code (FPT code), which follows the trajectories of particles considering their gyromotion.

From the simulations performed (an instance is shown in Fig. 2.42) it is was apparent that the magnetic configurations with majority of magnetic field lines in the horizontal direction (x-directions) are the best and among them the new so-called 3060 configuration. In that case the largest number of particles is trapped in the driver (46.3%) and the average length of the trajectories is the longest, meaning that electrons stay for a long time in the driver, contributing more to the ionization of the Hydrogen gas and consequently to the production of plasma. The new 4060 configurations are very close to 3060 in that respect.

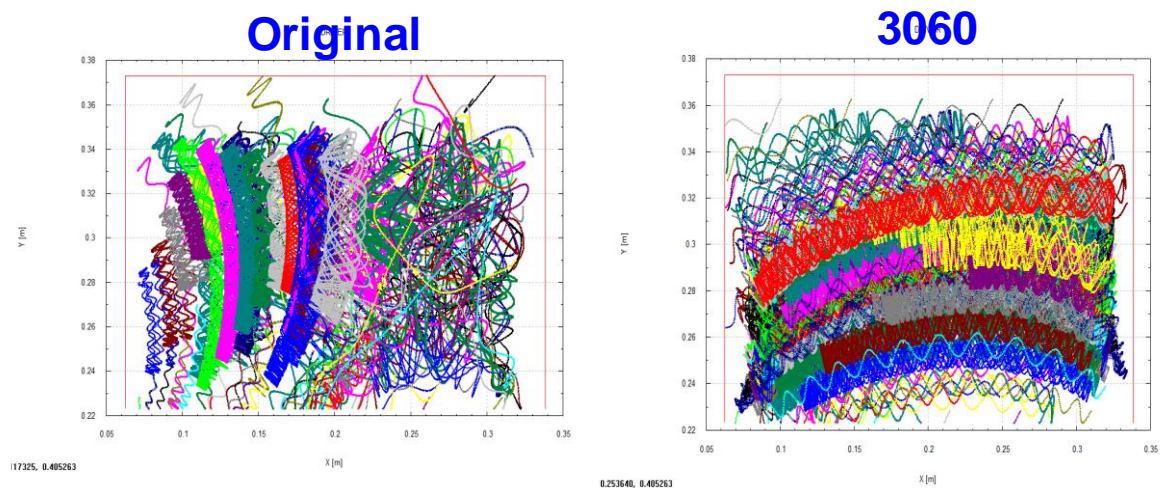


Fig. 2.42 Comparison of electron trajectories in the original (left) and in the new (right) configurations of the SPIDER magnetic filter field.

Further, the FPT code has been used to perform simulations of the electron trajectories in the real magnetic filter field configuration in SPIDER with the aim to reveal reasons for the different performance of the central and bottom drivers. Calculations have been done for the 3D magnetic field configuration for both drivers (central and bottom) assuming different plasma temperatures and potential profiles (model profiles and experimental profiles). Results of simulations indicate that the observed different behaviour of the drivers cannot be associated to the electron dynamics in the driver regions.

2.1.4.4. Simulation of plasma dynamics

During late 2019 and 2020, the plasma properties were measured along axial profiles in the SPIDER ion source. The availability of ion density, electronic temperature and plasma potential motivated a strong effort to bring the pre-existing GPIC code to maturity, and to apply it to the study of the plasma expansion region in SPIDER. A thorough set of collisional processes related to low-temperature electron collisions was implemented. It was possible to achieve a prompt convergence by exploiting a feedback control on neutral density that used the target density and electron temperature in the driver centre. The density gradients and the electron cooling through the filter-field were successfully simulated, in various conditions of background gas pressure and plasma properties inside the driver, as shown in Fig. 2.43. The reduced dimensionality of the PIC model (2D3V) did not affect much the result in the expansion region, as the self-consistent 2D electric fields in a plane perpendicular to the filter field grasp most peculiarities of perpendicular transport. Even though Coulomb collisions for electrons were not active in the simulation, the comparison to experimental data showed an excellent agreement confirming that in SPIDER-relevant conditions, electron cooling is mostly a result of collisions with neutrals.

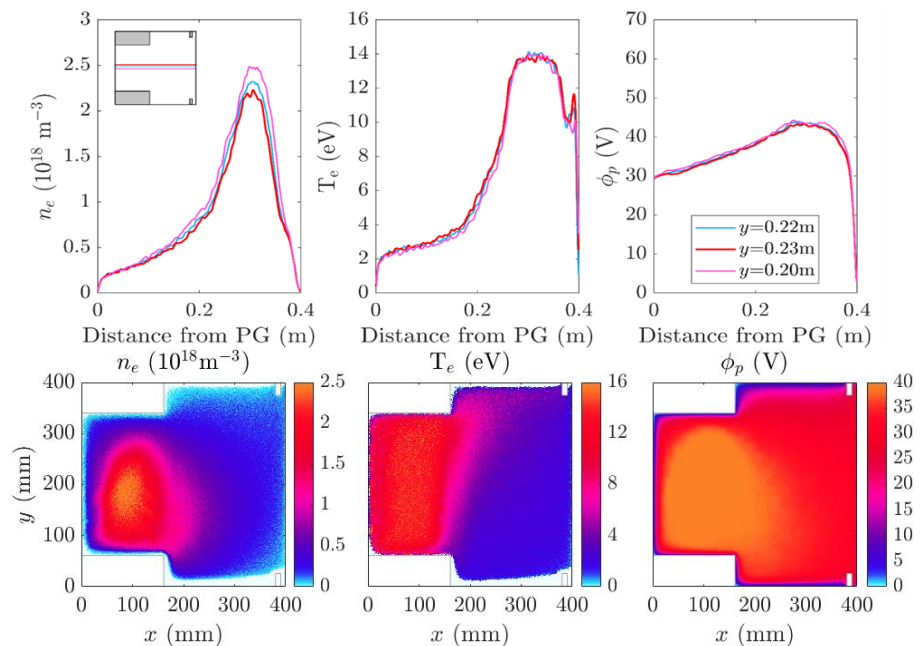


Fig. 2.43 Spatial profiles of plasma parameters.

During the development of this model, a simplified structure of confinement magnetic field was applied to the driver rear plate where cusp fields are installed, and none was applied to the Plasma Grid. In order to determine a proper boundary condition at these surfaces, the effect of cusp magnets was simulated in a dedicated sub-model, which allows to quantify the loss fraction and plasma exclusion zones; these are poorly quantified by analytical relations for a

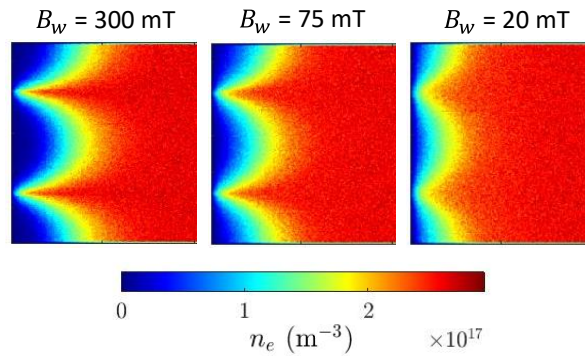


Fig. 2.44 Effect of cusp magnets on boundary plasma.

low induction field strength at the walls (as it is the case for SPIDER). An example of results is shown in Fig. 2.44. The results of this sub-model will provide a proper boundary condition to the large PIC model of the plasma expansion (described before in this same section). Future work will focus on the extraction region in front of the Plasma Grid, where the bias plate acts as a scraper for electrons.

In parallel, an activity has started to develop a 2D fluid model for the plasma in SPIDER. First, a numerical code, solving the general convection-diffusion equations in 2D, has been developed and tested. The numerical discretization is done on a staggered non-uniform mesh and is based on the 9-point stencil in order to properly approximate the strongly anisotropic plasma transport in the magnetic field. The convective terms are discretized using the Patankar method, including the possibility of using Central Difference, Upwind, Hybrid Power law and Exponential schemes. Different numerical solvers for the inversion of the resulting matrix of the system of linear equations have been developed and tested, among them: Modified Strongly Implicit (MSI) Procedure, Alternating-Direction Implicit (ADI) method, Generalized Minimal Residual method (GMRES) and Biconjugate Gradient Stabilized method (BiCGSTAB). It was found that the BiCGSTAB solver is the most stable and the fastest, at least for test cases considered so far. In the future the model will be developed with realistic boundary conditions and compared with the experimental measurements.

2.1.4.5. Cryogenic pump regeneration model

Partial regeneration of SPIDER cryogenic pumps was demonstrated during this year. The capability to prevent oxygen and nitrogen release during regeneration is an asset for next SPIDER operation with Caesium. Controlling thermal desorption of Hydrogenic species from charcoal-covered panels is a topic of research very important also in view of the operation of MITICA. The development of a model of thermal desorption based on equilibrium isotherms was started during the last year. The results based on a Temkin isotherm are shown in Fig. 2.45. The measured pressure, and the fractional coverage extrapolated from the

measurement, are shown in red for the partial regeneration of one single cryopump loaded with Deuterium; the results of the pressure calculated by the model, and instantaneous release of Deuterium for the measured temperatures are shown in green. The desorption energies used in the model, for the full monolayer and zero coverage, are in line with the few data available from the literature. This numerical investigation will continue to fill the gap with the experimental measurement, by the implementation of different types of isotherms, or of the diffusion through porous materials.

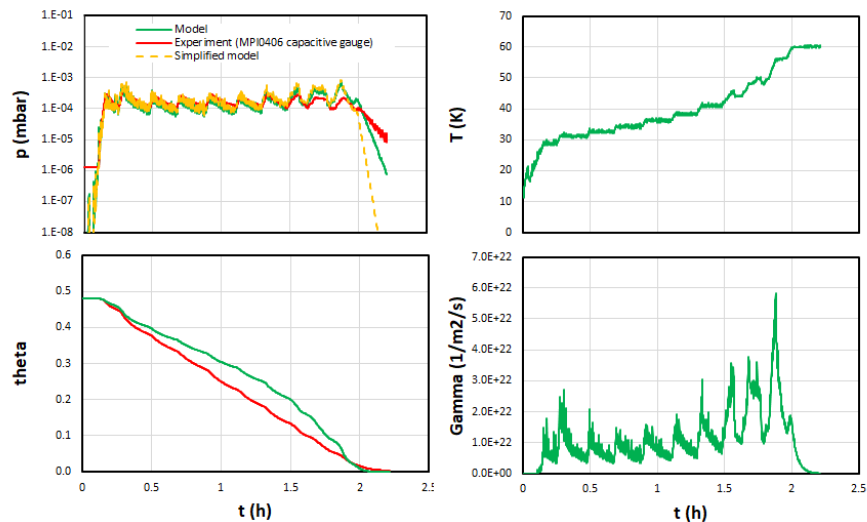


Fig. 2.45 Modelling controlled regeneration of SPIDER cryogenic pumps.

2.1.4.6. Code benchmarking & accelerator design validation (collaboration with QST)

A comprehensive benchmark of different numerical models used at Consorzio RFX for the extraction and acceleration of a H^- beam, has been carried out by comparison with measurements made on the MeV ion source Test Facility (MTF) at QST (Japan) in 2019.

MTF was operated at 500 kV as a three-stage multi-aperture accelerator. Experiments were conducted on MTF aiming at accelerating a H^- beam with high energy and good optics for a long duration of the beam (around 100s). These experiments allowed to measure the beamlet divergence and deflection as well as the heat loads due to particle impinging on the accelerator grids, over a wide range of operating parameters. The predictions of beam acceleration codes (Opera, COMSOL, SLACCAD, EAMCC3D) have been compared to the experimental measurements. In the calculations, the ion current density profile at the beamlet meniscus was assumed to be non-symmetric with respect to the beamlet axis, as indicated by recent studies that correlate the non-uniform extraction of negative ions to the strength of the applied transverse magnetic field. The good agreement between the measurements and the beam optics simulations has strengthened the credibility of this correlation. The heat loads on the

accelerator grids predicted by simulations are also compared to the heat loads measured by water calorimetry during experiments.

This comparison has allowed to obtain the following conclusions ¹³:

- The measured divergence on the reference MTF pulse was ~6.5 mrad and was consistent with the simulations of COMSOL and EAMCC3D within ± 1 mrad. Opera and SLACCAD also correctly evaluate the beamlet divergence and the optimum parameters that minimize it
- Opera correctly simulates the beam trajectory and its deflection at the accelerator exit when the current density profile asymmetry as the meniscus is included in the model. The assumption of a radially symmetric profile implies a strong underestimation of the beamlet deflection on COMSOL, EAMCC3D and Opera (with uniform meniscus).

Both EAMCC3D and COMSOL give a correct order of magnitude of the total power deposited on the grids, but underestimate the heat loads on the first two acceleration grids. The reason for this discrepancy might be the assumption that the nine beamlets carry the same optimal current density that minimizes the divergence and the underestimation of the beamlet deflection caused by the assumption of uniform current density at the meniscus.

2.1.5. ***Vacuum high voltage holding modeling and experiments***

2.1.5.1. ***Vacuum High Voltage modelling and preparation of MITICA HV holding tests***

The voltage holding capability of the ITER HNB and MITICA Beam Source insulation at 1 MV in vacuum is a very challenging issue, which could not be fully addressed so far on the basis of experimental results and of theoretical models available in literature.

In the final design of the Beam Source ¹⁴, the most critical gap appears to be the long gap between the -1MV surface of the Beam Source and the Vacuum Vessel. In this gap, which is of the order of 1 m, the “background” gas pressure is expected to be between 10^{-5} Pa (with no gas injection) and $2 \cdot 10^{-2}$ Pa, (when the Plasma Chamber pressure is ~ 0.3 Pa) with all the cryopumps operating at full pumping speed (4700 m³/s, see ¹⁵).

¹³ S. Denizeau, D. Aprile, P. Agostinetti, F. Veronese, T. Patton, A. Pimazzoni, J. Hiratsuka, M. Ichikawa, G. M. Saquilayan, A. Kojima, M. Kashiwagi, G. Chitarin, SOFT 2020

¹⁴ N. Pilan *et al.*, "Numerical–Experimental Benchmarking of a Probabilistic Code for Prediction of Voltage Holding in High Vacuum," in *IEEE Transactions on Plasma Science*, vol. 46, no. 5, pp. 1580-1586, (2018)

¹⁵ N.Pilan, P.Veltri and A. De Lorenzi, Voltage Holding Prediction in Multi Electrode-multi Voltage Systems Insulated in Vacuum, IEEE 18 (2011)

Tests carried out by QST in 2016 have shown that splitting a long gap by means of one or more intermediate electrostatic shields can greatly improve the voltage holding capability of the 1 MV insulation ¹⁶.

A sequence of HV insulation test campaigns has been planned in collaboration with QST (see Fig. 2.46) using mock-up electrodes reproducing in detail the geometry of the Beam Source and Accelerator. The last test campaign will be carried out inside the MITICA vessel in NBTF and will incorporate all the essential features both of the single-gap and of the multi-stage insulation, so as to obtain reliable data on voltage holding at 1 MV before the installation of the real components.

For this reason, a first experimental campaign using mock-up electrodes has been decided for evaluating the voltage holding behaviour of MITICA source with and without an intermediate electrostatic shield.

This approach is intended to reduce the risk related to the HV insulation at 1 MV and, if necessary, to allow to develop the most effective solutions. The tests will be performed in the MITICA Vessel (already available in the NBTF site) both in vacuum and in low-pressure gas.

The main objectives of the test campaign in NBTF are the following:

1. verify and improve the insulation of MITICA up to 1 MV in vacuum and low-pressure gas, before the installation of the real Beam Source
2. establish and validate Voltage Holding scaling laws for large gaps and multiple electrodes (required for effective design optimization)

In order to perform the campaign, several activities are required: the design and realization of the mock-up of the beam source and of a planar anode, including an adjustable support for modifying the gap length; the realization of a gas injection system for controlling the pressure inside the BSV; the preparation of the equipment for measuring voltage and currents, both

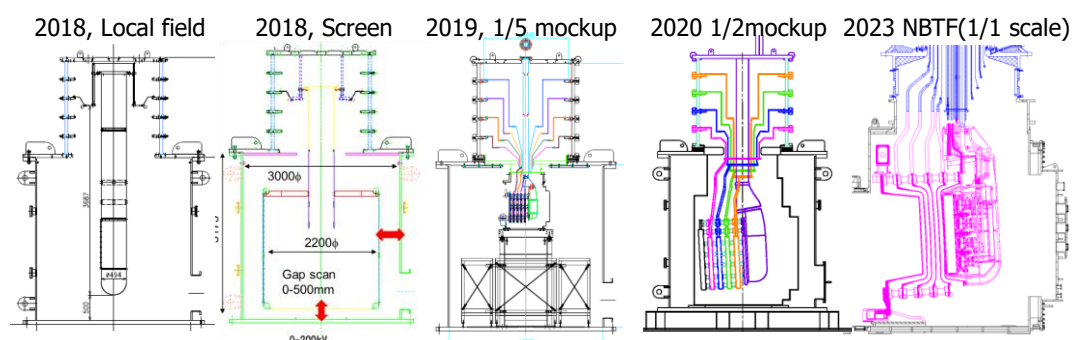


Fig. 2.46 sequence of HV insulation tests planned at QST and in NBTF for ITER HNB and MITICA Beam Source in vacuum

¹⁶ A. Kojima et al, Demonstration of 1 MV insulation for the vacuum insulated beam source in the ITER neutral beam system, Nucl. Fusion 59 086042 (2019)

steady-state and during breakdown, and the X-ray spectrum and for capturing images of the breakdown path.

The test requirements can be summarized as follows:

1. tests shall be carried out in a pressure in high vacuum ($5 \cdot 10^{-5}$ Pa) and in low-pressure gas ($5 \cdot 10^{-2}$ Pa)
2. applied voltage shall be up to 1 MV, number of Intermediate electrostatic shields shall be minimum
3. intermediate electrostatic shields shall have sufficient molecular gas conductance (single- or double-walls with staggered apertures are necessary)
4. damages caused by transient overvoltages on the HVB shall be avoided
5. tests shall be completed within the allowed time-window (BS delivery: ~ beginning 2022)
6. testing of alumina post insulators not necessary
7. a realistic geometry is necessary for all the electrodes (insulation around the grid support flanges has never been tested in vacuum, no verified model exists for such multi-electrode geometry)

The test setup will include the following electrodes:

- ME10: full size, detailed mock-up of electrode at -1 MV, compatible with standalone use, mechanically supported by HVB
- ME08, ME06, ME04, ME02, ME00: modular mock-ups of accelerator electrodes at 800, -600, -400, -200 and 0 kV, mechanically separated from ME10
- GP00: grounded platform to cover the bottom of BSV, supported from BSV

The mockup electrodes (ME02 – ME08) will include a flat grid (with no apertures) with flange and external guard shield, ME02-ME08 supported by a lightweight insulating structure fixed to the BSV.

The position of grounded platform (GP00) can be manually adjusted (useful during a first phase and for evaluating safety margin)

Main issues being addressed by this test strategy are the following:

- surface/size of electrodes and all details of the electrostatic configuration are significant with respect to real BS
- Staged approach to construction and tests
- gravity load on HVB is due to ME10 only (250 kg max ?)
- manufacturing/delivery time of solid insulators is reduced with respect to alumina post insulators
- intermediate electrostatic shields ES06 and ES02 can be added if necessary

However, some issues are still to be addressed:

- surge arresters: they are necessary to protect HVB ceramic rings against overvoltages >200 kV, spark-gaps located just below the HVB are probably the only viable solution (sealed spark-gaps could avoid dependence on BSV vacuum pressure and conditioning)
- intermediate shields with large number of apertures have never been tested and optimized (size and number, single/double wall, stagger and distance between walls). Double-walled shield have never been tested by QST: dedicated characterization experiments in HVPFT test stand are under consideration
- effect of pressure increase due to gas flow across intermediate shields (having non-negligible gas conductance) cannot be tested directly, since controlled gas injection from HV side is practically impossible using mock-up electrodes
- vacuum pump-down time of BSV+BLV is ~ 250 h to reach $5 \cdot 10^{-5}$ Pa according to recent estimations with additional turbomolecular pumping capacity of $10 \text{ m}^3/\text{s}$
- assembly procedures and methods for diagnosis of breakdown location in the presence of intermediate shields need to be investigated

The campaign will be carried out in stages according to this sequence (see Fig. 2.47):

- test ME10, initially with small gap length (grounded platform GP00 in high position)
- repeat tests with Increased gap length (lower GP0 position)
- install ME00 and repeat tests
- install ME02, ME04, ME06, ME08 and repeat tests
- if necessary, install ES06 and repeat tests, if voltage holding is sufficient, stop tests.
- if necessary, install ES02 and repeat tests

Activities regarding the design of the first configurations to be tested have already started, together with the identification of the additional pumping system and its integration with the MITICA vessel, the electrical sensors and the required cameras of various types needed to monitor the experiments, and the specific control system to manage the testing campaign.

In Fig. 2.48 and Fig. 2.49 the status of the design can be seen: extensive numerical simulations are being carried out to verify the electrical and the structural behaviour, together with the integration with the HV bushing procured by JADA, onto which the ME10 will be hanging on.

Two Cryopumps Coolvac 10000 will be procured and will be connected to the ports targeted for the feedthrough of the reference MITICA cryopanel, via a dedicated adapter under design.

5 cameras have been identified as relevant for the tests and are under detailed assessment for procurement:

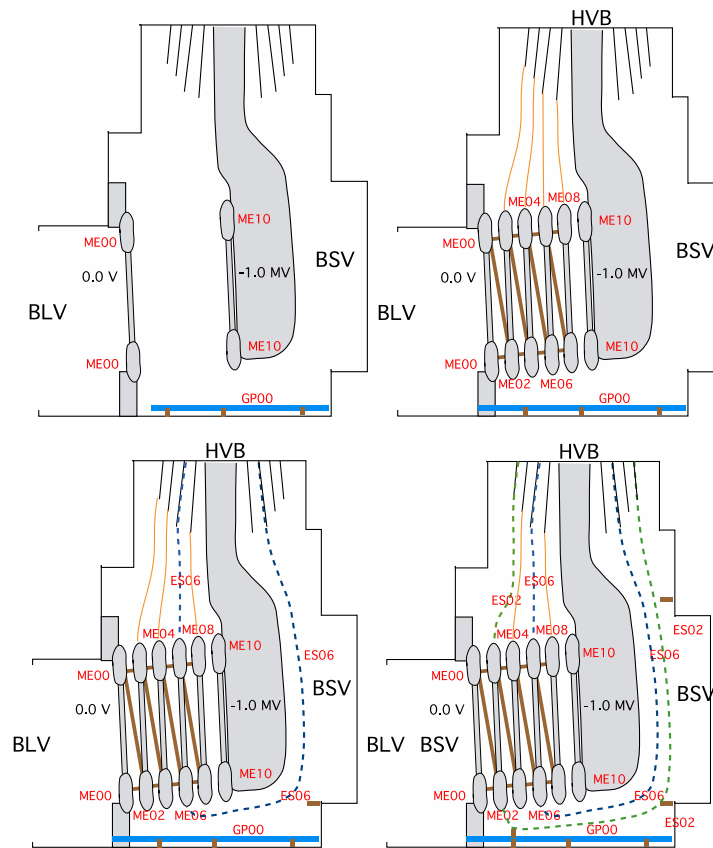


Fig. 2.47 Sketch of the experimental sequence for the HV tests in the MITICA vessel, showing the Mock-up Electrodes (ME10, ME00), the grounded platform (GP00), the electrodes of the electrostatic accelerator (ME02, ME04, ME06, ME08) the intermediate electrostatic shields ES06 and ES02.

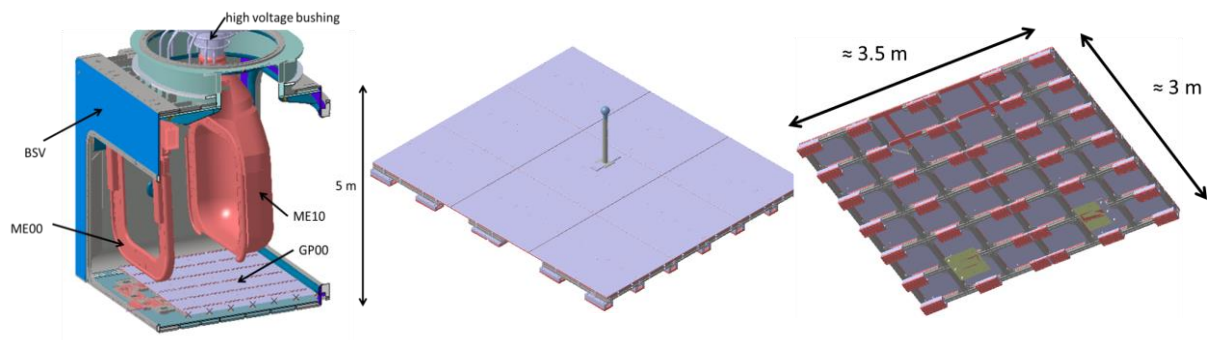


Fig. 2.48 Overall status of the design for GP00, ME10 and ME00 electrodes.

- 2 cameras on visible range
- 1 high frequency camera
- 1 infrared camera (to be confirmed)
- 1 safety cam

A potential issue regarding viewport glasses breakout has been identified and is being investigated, in order to minimize the corresponding risks.

Conductive glasses are a possible mitigation action

Also mirrors, in order to reach not directly visible areas, are under investigation

2.1.5.2. HVPTF and HVSGTF experiments

NBTF Team has two facilities at its disposal for the study of high voltage withstand phenomena in vacuum (HVPTF) and for the study of the formation of discharges in vacuum (HVSGTF). Below are the main results obtained during the experimental campaigns carried out during 2020.

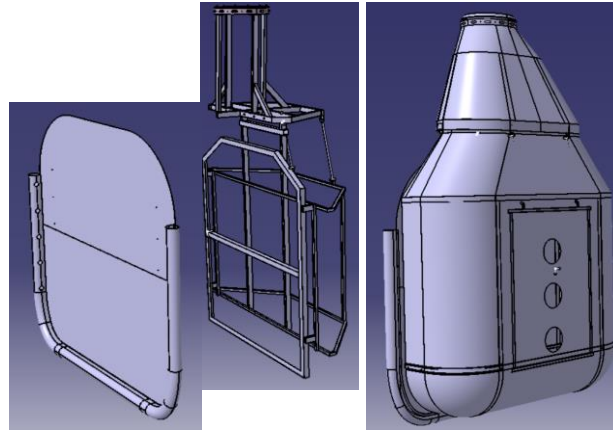


Fig. 2.49 Details of the design for ME10 and ME00 electrodes.

HVPTF experiment activity and main results:

Two Saes Getter Non-Evaporable Getter (NEG) modules HV800 were installed and tested by applying HV voltage to a sphere plane configuration with a gap length of 33 mm. The test was carried out upon pumping the vacuum chamber by NEG modules and by the 1000 l/s turbopump usually adopted at the HVPTF, see Fig. 2.51.

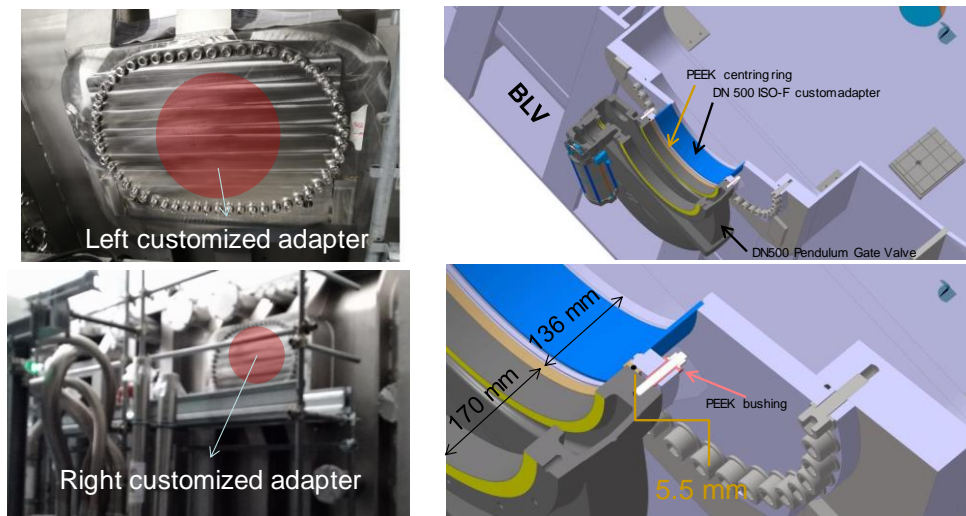


Fig. 2.50 Integration of additional pumping system

The test was carried out in high vacuum at a pressure of 10^{-8} mbar, lower than the typical pressure (10^{-7} mbar) of HVPTF. The additional pumping modules have reduced the deconditioning effect, which occurs during the nights, when the high voltage is not applied, nonetheless no appreciable improvement of the voltage holding in high vacuum was observed.

A needle-plane configuration was implemented to enhance the electron emission from the

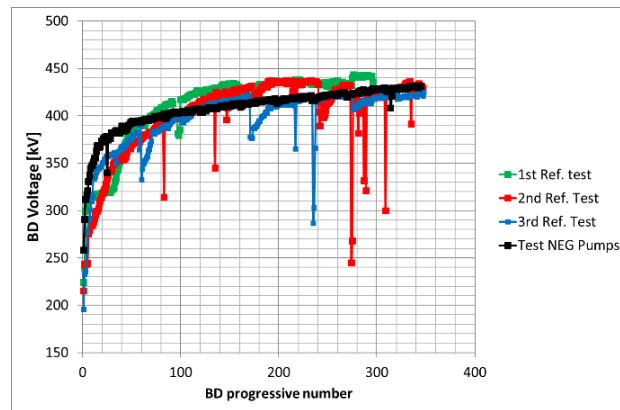


Fig. 2.51 Comparison of conditioning histories, coloured plots (RGB) refer to reference cases, black plot refers to the case with NEG pumps

cathode, the test was carried out to calibrate the Time-Correlated Single Photon Counting system routinely adopted at the HVPTF, see Fig. 2.52. The test allowed to measure the X-ray spectrum generated by a mono-energetic electron beam impinging on the anode.

A simple analytical model based on the Kramer equation from the bremsstrahlung radiation has been benchmarked with experimental results. The model estimates the electron current exchanged between electrodes from the X-ray detector located outside the HVPTF vacuum chamber.

A conceptual design of a multi pixel collimator to resolve the spatial distribution of the X-ray emission has been completed, see Fig. 2.53. The hypothesis of the mutual exchange of



Fig. 2.52 Infra-Red picture of the Needle-plane test. Electron backscattering can cause more than one hot spot on the anodic surface

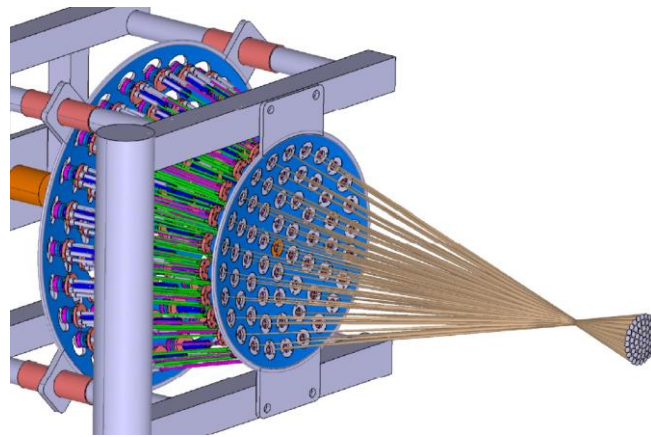


Fig. 2.53 Multi pixel collimator to reconstruct the spatial and temporal emission of X-rays due to bremsstrahlung radiation from anodic surfaces

charged particles and the existence of (micro) discharge attractors has been confirmed by specific high voltage tests by using concave electrodes with large bore diameter, see Fig. 2.54 and Fig. 2.55.

A Phantom V2012 fast camera has been successfully tested at the HVPTF: both the dynamic of micro discharges and the effect of the breakdowns have been observed.

Despite the onset of dark currents ($< 1\mu\text{A}$), micro discharges (20-500 μA) and eventually breakdown ($> 1\text{A}$) determine the hold-off voltage of a system insulated by large vacuum gaps, the HV tests with concave electrodes clarified that the position of micro discharges (toward the accumulation points) can be different from the position of breakdown.

HVSGTF experiment activity and main results:



Fig. 2.54 Picture of the concave electrodes taken during the assembly (left). Hot spot on the centre of the concave anode during the HV conditioning (right) in presence of microdischarges

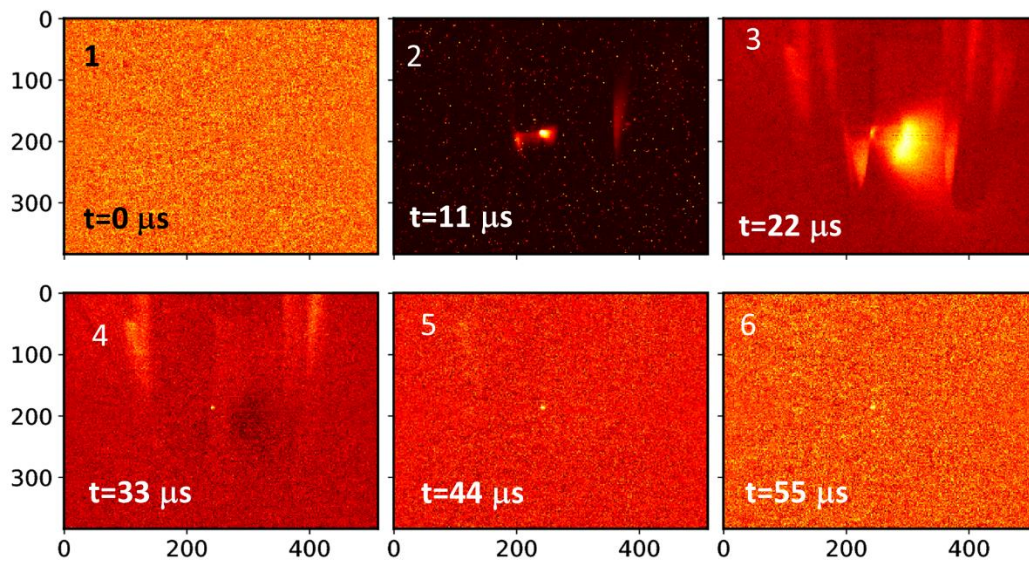


Fig. 2.55 Consecutive pictures of the concave electrodes during a breakdown. Cathode on the left and anode on the right

At the HVSGTF high voltage tests were carried out to verify the time evolution of the measured current at constant voltage. The tests were done considering gap lengths of 0.5, 1 mm. A sensible reduction of the measured current was observed after some hours of operations.

A preliminary test with a Gas Electron Multiplier (GEM) was carried out to reconstruct the spatial distribution of the X-rays produced during the HV conditioning of the largest gap.

At the HVSGTF further experimental campaigns were carried out to study the Voltage-Current characteristics for vacuum gaps of: 0.5, 1, 2, 3, 4, 5 mm measuring currents from few to 100 microA. The general behaviour observed in 2019 was confirmed: a progressive reduction of cathodic electric fields E_c at constant current I occurs when applying progressively high voltage cycles. A clockwise hysteresis in the plane $E_c - I$ has been observed during the execution of the HV tests, see Fig. 2.56.

A silicon detector and a special beryllium window, with very low filtering effect, has been used to study the distribution of the soft x-ray emitted during the HV conditioning, it has been possible to appreciate the characteristic emission of iron, nickel and chromium of the stainless steel anode.

SEM –EDAX analyses of electrode surfaces, before and after HV conditioning, were carried out on electrodes separated by a vacuum gap of 1mm, see Fig. 2.57.

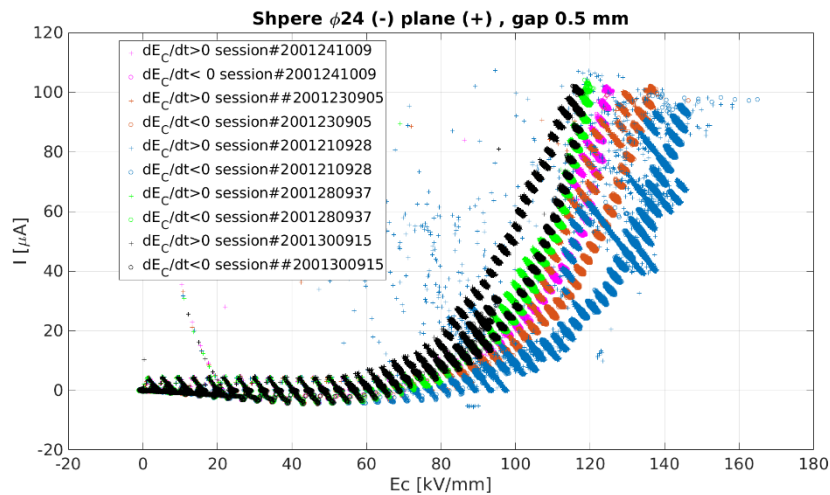


Fig. 2.56 Current vs. Electric field at cathode in consecutive sessions at HVSGTF

The analysis reveals the presence of micro particles detached from anode and impinging the cathode, this material could justify the enhanced current emission generally observed during the first HV conditioning.

Fig. 2.56 and Fig. 2.57 show that, during subsequent measurements, the electric current gradually increases and the cathode surface deteriorates. So, we can assume a gradual increase of the cathode emission surface. Hence, the comparison of experimental data with the BIRD model has to take into account this “free” parameter. However, to better compare experiment to theory, it is better to deal with a constant emission surface. This can be achieved in a low-current, low-voltage regime.

2.1.5.3. HV holding modelling

Regarding the BIRD Model, the need to have a good electrical voltage-holding in high vacuum requires a clear knowledge of the processes involved in Electric Field Emission. The

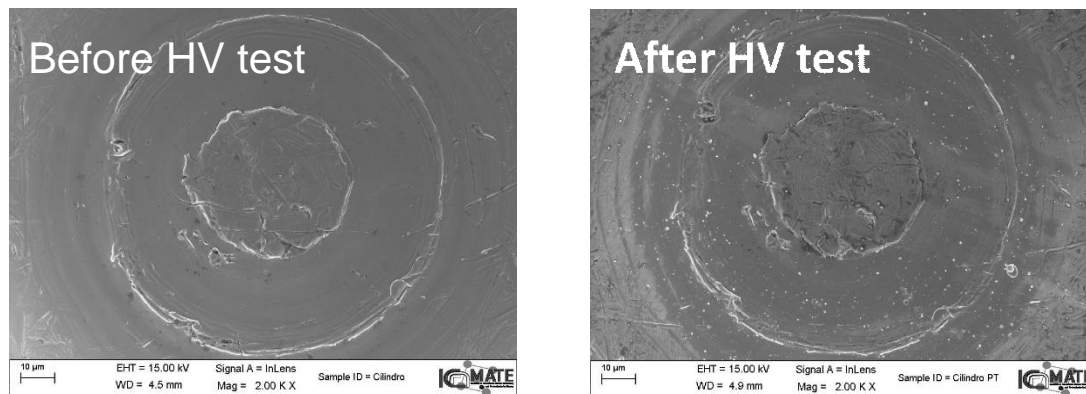


Fig. 2.57 SEM images of cathode, before and after the execution of the HV test at the HVSGTF

mechanism studied and proposed by Fowler and Nordheim (FN), that takes into account a quantum tunneling of electrons out of a pure metal, suffers from two main issues. Firstly, the forecast current is extremely small, too small compared to experimental data. Secondly, the fact that metal surfaces are usually covered with a thin layer of oxide, or at least dotted with foreign substances, is ignored.

The BIRD model embraces the idea that the electrode surface is made up of an ideal dielectric layer. In this case no electrons can cross the layer and the emitted current is given by the extraction of the outermost polarization electrons. In this process the electric field in the dielectric layer gradually increases up to the dielectric strength value, where a rupture of the layer happens. The current density of the BIRD model, as a function of the electric field E : $J_B = k_1 E^2 e^{-\frac{k_2}{E}}$, resembles that of the FN model, except for the value of the two constants k_1 and k_2 . The new constants predict higher electric currents, more in line with the experimental values.

The model has been previously developed¹⁷ on a semi-classical ground, starting from a classical point of view and then imposing at the end of the calculation the quantum uncertainty relations. A more solid approach has then been attempted, by solving the Schrödinger equation for an electron trapped in a polarization structure. Using then the decay coefficient predicted by Gamow in his pioneering work on α – particle decay, the same law of the semi-classical approach has been found. However, some doubts emerged about the validity of Gamow's law and therefore the problem cannot yet be considered solved.

The application of the BIRD model to the experimental data reveals that the emitted current is amplified by a factor $A(V)$ that depends only on the voltage between the electrodes: $I = A(V)S J_B(E)$ (here S is the emission surface) and that a good fit for this amplification factor is $A(V) = 1 + k_0 e^{-\frac{k_3}{V}}$. More in-depth investigation will have to be done to better understand the origin of this factor.

2.2. ITER NBI Physics activities and accompanying program

2.2.1. Introduction

Aimed to contribute to the NBI for DEMO, to support the NBI R&D at the NBTF and to train the personnel, complementary research activities have been carried out during 2020. These activities were mainly devoted to the operation of the NIO1 negative ion source within the

17 E. Spada, A. De Lorenzi, N. Pilan and V. Antoni, "Theoretical Basis and Experimental Validation of the Breakdown Induced by Rupture of Dielectric Layer Model," in IEEE Transactions on Plasma Science, vol. 47, no. 5, pp. 2759-2764, May 2019

EUROfusion program. Beside these activities, two other minor activities continued on a voluntary basis in collaboration with Pisa and Bari University (see 2.2.5).

2.2.2. *NIO1 Experiment*

The EUROfusion activities on the NIO1 experiment were focused on two main topics:

- operation, characterization and optimization of the negative ion source with Cs evaporation
- Studies and conceptual design on plasma neutralizer experiments in NIO1.

Such activities are described in detail in a dedicated report.¹⁸

2.2.2.1. *Source operation with Cs evaporation*

The Cs oven for NIO1 was filled, installed in the source and integrated in the NIO1 control system by February 2020. During several days of operation with active oven heating, however, Cs was not detected in the source by Laser Absorption Spectroscopy (LAS) nor by Optical Emission Spectroscopy (OES). An inspection of the oven reservoir revealed that the Cs got totally oxidized, probably during the previous shutdown.

The COVID lockdown blocked maintenance activities until June, when it was possible to substitute the oven valve, remanufacture a new reservoir without Ar vent line for better temperature uniformity control, procure new Cs, refill the oven and reinstall it in NIO1. The subsequent source operation in July had to face several issues related to the pumping system and to a contamination of the gas injection line. Both the systems were fixed and upgraded, in particular a compact rotary pump was installed to keep the final, most delicate segment of the gas injection line in vacuum when the source is not in operation.

Cs was finally detected in the source by the OES diagnostic on 2/09/2020. This event was facilitated by the oven heating system that was accidentally left active during the previous night; having left the oven duct at 170° helped the Cs vapours to drift along the duct to reach the source. The introduction of Cs in the source gave visible effects in beam extraction. Fig. 2.58 shows the time trends of the Extraction Grid Power Supply (EGPS) current (in first approximation, co-extracted electron current) and AGPS current (i.e. extracted beam current); extraction and total acceleration voltages were 700 V and 6000 V, respectively. It can be observed that the immediate effects of Cs deposition mainly led to a reduction of the co-extracted electron current, rather than to an increase of the extracted beam current.

¹⁸ M. Barbisan, R.S. Delogu, A. Pimazzoni et al., Report on the activities on the plasma neutralizer design using NIO1 and the NIO1 experiment with negative ions produced by surface interaction with Cs – 2020, final report on deliverable HCD-3.2.01-T030-D001, IDM document EFDA_D_2P4P8E.

In the following day, by operating the source with 1600 W RF power, 0.75 Pa pressure, and 240° C reservoir temperature (cold spot at 180°C) it was possible to reach the best beam performances of the campaign: an extracted current density of 67 A/m² and a co-extracted electron current below 1 (with the caveat that the cryopumps were not active, so that part of the current may be due to secondary electrons).

During this and the following operation days it was possible to characterize the behavior of source and acceleration system as function of their control parameters. An example is given in Fig. 2.59, showing co-extracted electron current (a), extracted beam current (b) and fraction of co-extracted electrons (c) in two total acceleration voltage scans, performed with two different values of oven reservoir temperature. The higher evaporation of Cs results in a lower fraction of co-extracted electrons.

A progressive reduction of source and beam performances however occurred after 3/9/2020, accompanied by a steady reduction of plasma luminosity. This was interpreted as a consequence of excessive Cs evaporation, poisoning the plasma. Several attempts were made to clean the source using the Hydrogen plasma action, with source bias voltages and extraction/acceleration voltages turned off to facilitate Cs⁺ flux towards the diagnostic chamber, but with no visible result. A last attempt was made on 23/09/2020 by producing an Ar plasma in the source for one operation day, but again with no effects.

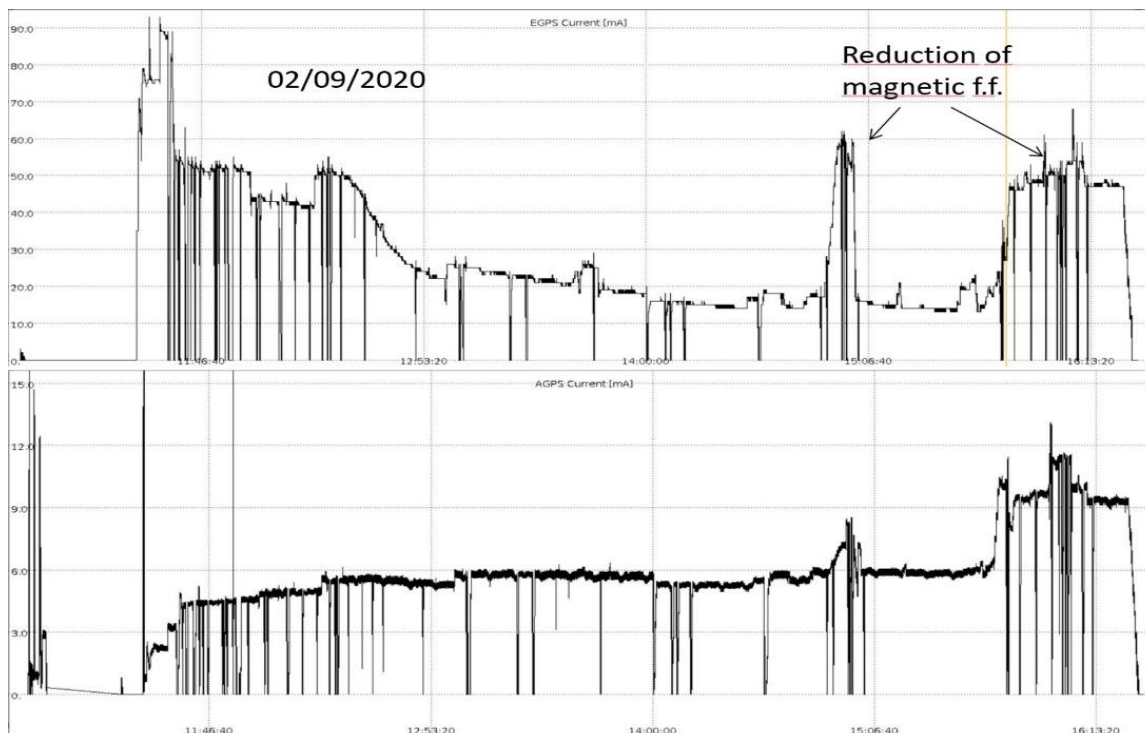


Fig. 2.58 Time trends of EGPS and AGPS currents on 2nd September 2020.

At the beginning of the experimental campaign the LAS diagnostic,¹⁹ which measures the neutral Cs density in proximity of the Plasma Grid, was active but not operational; it was indeed not possible to find the Cs 852 nm absorption line by tuning the laser wavelength. The issue was understood on 14/09/2020: the laser was not compliant with the requested specifications and with the individual tests provided by the manufacturer; this was temporarily solved by using another similar laser available at Consorzio RFX for the SPIDER experiment. The data provided from the LAS diagnostic indicated that the Cs density inside the source, even with the Cs oven turned off, was in the order of 10^{16} m^{-3} , i.e. one order of magnitude larger than what measured in other caesiated negative ion sources.²⁰ This confirmed the over *Caesiation* of the source. The LAS diagnostic also allowed to estimate the ionization degree of Cs in the source (about 60-70%) and the dependence of Cs density on the source walls temperature. An example is given in Fig. 2.60, showing the time evolution of Cs density together with the fluctuations in the cooling water temperature, as measured by the thermocouples at the return sides of the PG-BP and source rear cooling sub circuits.

After the end of the experimental campaign the Cs oven and the source were uninstalled and inspected. In the oven, the Cs in the reservoir was found to be perfectly preserved; no evident

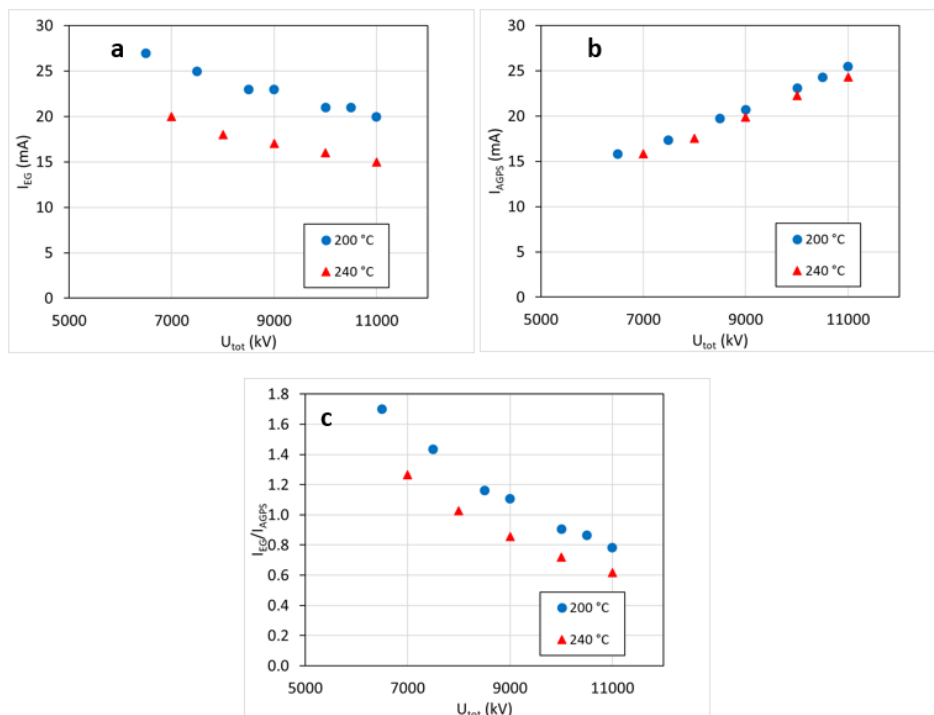


Fig. 2.59 EGPS current (a), extracted beam current AGPS (b) and their ratio (plot c) in a total acceleration voltage scan, with 1.2 kV extraction voltage. RF power was 1600 W, source pressure was 0.75 Pa, SBPS 20 V (source bias), BBPS (bias plate bias) 0.3 A, PG filter current 10 A.

¹⁹ U. Fantz et al., AIP Conf. Proc. 1390, 348 (2011).

²⁰ U. Fantz, C. Wimmer, J. Phys. D: Appl. Phys. 44 (2011) 335202.

deposition of Cs in parts of the oven different from the reservoir were found. The inspection of the source showed a clear deposition of Cs on the PG, on the BP, on the Mo protection foils, on the Pyrex cylinder. The Cs was even able to reach the rear sides of the Mo foils, that are expected to be inaccessible because in close contact with the Cu body of the source; the Caesium was also able to reach the windows at the sides of the Plasma Grid and at the rear of the source. All the source components were finally cleaned in the CATS test bed of the Neutral Beam test Facility, dedicated to Cs handling.

In future, the pumping system will be renewed to improve the reliability of the system with Cs evaporation and the availability of the cryopump system to keep the production of secondary electrons in the acceleration system as low as possible. The cooling system will be also upgraded including a heater to raise the Plasma Grid and source body temperature, besides improving their time stability.

2.2.2.2. Modeling of a plasma neutralizer for NIO1

The basic concept of a plasma neutralizer is to exploit the fact that collisions of H^- ions with H^+ are more efficient than collisions with the H_2 background gas in neutralizing the H^- beam. As the beam propagates in the beamline, a certain fraction of H^- is neutralized into H_0 and a part of the latter is ionized again into H^+ . To maximize the neutral fraction of the beam, the so-called target thickness, i.e. the line integral of the gas density along the beam path, has to be optimized. Reference calculation about the beam composition as a function of a target thickness for the NIO1 nominal beam energy of 60 keV beam are reported in Fig. 2.62a, while Fig. 2.62b gives the dependence of the neutralization efficiency on the ionization degree of

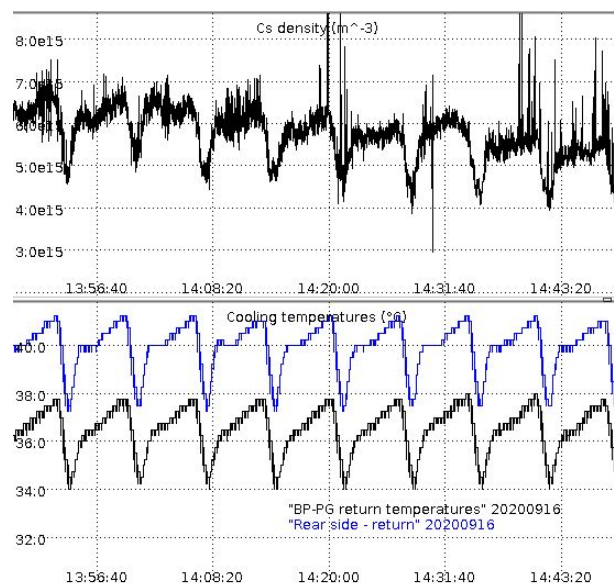


Fig. 2.60 Top: limited interval of Cs density measurements (LAS) as function of time during 16/09/2020. Bottom: Cooling water temperatures, as measured by thermocouples at the exit of the BP-PG and rear multipole circuits.

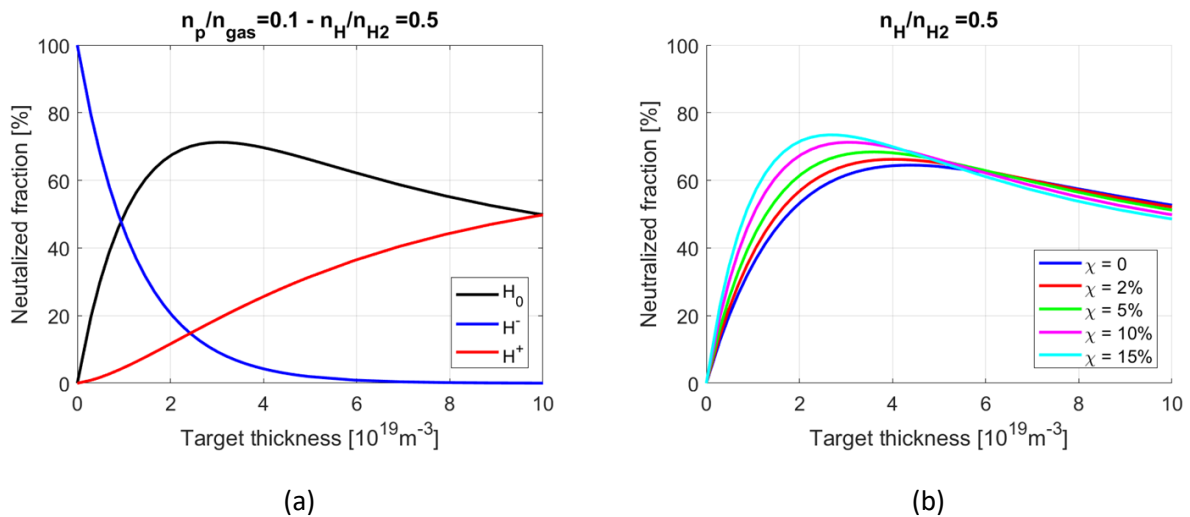


Fig. 2.62 Beam composition as a function of the target thickness for a plasma with an ionization degree $\chi = n_{\text{plasma}} / (n_{\text{plasma}} + n_{\text{gas}})$ equal to 9% and $n_H/n_{H_2} = 0.5$. (b) Fraction of neutrals as a function of the target thickness for different ionization degrees assuming $n_H/n_{H_2} = 0.5$. Beam energy is set to 60 keV.

the plasma. It is worth noticing that an ionization degree of 15% should guarantee an improvement of the maximum neutralization efficiency of about 10%.

As demonstrated elsewhere²¹, a self-induced plasma neutralizer in NIO1 would be very inefficient, as the ionization degree would hardly exceed 0.5%. Starting from models available in literature²² a conceptual design was carried out for a plasma neutralizer in NIO1, assuming to use biased filaments as external plasma source and a Halbach geometry array of permanent magnets to confine the plasma, as shown in Fig. 2.61. A neutralizer length $L = 1.2$

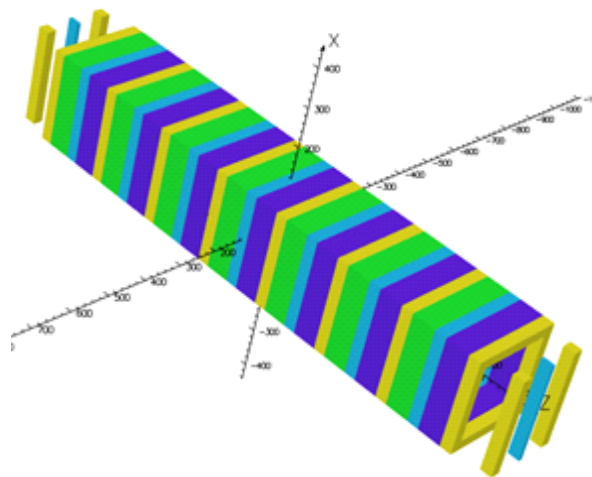


Fig. 2.61 . Confinement by permanent magnets arranged in a Halbach array layout (different colors represent different magnetization). Magnets arrangement in OPERA 3D model, $L_1 = 30$ mm, $L_2 = 60$ mm.

²¹ E. Sartori et al. AIP Conf.Proc. 1869, 050002 (2017); <https://doi.org/10.1063/1.4995783>

²² I. Turner, A.J.T Holmes, Fus. Eng. Des. 149 (2019) 111327

m was considered with an average gas density of $2.25 \cdot 10^{19} \text{m}^{-3}$. The width and height of the plasma column was set to 170 mm assuming to place the magnets at 90 mm from the beam axis.

The role of recombination was added to the model by considering all of the reactions reported in Table 2.1.

Table 2.1 List of reactions which are considered in the model.

1. $\text{H} + \text{e} \rightarrow \text{H}^+ + 2\text{e}$	H ionization by electron
2. $\text{H}_2 + \text{e} \rightarrow 2\text{H} + \text{e}$	H_2 dissociation by electron
3. $\text{H}_2 + \text{e} \rightarrow \text{H}_2^+ + 2\text{e}$	H_2 ionization by electron
4. $\text{H}_2^+ + \text{e} \rightarrow 2\text{H}$	H_2^+ recombination
5. $\text{H}_2^+ + \text{e} \rightarrow \text{H}^+ + \text{H} + 2\text{e}$	H_2^+ dissociation by electron
6. $\text{H}_2^+ + \text{H}_2 \rightarrow \text{H}_3^+ + \text{H}$	H_3^+ formation
7. $\text{H}_3^+ + \text{e} \rightarrow \text{H}^+ + \text{H}_2 + \text{e}$	H_3^+ dissociation by electron
8. $\text{H}_3^+ + \text{e} \rightarrow \text{H}_2 + \text{H}$	H_3^+ recombination
9. $\text{H} + \text{e} \rightarrow \text{H}(2\text{s}, 2\text{p}) + \text{e}$	H electronic excitation by electron
10. $\text{H}_2 + \text{e} \rightarrow \text{H}_2(\text{B}, \text{C}, \text{D}) + \text{e}$	H_2 excitation by electron
11. $\text{H}_2 + \text{e} \rightarrow \text{H}_2(v=1) + \text{e}$	H_2 vibrational excitation by electron

This improvement showed that recombination can strongly limit the achievable plasma density (see Fig. 2.63a): this warning is even more relevant in the case of DEMO. The scaling of the densities of different ion species with the filament current is shown in Fig. 2.63b.

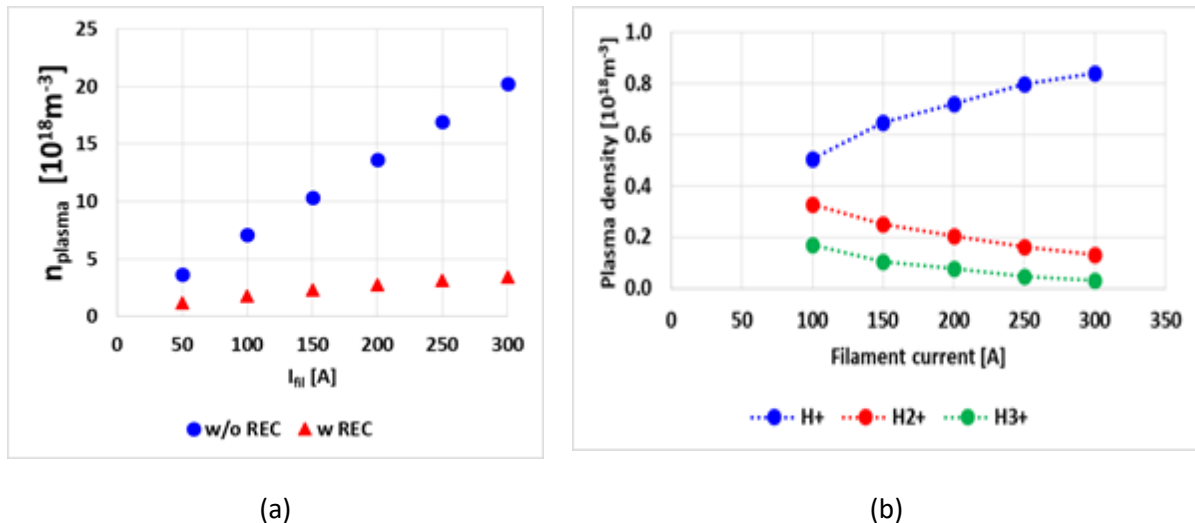


Fig. 2.63 (a) Comparison between the case with and without recombination. (b) Density of different positive ion species considering recombination and assuming $T_{\text{H}^+} = 0.5 \text{ eV}$, $T_{\text{H}_2^+} = 0.35 \text{ eV}$, $T_{\text{H}_3^+} = 0.29 \text{ eV}$, $T_{\text{H}} = 0.25 \text{ eV}$, $T_{\text{H}_2} = 0.18 \text{ eV}$. Filament bias set to $V_{\text{bias}} = 70 \text{ V}$.

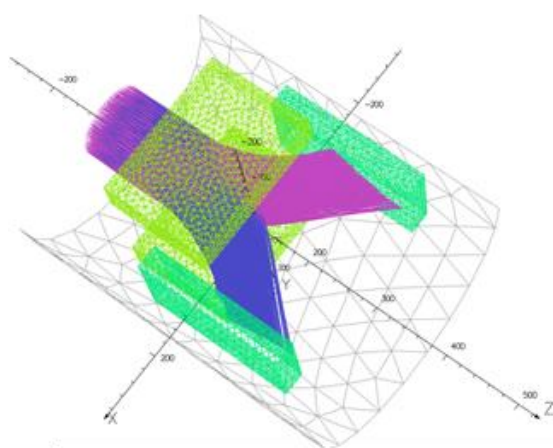
A conceptual design for a residual ion dump was performed and a Monte-Carlo particle tracing code was developed to assess the beam transmission through the neutralizer showing that the beam should be almost fully transmitted.

The only relevant losses were found in the RID, as shown in Fig. 2.64. These losses should be reduced to zero by means of a ferromagnetic cage.

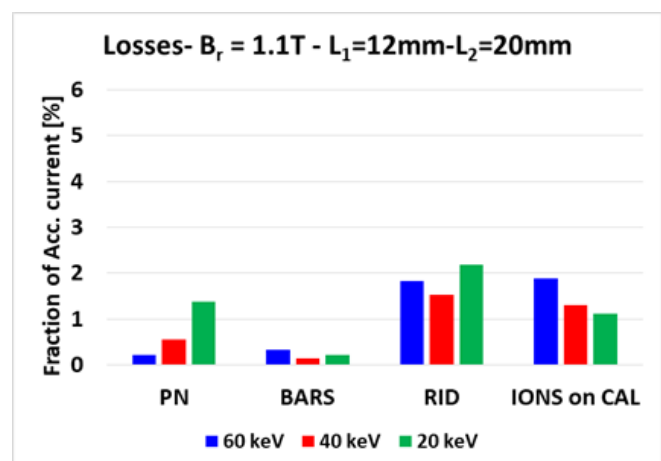
The developed models would be further developed and used extensively to carry on a more detailed design of a plasma neutralizer for NIO1.

2.2.3. *NBI Complex system and controllability*

In previous works modern concepts of network theory have already been successfully applied to NBI networks^{23 24}, that is, to the physical processes affecting generation, extraction and acceleration of negative ions. In particular the simple case of the negative ion source NIO1 has been investigated. The same technique has been applied to CO₂ dissociation reaction networks to examine the possibility of controlling CO₂ dissociation by controlling a subset of the involved chemical species. Chemical reaction networks can be seen as graphs where reactants and products are considered as nodes of the network. Driver nodes of a reaction are thus those species whose role in the reaction is particularly relevant. CO₂ dissociation reaction networks²⁵ have been described as graphs and their driver nodes found, that is, the minimum number of chemical species required to drive the whole process. Full and reduced²⁶ systems can be identified, and different network models are derived from them. Controllability analysis of the network models shows the pivotal role played by some species in the full network that are not present in reduced networks.



(a)



(b)

Fig. 2.64 (a) Schematic of the residual ion dump. Two SmCo magnets (1.1T remanence, 170x140x50 mm³) and two graphite plates (170x120x30 mm³). (b) Calculated beam losses for different beam energies (PN: plasma neutralizers, BARS: entrance and exit magnets, CAL: calorimeter).

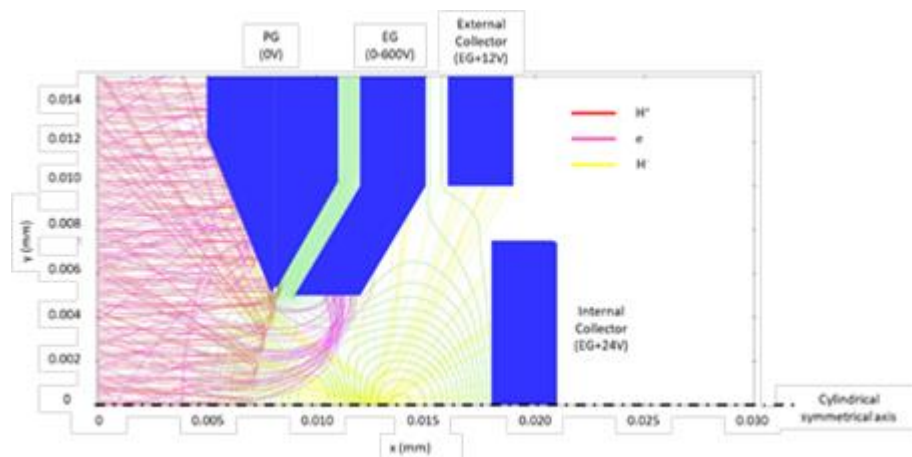


Fig. 2.65 IBSimu simulation for Hydrogen plasma with the new extraction configuration. The new item is the extraction grid EG which can be biased up to 600V. The magnetic field imposed is 15mT (the real magnetic field reaches a peak of 30mT near the inner collector).

Examination of all driver node sets shows that in the full system three driver node clusters are present that are not in the reduced system: CO exited states, O2 exited states, O4 ions. In particular, O4 is involved in relevant O2-producing reactions with high rate. O4 reactions are therefore reintroduced in the reduced network so that the total number of species is increased to 12 (including O4 reactions also requires the inclusion of O3 and O3-). The controllability analysis of the reduced system plus the O4 ions shows that the system is controllable with two nodes (instead of one). Notably, the driver node spectrum is different with respect to the spectrum of the original reduced network, and now includes O3.

Comparison of reduced model with a full model indicated that only 71% of the relationship between species is accounted by the reduced one, so that the controllability is expected to be different from that of a full model. The reduced model upgraded by adding the reactions involving O4 ions compared with the full one shows that the rate of overlapping rises to 92%. The results confirm the key role played by O4 ions in the process of CO₂ dissociation and seems to indicate that even a reduced model can in principle offer a controllability compared to a full set of reactions provided those involving the above mentioned species are included.

2.2.4. *Alternative ion Sources*

An additional electrode has been designed and manufactured to improve the extraction mechanism in ATHENIS facility. The aim is to avoid the plasma expansion in the beam region and to collect most of the electrons on the additional plate instead of the final collection probe. This time, IBSimu has been used as software to predict the behavior of the new configuration. Fig. 2.65 shows the new extraction grid configuration. The improved electric field generates a correct meniscus in order to shield the plasma from the plasma region. The red lines, which represent the positive Hydrogen ions of the plasma, are well repelled from the

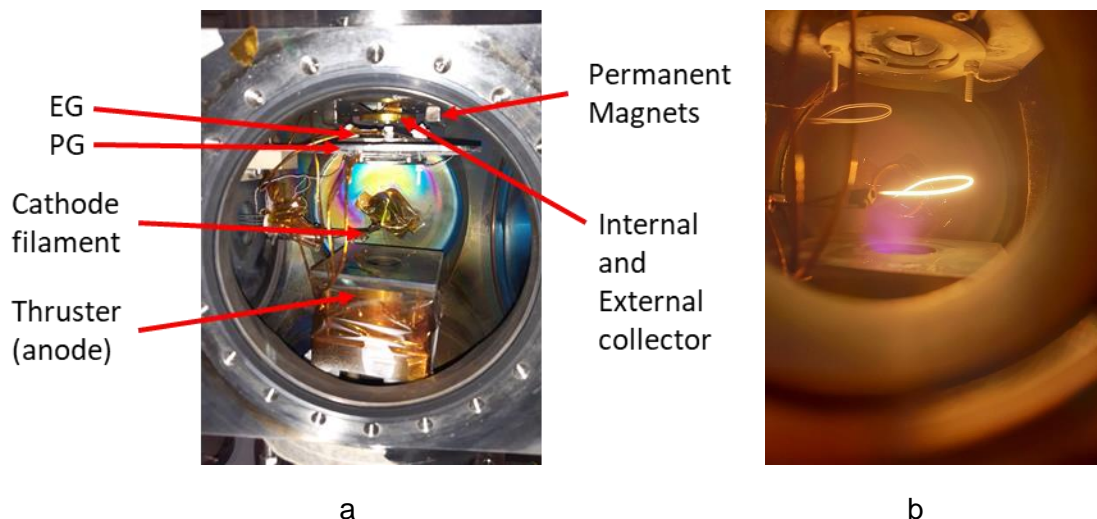


Fig. 2.66 ATHENIS layout. a) Assembling. b) Operation with N2

Plasma Grid (PG) and the new electrode (EG). The electrons (purple lines) are collected by the EG thanks to the magnetic field filter (15mT), while most of the negative ions are collected by the two collector probes (external and internal).

Fig. 2.66a shows the assembling of the all configuration (thruster + extraction system). Fig. 2.66b shows the operation with Nitrogen. The aim is to check the reliability of the extraction system simulations, that is to determine whether the electrons are filtered or not before using Hydrogen and Caesium. From preliminary operations, with a pressure of 0.2Pa, $V_{\text{anode}}=90\text{V}$, $I_{\text{anode}}=1.2\text{A}$, $V_{\text{cathode}}=0\text{V}$, $I_{\text{cathode}}=6.5\text{A}$ and $V_{\text{EG}}=300\text{V}$, we collected $I_{\text{EG}}=0.255\text{A}$, $I_{\text{external}}=1.8\text{mA}$ and $I_{\text{internal}}=0.25\text{mA}$. This means that the ratio between extractor current and collector current is around 125, which is a remarkable improvement compared to the previous operations and which should guarantee that the current collected during Hydrogen and Caesium operations should be caused by negative ions.

2.2.5. Collaborations

Collaborations continued with other EU laboratories working on NBI within the EUROfusion program: with Pisa University for the optimization of ATHENIS the alternative ion source based on the Hall effect thruster concept, and with Bari University, for the application of a novel complex network analysis tool, originally developed to control the processes in NIO1, to the chemical network of the CO2 dissociation. The latter can be considered as an exercise preliminary to an analogous one planned for the processes in NIO1 with Caesium.

2.3. ITER Diagnostics

2.3.1. Development of Software Algorithms for ITER Magnetics Diagnostic

In the frame of F4E-OPE-0883, CRFX contributed to the activities of WP 6.1 – 6.4 and 7.3.

2.3.1.1. WPs 6.1-6.4 Estimate halo currents and development of numerical tools

A numerical tool (Halo-ID) has been developed for the estimation of the poloidal current flowing in each sector of the ITER vacuum vessel according to the method investigated on the grounds of the activities carried out in the framework of the F4E GRT-047.

The numerical reconstruction consists in estimating the halo currents flowing through non-instrumented *tiles* (i.e. “wetted surfaces”) by interpolating, along the toroidal direction, the available Rogowski measurements of each instrumented *tile* which collect the current flowing through the earth straps installed on the rear side of the Blanket Modules (BMs) or legs of Dome, Inner and Outer Vertical Targets of instrumented divertor cassettes:

The present layout of sensors includes a total of 231 Rogowski sensors:

- 55.AN (Divertor): sets of Rogowski coils to measure the current distribution in 6 toroidally separated divertor cassettes, 10 sensors per cassette: in total, 60 sensors
- 55.AP (Blanket): pairs of Rogowski coils measuring the transient current flowing through selected blanket module earth straps in a disruption: in total, 171 sensors distributed as follows
- 81 sensors in the Inner Blanket Modules (IBM): 9-fold from BMs 1 to 9
- 90 sensors in the Outer Blanket Module (OBM): 18-fold on BM10, 9-fold in the others

The Halo-ID code is developed in Matlab environment and includes a Graphic User Interface implemented in Matlab App Designer environment. The validation of the code has been carried out against a set of reference data consisting in snapshots of the reference scenarios. The proposed methodology has also been verified by simulating fault conditions in which a subset of sensors are supposed to be not available.

2.3.1.2. WP 7.3 Onsite calibration, test and commissioning of magnetic diagnostics

The activities addressed the basic requirements of identification and polarity check of installed sensors, for which a robust solution has been presented, valid for the majority of sensors. Some specific sets of sensors have peculiarities that need custom solutions, some of them have been discussed.

The calibration task was also investigated: several issues have been presented and discussed, with the aim of identifying the best approach for the next phase of the work.

3. RFX Fusion Science and Technology: RFX-mod2 and Plasma Physics

3.1. Introduction

Due to the RFX-mod shut-down while waiting for RFX-mod2 and to budget limitations of the MST experiment, the experimental activities on RFP devices have been reduced in the last years. However, data analysis, modelling and theory developments have continued, as reported also in previous activity reports, and the discussion of RFX-mod2 scientific programme has progressed. A contribution to the design of the experiments for the upgraded device has been given by the revision and collection of the main scientific results of all RFP experiments in the last decades. These have been summarized in a review paper for Nuclear Fusion which is now in the proof revision stage. All the referees noted how ample and interesting are the achievements obtained by the RFP community, and thanks to their suggestions the paper is now more complete and projected towards the scientific exploitation of the new device RFX-mod2. It is also worth mentioning that the RFP contribution to the general understanding of the isotopic effect in fusion plasmas has been acknowledged as a dedicated article of a topical Plasma Physics and Controlled Fusion volume presently in preparation.

In 2020, the activities on RFX-mod2 have been slowed down by the covid-19 pandemics. Diagnostic revamping or development activities have been scheduled and performed following strict security prescriptions.

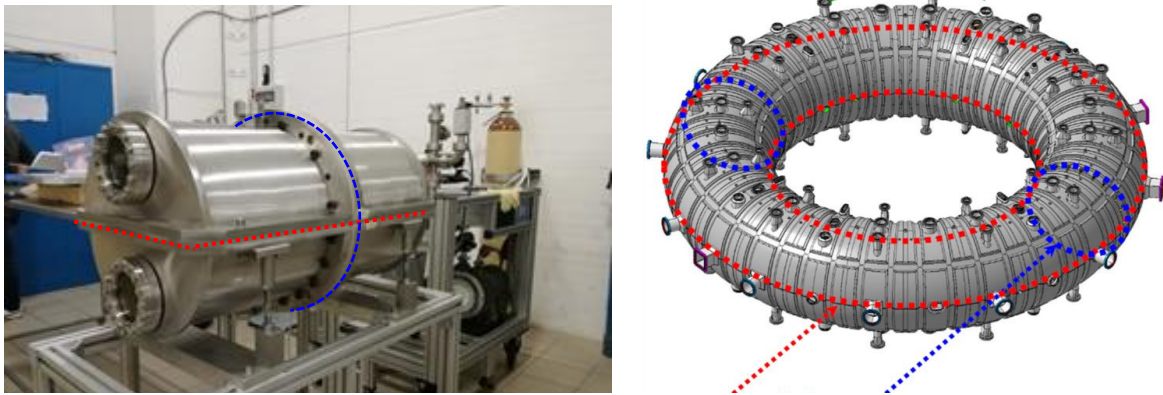
Besides, the activities concerning the design and implementation of the machine toroidal assembly modifications, co-funded by the local authority Regione Veneto in the framework of the industrial innovation program POR-FESR 2014-2020, suffered an interruption between mid 2019 and mid 2020 due to a financial default of the main manufacturing company involved in the related project "MIAIVO" (Ettore Zanon spa). Nonetheless, thanks to a significant commitment of all the stakeholders, the project has been recovered with a new company (Zanon Pressure Equipment srl) taking over the duties of the defaulted one and with the postponement of the completion of the project to the end of 2021 granted by the financing body. Even though with a significant delay, the design of the modifications was completed and the manufacturing phase started during the last quarter of 2020.

3.2. Implementation of the machine toroidal assembly modifications

3.2.1. Vacuum Tight Support Structure (VTSS)

As far as VTSS is concerned, the main activities has been focused on the validation of the vacuum-tight electrical-insulated crossed joints at the poloidal/toroidal gaps of the new

vacuum vessel (Fig. 3.1) in the reduced scale “VTSS mockup”, which turned out to be a technical critical point in the preliminary phase of the MIAIVO project.



Crossed joints representing **toroidal** and **poloidal** gaps of VTSS

Fig. 3.1 “VTSS-mock-up” (left) set up to validate the vacuum-tight electrical-insulated crossed joints of the VTSS

An innovative solution of gasket based on the combination of high-performance polymers and acrylic syntactic foam materials has been developed and successfully tested in the mockup at the expected operating conditions, with leak rates $< 1E-9$ mbar·l/s up to 100°C (Fig. 3.2)²⁷.

After the restart of the design activities with the new industrial partner (ZPE), the detailed CAD model of the VTSS has been completed and the finalization of manufacturing drawings and procedures has been started up (Fig. 3.3).

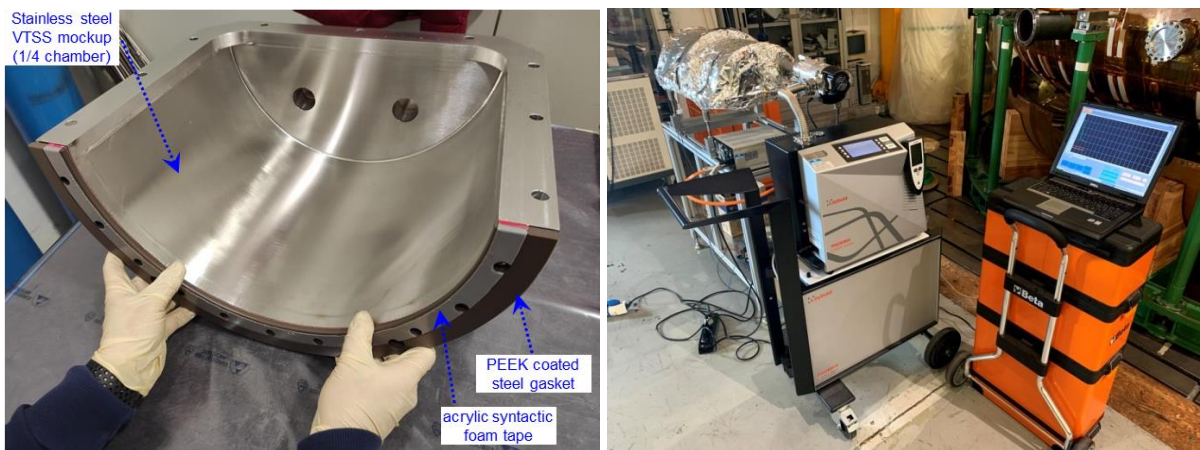


Fig. 3.2 “VTSS-mock-up” during assembly of poloidal gap (left) and thermal tests (right)

²⁷ S.Peruzzo, et al., Design validation of the vacuum-tight electrically insulated crossed joints of the new Vacuum Vessel for the RFX-mod2 experiment, presented at 31st Symposium on Fusion Technology (SOFT 2020)

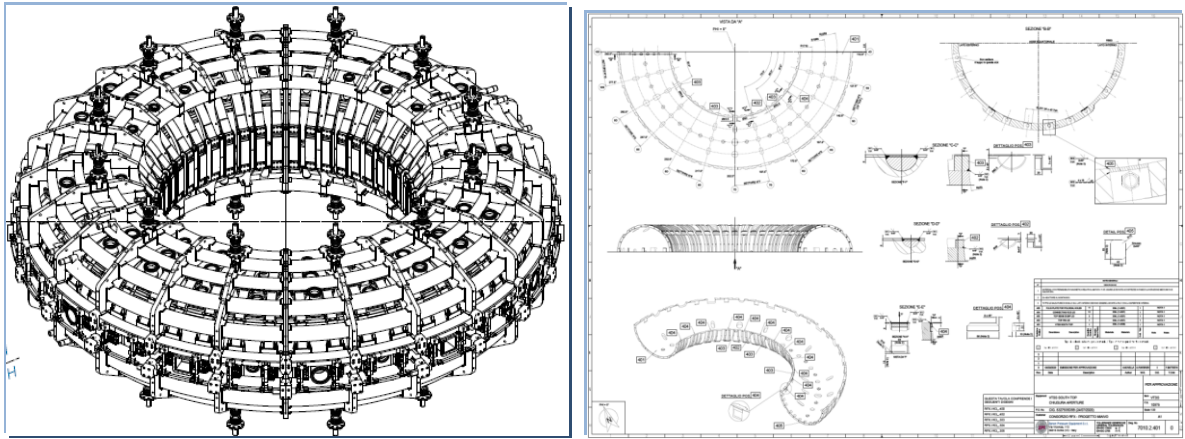


Fig. 3.3 CAD model of the VTSS assembled with poloidal and toroidal coils (left); VTSS manufacturing drawing (right)

3.2.2. Passive Stabilizing Shell (PSS)

The finalization of the design of the PSS assembly has been progressed and almost completed on the various aspects of the design.

Detailed 3D CAD model and exhaustive electromagnetic and mechanical verification of the PSS assembly have been completed, with particular reference to the new components of the support structure (72 poloidal stiffening rings) necessary to sustain the 3mm copper shell within the vacuum vessel (Fig. 3.4)²⁸ and to the integration of the wide set of in-vessel sensors located in the narrow space between the first wall tiles and the inner surface of the shell.

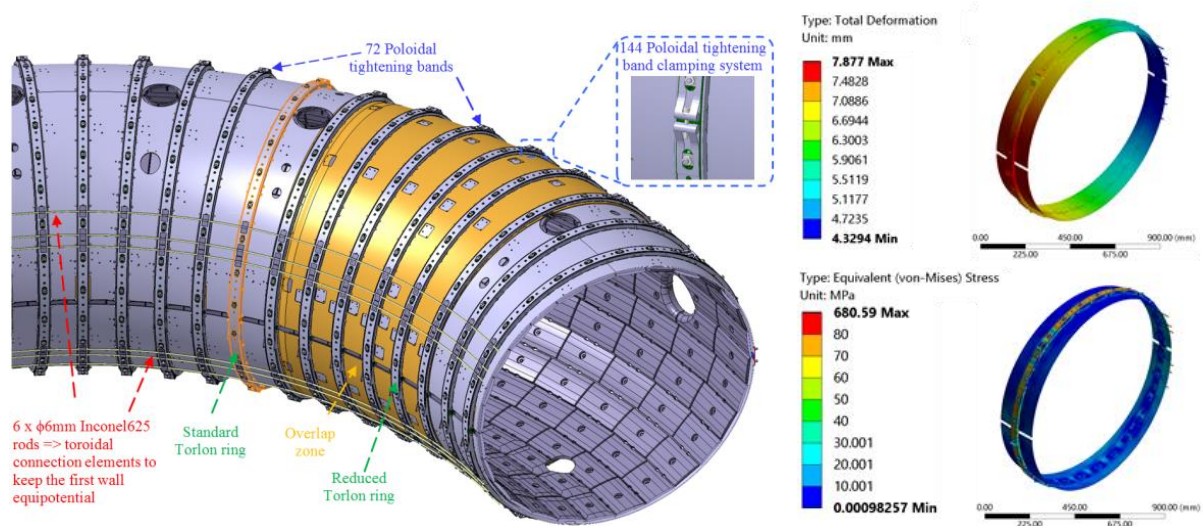


Fig. 3.4 CAD model of the PSS assembly (left); results of elasto-plastic analysis (right)

²⁸ G.Berton, et al., "Design of the new supporting structure for the Passive Stabilizing Shell of RFX-mod2" presented at 31st Symposium on Fusion Technology (SOFT 2020)



Fig. 3.5 Manufacture of Torlon rings prototypes: (a) injection mould; (b) ring sectors prototypes; (c) assembly test on the PSS

A specific procurement contract for the manufacture of the first prototypes of the supporting rings made of PAI-Torlon has been completed with a specialized company (Cattini srl) and the reliability of the manufacturing process of the rings composed of sectors of this unconventional high-performance polymer has been demonstrated (Fig. 3.5).

A full scale mockup of a rectified 30° sector of PSS has been designed and manufactured to test the soundness of the manufacturing procedures and the assembly sequence (Fig. 3.6).

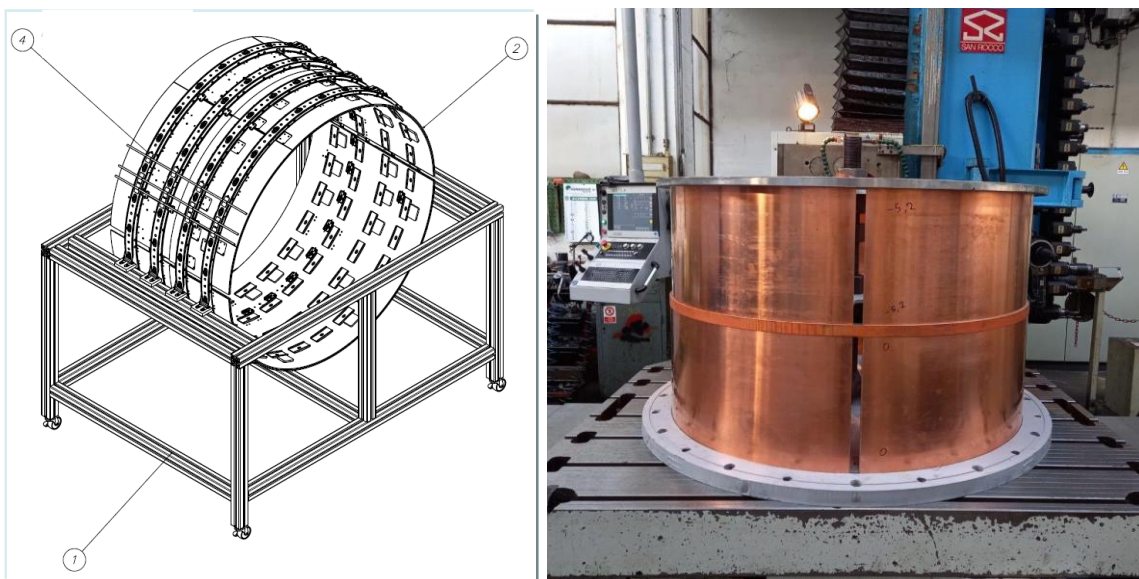


Fig. 3.6 full scale PSS mockup (rectified 30° sector): manufacturing assembly drawing (left); machining phase (right)

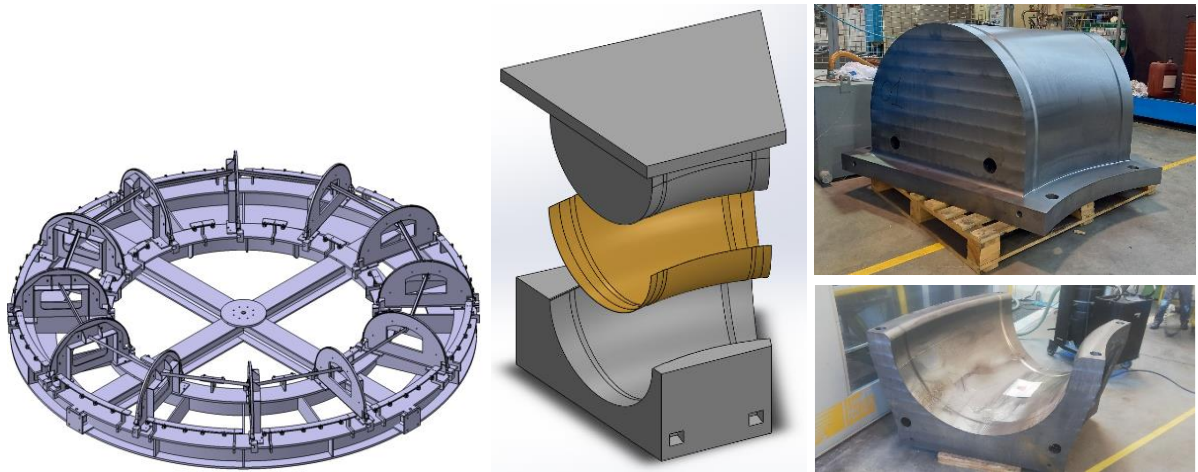


Fig. 3.7 Design of auxiliary supporting structure for PSS machining (left); punch & die for the moulding of new overlapped sectors of the PSS – design (center) and manufacture (right)

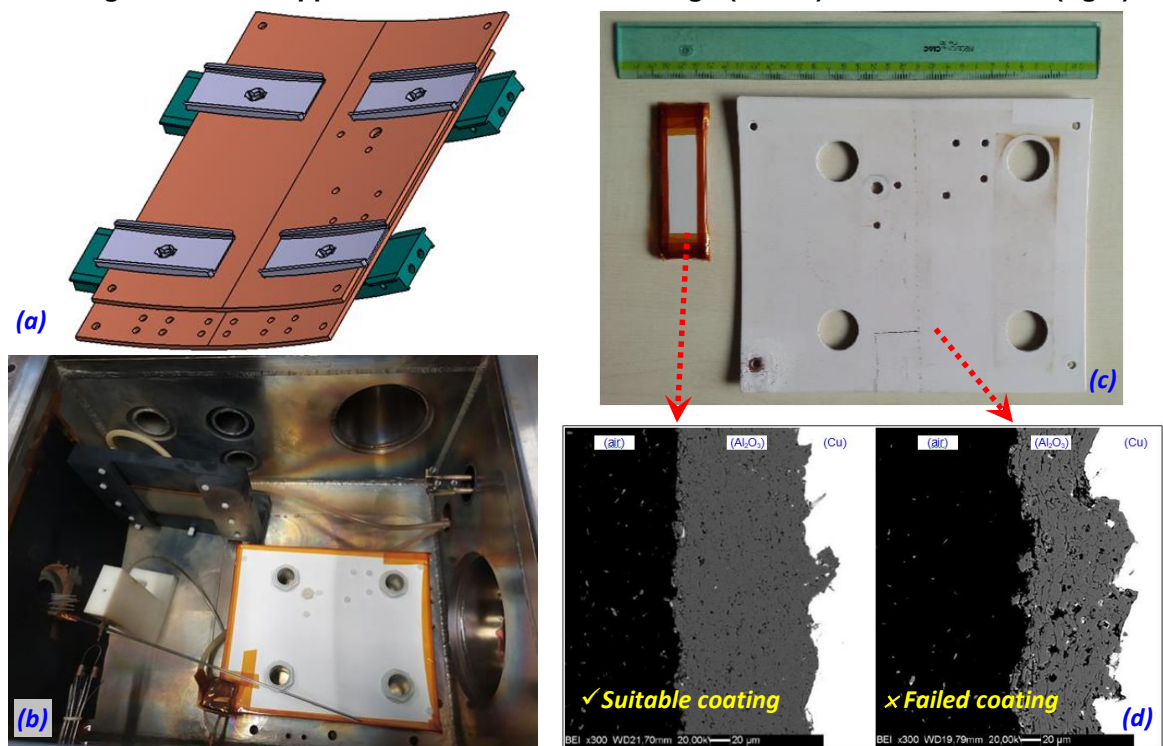


Fig. 3.8 Tests on alumina coating for invessel components: (a) design of PSS mini-mockup; (b) sample within vacuum chamber; (c) samples after tests; (d) sample micrographic section

In the meanwhile the auxiliary tooling for machining the final PSS component has been developed and is presently under construction (Fig. 3.7).

A thorough set of tests has been carried out to optimize the alumina coating process to be applied by atmospheric plasma spray on in-vessel components, to prevent detrimental electrical discharge during operation in presence of weakly ionized gas at the plasma boundary. With the tests, performed on several prototypes within the experimental set up

arranged in the previous phase of the project (ref. 2019 Activity report), a suitable Al₂O₃ coating in terms of thickness (100÷150 µm) and porosity (<1,5%) has been identified (Fig. 3.8)²⁹.

3.2.3. *First Wall*

The design of the first wall, composed of a set of 2016 polycrystalline graphite tiles attached to the internal surface of the PSS, has been completed³⁰ with the finalization of the detailed 3D CAD model and the realization of a representative number of prototypes to confirm the soundness of the manufacturing procedures (Fig. 3.9).

A contract for the procurement of the entire bulk of raw graphite material has been already launched, whereas a further specific contract for the machining of the complete set of first wall tiles is expected to be launched by the first quarter of 2021.



Fig. 3.9 (a) CAD model of the entire first wall protecting the bottom part of the PSS; (b) detail of tiles at equatorial access of the VTSS; (c) + (d) graphite tile prototypes

3.2.4. *Development of components made by additive manufacturing*

In the framework of the MIAIVO project, a specific task is devoted to the development and characterization of in-vessel components made by means of additive manufacturing.

²⁹ L.Peruzzo, et al., “Analisi al microscopio elettronico (SEM) di campioni in rame con ricoprimento in allumina, prototipi per la scocca di RFX-mod2”, RFX Technical Note <RFXmod2-TN-027> (2020)

³⁰ M. Dalla Palma, et al., “Design of the RFX-mod2 first wall”, *Fus. Eng. and Design* **160** (2020) 111795; <https://doi.org/10.1016/j.fusengdes.2020.111795>

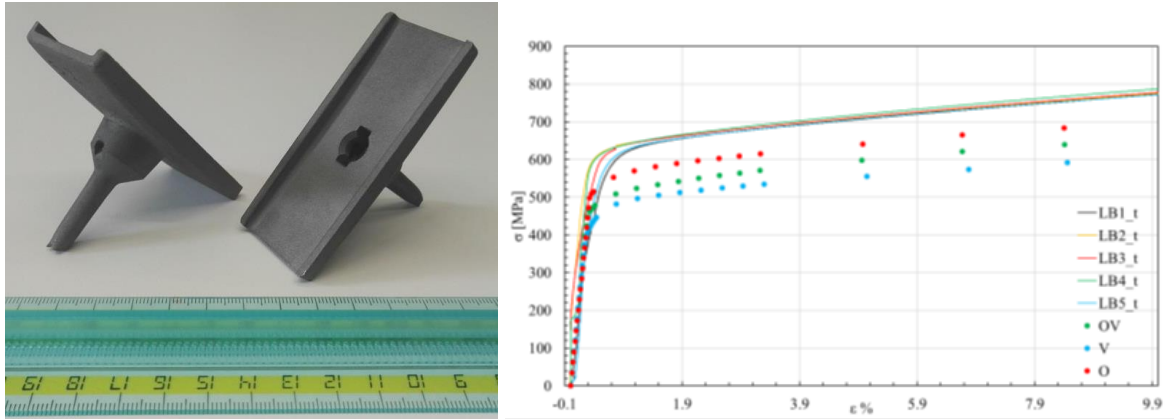


Fig. 3.10 tests on components made by Additive Manufacturing: prototypes of “locking bush” made of stainless steel (left); results of mechanical tests performed on AISI 316 samples - yield strength > 500 Mpa (right)

First prototypes of the stainless steel “locking bush” (the elements designed to fix the First Wall tiles to the PSS) have been manufactured, in collaboration with the industrial partner SISMA, and tested to confirm the reliability in terms of mechanical strength (Fig. 3.10).

First prototypes of the antennas for plasma position reflectometer diagnostic system (ref. Section 3.4.1) have been manufactured and tested to assess the electromagnetic performance of components made of different Cu alloys (Fig. 3.11). Due to the intrinsic high roughness of the Additive Manufacturing process, a surface finishing is necessary to achieve the operating requirements; this detail will be developed in the last phase of the project.

3.3. Revamping of Experimental plants and Auxiliary systems

Owing to the reschedule of the MIAIVO project, with the postponement of the completion of the machine toroidal assembly modifications by the end of 2021, the activities related to the revamping of experimental plants and auxiliary systems have been consequently deferred to

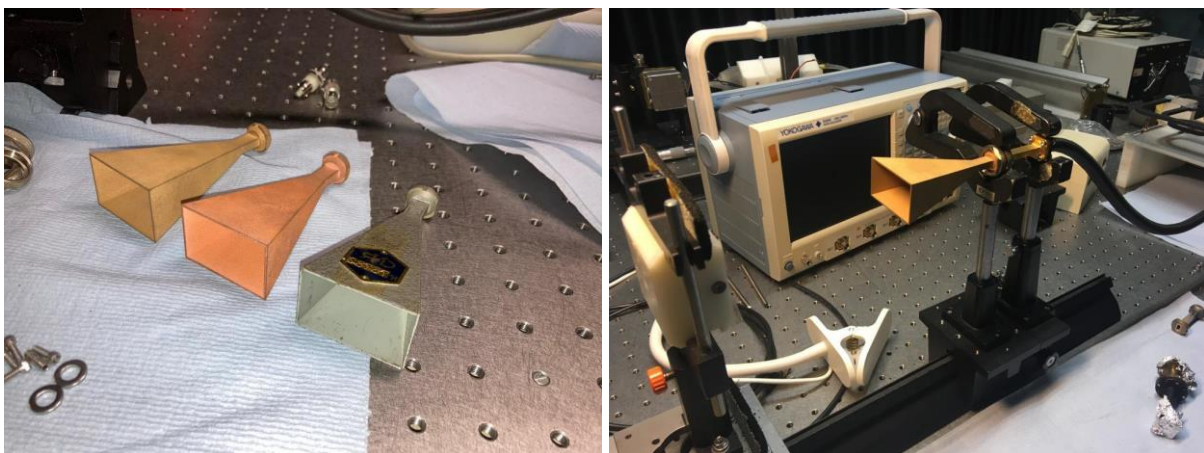


Fig. 3.11 tests on components made by Additive Manufacturing: prototypes of “RF antennas” made of Cu alloys (left); experimental set up for bench test (right)

2021. A detailed plan of activities and resources needed to restart operation in 2022 has been developed³¹.

3.4. Design and installation of diagnostic systems for RFX-mod2

The activity in 2020 focused on the diagnostics required for the first operations of RFX-mod2 and for the systems that need to be installed inside the machine.

3.4.1. Internal Sensors/Systems

3.4.1.1. General Layout and Common Interface

The layout for the in-vessel sensors has been finalised³² and recently integrated with a set of High Frequency magnetic sensors³³ (Fig. 3.12). A preliminary layout of the connection scheme has been checked against the effective possibility of laying out the cables and to bring the signals out of the vacuum vessel. The CATIA extension tool needed for the detailed design of the connection is under evaluation.

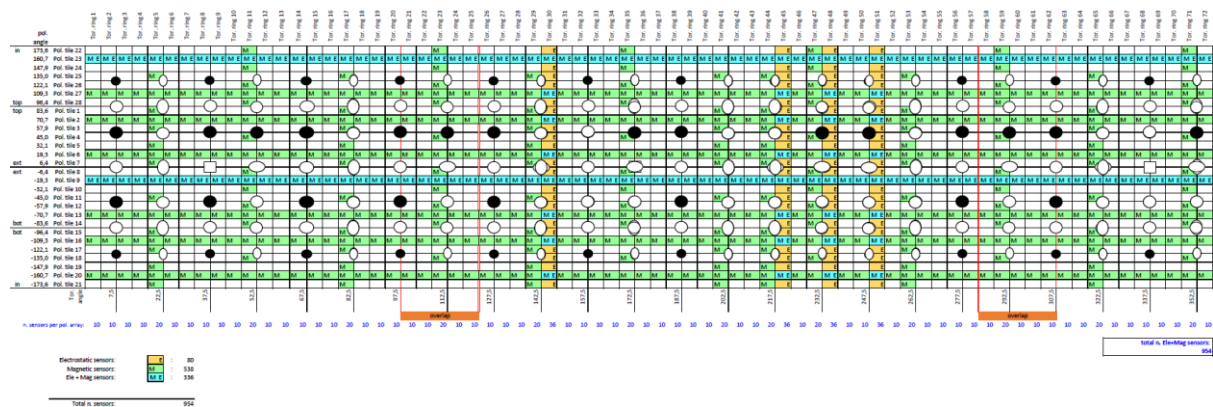


Fig. 3.12 layout of the entire set of magnetic and electrostatic sensors (tot. n.= 954) on a simplified plane geometry net of the toroidal PSS surface

In view to provide an ordered layout and a manageable installation, special open cable support trays have been developed. These supports have been manufactured by laser cutting and folding of 0.1 mm thick stainless steel sheets and tested on a dedicated mock-up (Fig. 3.13). These components are to be spot welded on the shoulders of the supporting rings of the PSS. Their placement can be freely adapted and the support elements easily mounted after the

³¹ M. Boldrin, et al., “Ripristino Impianti Sperimentali di RFX”, RFX Technical Note <RFXmod2-TN-038> (2020)

³² [RFXmod2-TN-029](#) D.Aprile, R.Cavazzana, S.Peruzzo: Schema delle forature da realizzare sulla scocca di RFX-mod2 per fissaggio dei sensori Elettrostatici e Magnetici

³³:RFXmod2_TN_050; S.Spagnolo, R.Cavazzana, L.Cordaro, N.Marconato, M.Zuin: Motivazione e layout dei sensori magnetici per fluttuazioni di alta frequenza su RFX-mod2

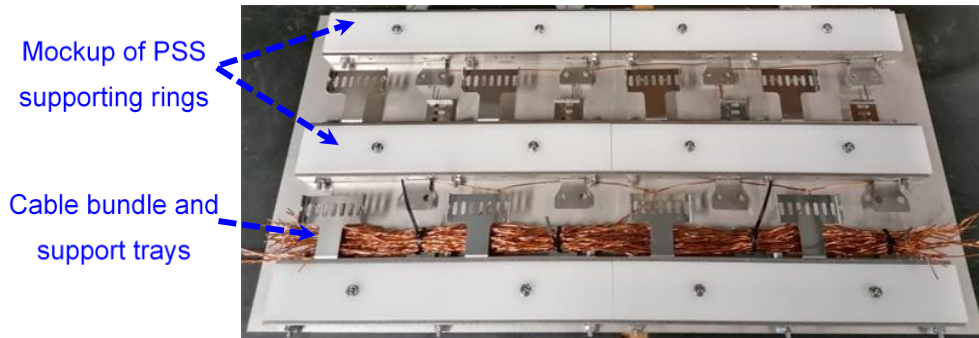


Fig. 3.13 Mockup for in-vessel cable loom test

PSS will be delivered to Consorzio RFX site, making them independent from the realization process of the core components of the PSS assembly.

Electrical vacuum feed-through flanges for D-subminiature from two different vendors have been tested against their insulation requirements. A combination of custom specified D subminiature flange ports and off-the-shelf connectors had been tested in air, in vacuum and in presence of plasma to up to 800 VDC (these components are usually rated up to 500 VDC). This achievement greatly simplifies the cabling process and reduces the overall cost, since with this specification the same type of connector can accommodate both magnetic and electrostatic sensors.

The fixture technology chosen for the magnetic pick-up coils and for the electrostatic probe shell side interface using ultrasonic riveting has been thoroughly investigated. This technology is normally applied on plastics with low temperature melting point (e.g. PVC and ABS) and therefore its use with PEEK (PolyEther Ether Ketone) rivets has been refined and validated, with successful results (Fig. 3.14). Moreover the ability of this fixture technology to withstand thermal cycling has been verified against creep, being proved to be a reliable fixing method for the purpose.

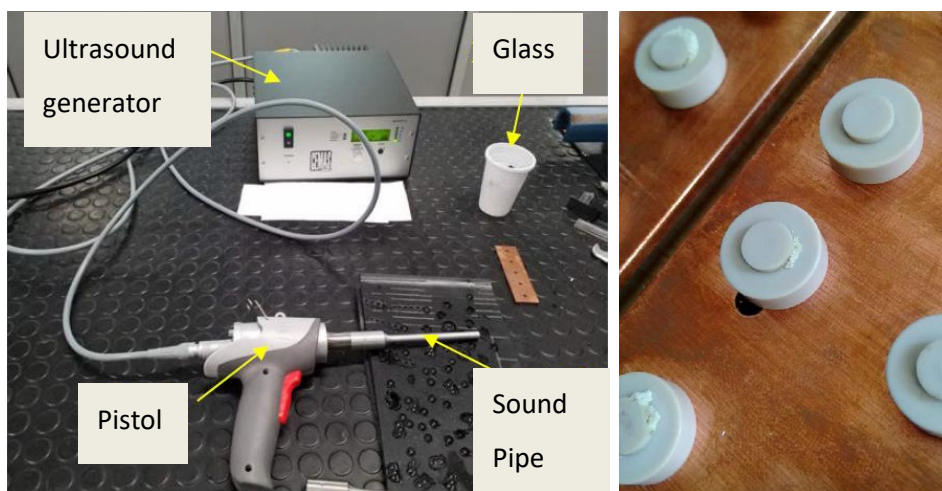


Fig. 3.14 Tooling for ultrasonic riveting (left); tests of PEEK rivets for sensor fixing

3.4.1.2. Magnetic sensors

The design of the pick-up coil sensors has been refined, in order to improve its reliability during and after the winding process³⁴: to this purpose the further refinement has been implemented on the pick-up support with 3D printing and the modified winding scheme successfully verified. On the basis of this result the design of the sensor support has been finalized and made ready for pre-series production tender. Moreover is now under development the vacuum impregnation process for the sensor windings in order to reduce its out-gassing and improve mechanical stability.

The magnetic sensors suite has been integrated with two additional group of special sensors: a set of bi-axial sensors placed on the external side of the PSS to measure and characterize shell currents and a set High Frequency (HF) magnetic sensors³⁵, with a design bandwidth of 5 MHz, vs. the 200 kHz range of the standard ones. All these new sensors are obtained by slight modification of the basic one, retaining the compatibility for winding process and ultrasonic riveting.

Considering the high number of sensors, the methodology for area calibration has been updated to speed up the process by performing the calibration on four sensors simultaneously. To this purpose a new support has been designed, now under fabrication, and a novel method for calibration using a multichannel DAQ system has been assessed. This new method improves the final precision, can check and compensate for errors due to harmonic distortion and frequency jitter, and is suitable for producing an automated report.

Along with the cable trays, on the dedicated mockup³⁶, the prototypes of saddle sensors and loop voltage have been tested. The outcome of these tests lead to a slight modification on the fixing clips and to the choice of the correct type and diameter of the copper wire needed for these sensors. The final fixing clips will also accommodate and keep in contact the thermocouples on the shell surface. Since the geometry of the magnetic saddle probes is a practical viable approximation of an ideal toroidal surface, the measurement errors introduced have been carefully estimated and turned out to be negligible³⁷, and if needed can be corrected.

³⁴ [RFXmod2-TS-003](#); N.Marconato: Specifica tecnica per la realizzazione degli avvolgimenti dei prototipi dei sensori magnetici locali per RFX-mod2.

³⁵ [RFX-mod2-TN-045](#); M.Bonotto, R.Cavazzana, D.Abate, N.Marconato: Progetto di un sensore per la misura del campo magnetico in alta frequenza.

³⁶ [RFXmod2-TN-028rev1](#); D.Aprile, N.Marconato, A.Tiso, F.Degli Agostini, R.Cavazzana: Design and realization of a prototype for testing magnetic loops for RFX-mod2.

³⁷ [RFXmod2-TN-044](#); D.Abate: Approssimazione corda-arco: effetto sulle misure magnetiche (di V-loop e saddle loop).

3.4.1.3. Electrostatic sensors:

RFX-mod2 will be equipped with poloidal and toroidal arrays of electrostatic probes, measuring edge n_e , T_e , plasma potential V_p , particle and energy fluxes and floating potential V_f fluctuations: two toroidal arrays of 72 probes each (one on the HFS and one on the LFS), along with four poloidal arrays of 28 elements (1 array of single probes, 2 arrays of 5-pin balanced triple probes and 1 array of ball-pen probes) were originally planned. The layout of the probes has been finalized, with some modifications. The final result is a compromise between the requirement of a high spatial resolution and the availability and location of signal feed-through ports (and, thus, of pins) to take the signals out of the vacuum chamber. In the end, 2 poloidal arrays (1 array of 5-pin balanced triple probes and 1 array of ball-pen probes) have been reduced from 28 to 18 elements, allowing a denser distribution (one probe on each tile) only on the LFS.

On the other hand, tiles equipped with two probes have been designed in correspondence of the second 5-pin balanced triple probes poloidal array, at the top and at the bottom of the chamber, to obtain measurements with a higher poloidal spatial resolution in the strike points regions during tokamak configurations.

As far as the probe development is concerned, a provisional design of the *Tile-Side* of the probe has been finalized and a prototype has been realized by the internal workshop and mounted on a tile prototype, realized by an external company. The assembly test revealed the necessity of a revision of the tolerances between mating parts. A provisional design of the *Shell-Side* of the probe has also been finalized and a prototype is under construction by the internal workshop. In particular, this part of the probe will be fixed to the shell with the same technology adopted for the magnetic sensors: the possibility to use peek rivets to fasten it to the PSS has been confirmed³⁸.

Finally, a market survey for the purchase of signal cables and of the boron nitride (ceramic material required for the realization of the insulating button directly faced to the plasma) has started.

3.4.1.4. Position reflectometer for tokamak position reconstruction:

In 2020, the activity on the design of new plasma position reflectometer has been affected by the limitations imposed to the whole experimental activity. In the first part of the year, the activity has been focused on the optimization of the reflectometer antennae design, within the

³⁸ RFXmod2-TN-037, M. Bernardi, et al, Validazione del sistema di fissaggio dei sensori in-vessel mediante ribaditura di rivetti in PEEK attraverso processo ad ultrasuoni; RFX-mod2-TN-047, D.Abate et al., Prova di creep (scorrimento viscoso) sui rivetti in PEEK 450G per il fissaggio dei sensori in-vessel di RFX-mod2

tight space constraints of the RFX-mod first wall. In particular, an electromagnetic model of the launch antennae has been implemented in COMSOL MultiPhysics. A detailed definition of the antenna has been proposed based on a parabolic reflector concept (Hogg horn), already implemented in other fusion devices like ASDEX-Upgrade. This antenna will be located in the High Field side region of RFXmod2. These kind of antennae will be manufactured via the additive manufacturing technique by the SISMA Company within the MIAIVO project (ref. Section 3.2.4). The same company provided us with few pyramidal antenna mock-up produced with this technique. A series of bench tests have been performed to verify real performance with respect to the traditional manufacturing³⁹.

Two other activities concerned the routing of the waveguides that will connect the High Field side antennae. The first one concerned the waveguides integration with the RFXmod2 model: a dedicated flange (on the top of the machine) and PEEK supports to anchor the waveguides to the mechanical structure have been designed. The second activity, concerned the investigation of a possible waveguide insulation coating, to avoid electrical contact with the RFX-mod copper shell; in case of fast termination in RFP configuration, in fact, the toroidal sector of the reflectometer can reach a spike voltage as high as 500 V. Bench tests have been performed to assess the electrical insulation provided by different materials: PEEK, PTFE and Pyro-Paint 634-ZO⁴⁰. Pyro-Paint 634-ZO appeared the most suitable solution.

3.4.2. *Diagnostics developments*

3.4.2.1. *Interferometry*

1. The diagnostic has been found to require a significant revamping: it has been decided to upgrade and modify it in order to overcome limitations of the previous design. On the one hand the CO₂ laser at 10.6 microns is confirmed for the measurement beam: a new source has been purchased to replace the old one. On the other hand it has been decided to change the wavelength of the laser used to compensate for the mechanical vibrations, in order to overcome issues related to the laser class applied so far (i.e. He-Ne at 3.39 microns). Indeed, the He-Ne lasers at 3.39 micron currently commercially available do not guarantee for the required single longitudinal mode operation. Furthermore, they are sensitive to the environmental temperature and previous experience at Consorzio RFX has shown that magnetic fields can strongly impact on their operation. Consequently a single-frequency DFB

³⁹ G. De Masi, "Test su antenne in ottone e bronzo stampate con tecnica Additive Manufacturing dalla ditta SISMA per il nuovo riflettometro diagnostico di RFX-mod2", technical note RFXmod2-TN-042 (2020)

⁴⁰ G. De Masi, et al., "Test di isolamento su guide d'onda rivestite in PEEK, PTFE e Pyro-Paint 634-ZO per il riflettometro di RFXmod2", RFX-mod2-TN-046 (2020)

Erbium-doped fiber laser with wavelength at 1.55 microns has been chosen, after verifying that this wavelength, albeit shorter than the one previously used, would in any case allow for the vibration compensation. A significant advantage of this laser is that it can be located far from the experimental room (and therefore from the magnetic field) and the light can be propagated through an optical fiber.

It has also been decided to try repairing the He-Ne laser at 3.39 microns, which is currently at Consorzio RFX, even though it is not clear if it is feasible. This laser could be applied as a back-up solution in case the performances of the interferometer with the new compensation laser (at 1.55 microns) will not be sufficient.

2. During the maintenance operation of the module A of the RFX interferometer, it was found out that several optics of the interferometer needed to be replaced. At the moment, the critical optics to be changed (windows, beam splitter, dichroic mirrors, Bragg cell) for the modified interferometer have been individuated and the majority of the quotations are already available. The purchase process will be started at the beginning of 2021.

3. The local and remote control system of the interferometer has been checked as well as the signal amplifiers and they are currently working.

4. Tests on the possibility to place both the lasers outside the experimental room have been started. The test is not yet concluded and it might be finalized by using the new CO₂ laser, which should arrive in the first months of 2021. Indeed, the laser at 1.55 micron will be outside the RFX experimental room, as mentioned in point 1 of this list, so this test will be useful mainly to gain insight into the stability of the CO₂ laser interferometer, when the laser source and the interferometer optics do not lie on the same optical bench.

3.4.2.2. Visible cameras

The design of the plasma camera view system, which began in 2019, has been updated and in particular the compatibility of the optical cones of sight with the newly RFX-mod2 designed graphite tiles have been checked: no interferences have been found. In parallel, a few companies have been contacted to evaluate the realization of a custom camera with sensor and electronics separated, in order to avoid any problem due to the high magnetic field in the locations close to the plasma. In fact, tests conducted on the RFX-mod available cameras have shown that above a certain value of magnetic field the power supply stops working. Placing the electronics a few meters away from the porthole, and keeping the sensor close to the plasma, is enough to solve this problem. The activity is still on-going due to the slow response by the companies.

3.4.2.3. Spectroscopic diagnostics

Refurbishment activity of spectroscopic diagnostics started in mid-2020. In particular a calibration of the VUV SPRED (wavelength 10-110 nm) spectrometer has been attempted. This spectrometer is a diagnostic for impurity identification in the RFX.mod2 plasma and it is therefore required in the first plasmas. This activity aims to test and document the calibration procedure, in preparation of a similar procedure that will concern the procurement of the VUV spectrometer for JT60SA. The calibration could not be completed because the old Micro Channel Plate detector, which was already replaced before the operation of RFX-mod in 2004, has been damaged due to the impossibility to keep it in high vacuum after the shutdown. After several iterations with the manufacture company (McPherson) a new MCP detector with a new phosphor deposition layer (replacing the 30 years old one) with similar characteristics to the old one have been ordered. Activity to re-activate other day0 spectroscopic diagnostic has been delayed to next year, when the RFX-mod2 device will be installed.

Taking advantage of the new RFX-mod2 first wall layout, a passing toroidal line of sight has been designed to allow a new measurement of Z_{eff} along a sufficiently long line of sight not intercepting the wall (the rationale is to maximize the signal from plasma with respect to possible wall reflections and pseudo-continuum emission from molecules close to the wall). Once the final design of graphite first wall have been completed, a careful analysis of possible interference of the line of sight with tiles have been performed. As a result, both a slight modification of the original optical design (a 5mm vertical displacement below the equatorial plane) and of the tiles around of the diagnostic accesses have been implemented in the design in order to avoid vignetting. As the evaluation of Z_{eff} requires an absolute brightness measurement, the transmissivity of the window is a key parameter. A simple, yet effective, calibration diagnostic based on a green diode laser (at a wavelength very close to the required Bremsstrahlung) has been designed using the same optical system, and it will perform calibration after each pulse. In case of an excessive reduction of transmissivity, due to the unavoidable carbon re-deposition, an in-situ laser-based window cleaning system based on Laser Blow Off (not requiring to break vacuum) has been conceptually designed.

The same diagnostic accesses will allow an easy (not requiring absolute calibration of the wavelength) determination of the toroidal flow of low ionization state impurities (typically located at the edge) by simultaneously measuring the line Doppler shift along opposite directions of the same LOS.

3.4.2.4. Thomson Scattering

During 2020, the design activity for the Thomson scattering diagnostics upgrade progressed with a detailed design of the vacuum interface and of the manipulator for beam dump extraction / insertion. Beam dump replacement without breaking vacuum is required either if

the beam is back reflected, since the reflector is exposed to plasma damage and its lifetime is expected to be short.

The manipulator is based on a translating structure holding the insertable arm; all is kept in vacuum and operated by means of two rotary feedthroughs, one dedicated to the arm translation and the other to the dump lock/unlock on the inner equator of the machine. The gearing system, at first designed with a single crankshaft, has been modified including a reduction stage, in order to mitigate the sliding friction and hence the jamming risk.

A third rotary feedthrough is reserved for the subsequent installation and operation of the Laser Blow Off target holder, consisting of a belt operated system at the arm end.

In parallel, several damage tests of the beam retroreflector have been performed. The beam enters the machine with elliptical footprint, with the major axis in vertical direction. The test pointed out that a layout featuring an intermediate beam waist and a concave retroreflector leads to a power density exceeding the reflector damage threshold. The baseline layout now feature a flat back-reflector working with a low divergence beam.

Finally after the definition of the vacuum interface, a new set of windows has been selected and purchased, ready for installation once RFX-mod2 will be in place.

3.4.2.5. Bolometric tomography

During RFX-Mod experimental sessions, one or more bolometric amplifiers stopped working, and they could not be mended. The common practice in the past was simply the replacement or waiting for the amplifier to recover by itself (that could happen in (days or weeks)). The problem has now been investigated more deeply and the conclusion has been that many amplifiers need to be repaired, both to have all bolometers working (12 sensors for each probe, 3 probes for a total of 36 channels) and to have a few spare units. The company that built the amplifiers has been contacted, next year the damaged / not working modules will be repaired.

The three manipulators were originally installed in the upper side of the RFX-Mod vacuum vessel. For experimental reasons, the manipulators will be moved to the lower side of the vessel, where the manipulators of the SXR tomography were installed. Consequentially the SXR manipulators will be moved on the upper side. This will require some modifications, in particular to the cabling.

In parallel with this activity, the interference between the lines of sight of bolometers and the new graphite tiles of RFX-Mod2 has been analyzed. As a result, some tiles had to be modified to cure a few lines of sight intersecting them, in particular those looking at the plasma edge,.

3.4.2.6. SXR tomography

Similarly to the bolometry, also several of the SXR tomography amplifiers have been found to need repair. The same company of the bolometric amplifiers will take care of the repair in

2021. Also the SXR tomography lines of sight have been checked for interference with the new graphite tiles, with results and solutions analogous to those of the bolometry.

3.4.2.7. Thermal Helium Beam

The THB diagnostic has been used in RFX-mod to determine edge profiles of n_e and T_e with high frequency resolution in three locations⁴¹. In its standard configuration, the THB acquires three HeI lines (667.8, 706.5, 728.1 nm) and from the ratios of their intensities, edge n_e and T_e are evaluated⁴². From the experience gained with the operation of the old THB system, an upgrade has been designed and is being implemented to improve the diagnostic in two aspects: (a) remove the systematic error due to the light re-absorption at high neutral Helium density (above 10^{17} m^{-3}), by adding the measurement of a fourth line (501.6 nm); (b) increase the signal level, especially for the 728.1 nm line, which limited the frequency range analysis in RFX-mod, by changing the detection chain. In particular, the multichannel photomultiplier (PMT) detectors are replaced by Multi-Pixel Photon Counters (MPPC), also known as silicon photomultiplier (SiPM), which are solid-state photodetector based on multiple avalanche photodiode (APD). In order to detect the four lines, spanning a wider spectral range, with the same Czerny–Turner spectrograph of the RFX-mod THB, a grating with a smaller dispersion (half of the previous one) is required. Correspondingly, the entrance slit size is halved. On the other hand, the new MPPC detectors are not sensitive to the magnetic field and therefore they can be located near the spectrograph with a much shorter fiber optic connection: the overall effect is that signal is significantly improved. The complete system has been aligned and calibrated and it is now ready to be used. The calibration has been performed by using a integrating sphere absolutely calibrated as light source. Since the MPPC detectors do not have a linear response, the light intensity has been varied, obtaining the calibration of the whole system as a function of the input brightness⁴³.

The THB in RFX-mod2 will be used also for measuring the edge n_e and T_e at the HFS, to study the poloidal magnetic topology of the boundary plasma. To do this, a new injection point in the inboard equatorial plane, integrated inside the RFX-mod2 vacuum vessel, has been designed and will be installed in RFX-mod2 in 2021. A preliminary design of the detection optical path have also been performed.

⁴¹ Agostini M, et al. Fast Thermal Helium Beam diagnostic for measurements of edge electron profiles and fluctuations. *Review of Scientific Instruments*. 2015 Dec;86 (12):123513.

⁴² Agostini M, et al. Optical measurements for turbulence characterization in RFX-mod edge. *Review of Scientific Instruments*. 2010 Oct;81(10):10D715.

⁴³ Agostini M, et al. Development and characterization of thermal helium beam diagnostic with four helium lines for RFX-mod2 experiment. *Review of Scientific Instruments*. 2020 Nov 1;91(11):113503.

3.5. Preparation for RFX-mod2 experiments

3.5.1. Changes and new algorithms for magnetic data analysis

The RFX-mod2 experiment will benefit from a renewed plasma front-end system to allow increasing plasma minor radius and reducing the distance between plasma and stabilizing-shell. This change imposes a major revision of all numerical routines developed for magnetic data analysis both dealing with axisymmetric quantities, as well as non-axisymmetric quantities. The adaptation is required due to the increased number of sensors foreseen in RFX-mod2. The work is in progress and will continue in 2021, but some aspects were already implemented in 2020. In this respect, all routines used for cylindrical and toroidal analysis were modified in order to apply the algorithm with a generic number of sensors: this involves both the spectral analysis as well as the eigenfunction computation in both geometrical descriptions. These routines were tested and debugged on RFX-mod pulse files setting in the routines the present layout of sensors. A new algorithm was devised for axisymmetric shift and shape of the plasma surface since new measurements are available with higher spatial resolution. The estimate of the aliasing pollution onto the sensors was readdressed and modified accordingly also taking into account the toroidal and poloidal supporting rings. The latter effect may be negligible due to the high resistance of the material used. However this might possibly be changed with a lower resistance material so the coding was implemented to be ready for initial operations. Further testing will be performed when a set of synthetic measurements will be available.

3.5.2. Analysis and documentation of the RFX-mod 2 magnetic control system

The RFX-mod magnetic control system has been designed and simulated in Simulink environment since the very beginning of the project. The corresponding C-code routines to be deployed to the real time control framework are generated by means of the Real Time embedded coder tool. Now, in view of the prospective operation of RFX-mod2, a thorough scrutiny of the nested block schemes making up the full system is under way. Beyond simplification and rearrangement of some control blocks and detection of possible errors, a documentation effort has been undertaken by exploiting the possibility of generating reports provided by Simulink. Texts have been written to explain the function of single blocks and nested schemes. A report can then be automatically generated by Simulink which indexes the text sections according to the position of the blocks and the sub-schemes in the whole control system. The level of details in the description would be aimed at offering a comprehensive guide for prospective users of the controls system or developers of new subsystems.

3.5.3. **Characterization of reconnection processes**

Magnetic reconnections in high current RFX-mod plasmas are often associated to partial or total transitions from a helical to an axisymmetric topology. A high time resolution soft-x-ray diagnostic (DSX3) allows to reconstruct the electron temperature evolution during these events. The data show that during these transitions the electron transport barriers are rapidly lost and the core electron temperature decreases from $\sim 1.5\text{keV}$ to less than 0.6keV (about -50%, see an example of T_e profile evolution in Fig.1-(a)); this happens also for minor events when the helical topology is not completely lost (T_e drops by about -30%). The variation of the electron thermal energy during reconnections together with the data of the input / radiated power, of the dissipated magnetic energy ΔW_m and of the electron heat losses are used to estimate the “surplus” amount of energy ΔU_s which could be involved in ion heating or in other non-thermal processes like particle acceleration. The statistical distribution for ΔU_s over an ensemble of events has a maximum around 80kJ but with a few events up to 200 kJ are also detected. There are several experimental evidences that this energy could be involved in ion heating as indicated both by the Neutral Particle Analyzer (NPA) - which estimates the ion temperature from the distribution function of the neutral atoms - and by the DD neutron detection; the analysis of the signals from these diagnostics and the estimate of the ion energy increase during magnetic reconnection are still in progress.

3.5.4. **Relation between density limit and Hartman number**

We analyzed the density limit in RFX in terms of the experimentally estimated dimensionless parameter Hartmann number, H , in a wide database of RFP discharges. This work is part of a broader framework (see Section 3.6) aimed at understanding the role of H in ruling the RFX-mod plasma behavior. On the one hand, 3D nonlinear MHD modeling shows that the H number rules the transition to quasi single helicity regimes, and, more in particular, the amplitude of $m=0$ modes. On the other hand, the experimental correlation between $m=0$ edge islands, causing the highly radiative annulus (MARFE) observed in high density discharges, and density limit has a solid background as documented in previously published papers^{44,45}. A direct experimental correlation between the presence of a MARFE and H have been established, finding a threshold value $H = 3.5 \times 10^6$ for the appearance of the MARFE, equivalent to $n/n_G = 0.56$. The transition to the density limit has been further confirmed by a

⁴⁴ G.Spizzo, G.Pucella, O.Tudisco, M.Zuin, et al, “Density limit studies in the tokamak and the reversed-field pinch”, Nucl.Fus. 55, 043007 (2019) <https://doi.org/10.1088/0029-5515/55/4/043007>

⁴⁵ M.E.Puiatti, P.Scarin, G.Spizzo, M.Valisa, et al., “High density physics in reversed-field pinches: comparison with tokamaks and stellarators”, Nucl.Fus. 49, 045012 (2009) <https://doi.org/10.1088/0029-5515/49/4/045012>

good matching between scaling of mode amplitudes in MHD numerical simulations and in RFX-mod experimental data: these evidences indicate that the density limit can be interpreted as a magnetofluid phenomenon governed by H . This scaling allowed also to infer an effective experimental viscosity, which turned out to be approximately two orders of magnitude larger than the value obtained using the Braginskij transport theory. Such a result has been further and independently confirmed by analyzing the temporal scales of the reconnection events, as described in Section 3.6: the estimated viscosity is greater by two to three orders of magnitude (more precisely, the anomaly factor ranges from 40 and 110 times the Braginskij estimate): interestingly, these values are compatible with the viscosity experimentally estimated in the Madison Symmetric Torus experiment as reported in ⁴⁶, where the anomaly factor ranges between 8 and 380.

3.5.5. *Collaboration with RELAX on relaxed states*

The visit by a Japanese RELAX scientist has been prematurely interrupted by the covid-19 lock-down. The visit aimed at comparing the experimentally measured states in the low aspect ratio ($R/a=2$) RELAX device with the cylindrical relaxation theory⁴⁷.

A substantial deviation of the experimental states from the theoretical predictions has been observed, in particular for cases corresponding to a large reversal of the edge toroidal field⁴⁸. In the attempt to explain this discrepancy, in 2020 we have considered the effect of the toroidal geometry by employing the VMEC and RelaxFit equilibrium codes.

First, the VMEC solver, has been initialized by the safety factor profile as deduced by the code RelaxFit that reconstructs the toroidal equilibrium by taking into account the experimental magnetic measurements. A good agreement between the two codes has been found.

Then, by initializing VMEC with the Single Helical Relaxed (SHR) q profiles, we have shown that the poloidal asymmetries both on the poloidal and toroidal fields due to toroidicity are changing the cylindrical values of the two dimensionless parameters, F and Θ , towards values that agree well with the experimental measurements as reconstructed by the RelaxFit code. These toroidal corrections of the cylindrical states, however, could hardly match the experimental reconstructed data if Θ is larger than 2. Therefore it has been concluded that the toroidicity is a key element to reconcile the SHR states with the experimentally measured values in the intermediate range of $F - \Theta$'s.

⁴⁶ R.Frström, B.E.Chapman, A.Almagri et al, Phys.Rev.Lett. 120, 225002 (2018).

⁴⁷ R. Paccagnella, S. Masamune, A. Sanpei, Phys. of Plasmas 25 (2018) 072507.

⁴⁸ R. Paccagnella, S. Masamune, I. Predebon, A. Sanpei, arXiv:2005.07414 (2020).

3.5.6. ***RFX-mod2 tokamak: DEMO-like shaped operations***

A detailed modelling activity has been carried out to demonstrate the feasibility of DEMO-like shaped tokamak operations (i.e. $k > 1.5$, $\delta > 0.3$) in RFX-mod2 experiment with both positive and negative triangularity⁴⁹. The new shape conditions would allow achieving higher plasma current and density values at the same toroidal magnetic field and safety factor limits of previous RFX-mod tokamak operations. These results are also of interest for the design of a new controller in which the reflectometry diagnostic will be used to control both vertical and horizontal position of DEMO-like shaped equilibria in the RFX-mod2 experiment.

Preliminary stability analysis on these DEMO-like shaped equilibria has been carried out revealing that shaped equilibria has lower no-wall and ideal-wall stability limits, and a considerably narrower wall-stabilized region, with respect to circular cross-section plasmas. Nevertheless, the operational space remains well below the calculated no-wall limits. Both circular and shaped plasmas show possible (linear) Tearing Mode instabilities ($n=1$) with growth rates scaling as $S^{-3/5}$ (where S is the Lundquist number). With finite pressure however, the DEMO-like shape introduces poloidal coupling between $n=1$ harmonics, which affect the scaling of the growth rate with pressure. In general, a richer poloidal spectrum is observed for eigenfunctions in shaped plasmas.

3.5.7. ***RFX-mod tokamak: negative triangularity preliminary equilibrium analysis***

A preliminary activity has been started in view of future systematic studies of still open issues involving negative triangularity operations such as low- q limit and kinetic stabilisation effects. Starting from RFX-mod experimental plasma discharge (#39122), presenting both L-mode and H-mode conditions, the related plasma equilibria have been computed and characterized. Thus, the shape of poloidal cross section has been mirrored with the same methodology of DEMO-like equilibria⁴⁹; hence, using the plasma equilibrium conditions of reference experimental shot as boundary conditions, new mirrored plasma equilibria in L-mode and H-mode were produced with fixed boundary calculations. The feasibility of these mirrored shapes was confirmed by computing the coil currents requirements and the solution was verified in a free-boundary calculation (with a maximum error of about 3cm in proximity of the X-point and mid-plane high field side). The equilibrium fields have been characterized in terms of some basic geometric quantities in view of further analyses, both within the separatrix and in the SOL. The equilibria have been fed to the CHEASE code for producing a high resolution version and output in EQDSK format, allowing an easy integration with other workflows (e.g. for stability studies). Finally, the setup for gyrokinetic calculations (with GENE) is ready to test the

⁴⁹ D. Abate, et al., PPCF. 62, 085001 (2020).

effect of a positive or negative triangularity on different kinds of micro-instabilities and turbulence.

3.6. RFX Theory and modelling activities

Nonlinear modelling and data analysis tools developed and adopted in our lab have accomplished major steps forward in dealing with physics issues encountered in the Reversed Field Pinches, Tokamaks, and possibly of interest for Stellarators too. In this spirit of a transversal approach to magnetic fusion, we have been addressing, in particular, self-organization processes, formation of internal transport barriers, temporary loss of operational point and relaxation-reconnection events with excitation of Alfvén waves, leading in 2020 to some publications^{50,51,52} and follow-up, as described below.

3.6.1. 3D nonlinear visco-resistive MHD modelling

These studies provided a fundamental pillar for the basic understanding of RFP *helical* self-organized dynamo since the early 90ties, and highlighted in the RFX/RFX-mod devices starting in the late 90ties. In the last years the implementation of more realistic 3D nonlinear MHD boundary conditions emphasized their key role in favoring the transition to the quasi-helical regimes as observed in RFP^{53,54,55} and Tokamak experiments⁵⁶ (quasi-helical *dynamo effect*, also referred to as *flux-pumping mechanism*⁵⁷ in the Tokamak case). Moreover, the implementation of suitable seed edge magnetic perturbations has been shown capable to force different pitches of the helical plasma shape, leading to the discovery of new RFP global

⁵⁰ Veranda M. et al *Magnetic reconnection in three-dimensional quasi-helical pinches*. *Rend. Fis. Acc. Lincei* (2020) <https://doi.org/10.1007/s12210-020-00944-4>

⁵¹ Cappello, Bonfiglio, Veranda, et al., Invited Talk 4th Asia-Pacific Conference on Plasma Physics, 26-31 Oct, 2020 <http://aappsdp.org/DPP2020/pdf/F-114.pdf> (recorded presentation available to registered participants till June 2021)

⁵² Veranda M., Bonfiglio D., Cappello S. et al, “*Helically self-organized pinches: dynamical regimes and magnetic chaos healing*” *Nucl. Fus.* 60 016007 (2020) <https://iopscience.iop.org/article/10.1088/1741-4326/ab4863>

⁵³ Bonfiglio D. et al, *PRL* 111, 085002 (2013) <https://doi.org/10.1103/PhysRevLett.111.085002>

⁵⁴ Bonfiglio D, invited talk 3rd AAPPs-DPP Hefei, China (2019), and Bonfiglio D et al *EPS* 2019 <http://ocs.ciemat.es/EPS2019PAP/pdf/P1.1049.pdf>

⁵⁵ Marrelli L., et al., *Nucl. Fusion* 59, 076027 (2019) <https://doi.org/10.1088/1741-4326/ab1c6a>

⁵⁶ Piovesan P. et al., *Nucl. Fusion* 57 116029 (2017) <https://doi.org/10.1088/1741-4326/aa700b>

⁵⁷ Jardin S.C., Ferraro N. and Krebs I., *Phys. Rev. Lett.* 115 215001 (2015) <https://doi.org/10.1103/PhysRevLett.115.215001>

helical regimes⁵⁸. A recent overview of the impact of dimensionless parameters and helical boundary conditions is presented in ref⁵⁹, where older works from our lab can be also found. During 2020 the activity in this regard continued, with the aim, in particular, to train a PhD student (first year) to 3D nonlinear MHD modeling activities⁶⁰. Thus, a basic benchmark study has been undertaken with respect to the linear stability theory for the external kink mode in the tokamak, according to Shafranov and Wesson approaches. A reasonable agreement is obtained in terms of stability thresholds and growth rates by visco-resistive (zero-beta) SpeCyl code in the limit of low dissipation and by adopting an edge pseudo-vacuum region. To improve the quantitative agreement, the implementation of new boundary conditions at the interface between plasma and edge vacuum-layer is presently under assessment, with particular attention to the flow field boundary conditions. Also, the role of the dimensionless Hartmann number (proportional to the inverse of the geometric mean of viscosity and resistivity), highlighted in 3D nonlinear visco-resistive magnetofluid modelling, has been further analyzed. Part of this work provides also a training for another PhD student (first year) to 3D nonlinear MHD modeling activities⁶¹. In particular, the comparison between mode amplitude scaling in numerical and in RFX-mod experimental data allowed to infer an effective experimental viscosity to be about two orders of magnitude greater than the value obtained using the Braginskij transport theory (see also sec 3.5.4). Such a result has been further, and independently, confirmed by comparing the temporal scales of the reconnection events, measured both in MHD modelling and in RFX-mod: they follow a modified Sweet-Parker scaling and their temporal features coincide when accounting for a two orders of magnitude increase of the plasma “effective” viscosity with respect to Braginskij relation. In addition, using the experimental estimate of the H number, we addressed its possible correlation with the density limit in RFX-mod. In fact, 3D nonlinear MHD modeling shows that the *H number* rules the transition to quasi single helicity regimes, and, more in particular, the amplitude of $m=0$ edge magnetic structures, which, in turn, determine the highly radiative strongly 3D annulus

⁵⁸ Veranda M. et al., “*Magnetohydrodynamics modelling successfully predicts new helical states in reversed-field pinch fusion plasmas*” Nucl. Fusion 57 116029 (2017) <https://doi.org/10.1088/1741-4326/aa7f46>

⁵⁹ Veranda M., et al, “*Helically self-organized pinches: dynamical regimes and magnetic chaos healing*” Nucl. Fus. 60 016007 (2020) <https://iopscience.iop.org/article/10.1088/1741-4326/ab4863>

⁶⁰ Spinicci L., XXXIV cohort, Phd in Fusion Science and Engineering (Università di Padova, Ghent University) «3D nonlinear MHD modelling studies: plasma flow and realistic magnetic boundary impact on magnetic self-organization in fusion plasmas»

⁶¹ Vivenzi N., XXXIV cohort, Phd in Fusion Science and Engineering (Università di Padova, Ghent University) «Modelling of helically self-organized plasmas with 3D nonlinear magnetohydrodynamics: dimensionless parameters and transport studies».

(MARFE) in the high density discharges^{62,63}. A discussion is ongoing whether the *unified density limit model*^{64,65}, based on a 1D power balance constrained by impurity radiation losses (recently validated against several different configurations: RFP, ohmic tokamak and stellarator), could be interpreted as a “mean field version” of the above mentioned fully 3D process observed in RFX-mod.

3.6.2. *Lagrangian Coherent Structures*

The development of refined techniques to detect Lagrangian Coherent Structures (LCS), i.e. surfaces ruling the “motion” of magnetic field lines inside a chaotic domain^{66,67}, allowed explaining the formation of temperature gradients even in regions characterized by chaotic fields, as shown in the example of the Fig. 3.15⁶⁸. The development of an “LCS tool” has been the main subject of a PhD thesis discussed in March 2020⁶⁹, and has been recently further finalized⁷⁰. The tool is ready now for further applications to fusion configurations, as recently proposed in ENR project⁷¹.

⁶² G.Spizzo, G.Pucella, O.Tudisco, M.Zuin, et al, “Density limit studies in the tokamak and the reversed-field pinch”, Nucl.Fus. 55, 043007 (2019) <https://doi.org/10.1088/0029-5515/55/4/043007>

⁶³ M.E.Puiatti, P.Scarin, G.Spizzo, M.Valisa, et al., “High density physics in reversed-field pinches: comparison with tokamaks and stellarators”, Nucl.Fus. 49, 045012 (2009) <https://doi.org/10.1088/0029-5515/49/4/045012>

⁶⁴ Zanca P., Sattin F., Escande D.F., Pucella G. and Tudisco O., “A unified model of density limit in fusion plasmas”, Nuclear Fusion 57 (2017) 056010 <https://doi.org/10.1088/1741-4326/aa6230>

⁶⁵ Zanca P. Sattin F., Escande D.F et al, “A power-balance model of the density limit in fusion plasmas: application to the L-mode tokamak” Nucl.Fus. 59, 126011 (2019) <https://doi.org/10.1088/1741-4326/ab3b31>

⁶⁶ Di Giannatale G. et al, Phys. of Plas., 25-5 052306, (2018) <https://doi.org/10.1063/1.5020163>

⁶⁷ Pegoraro F. et al, PPCF 61 044003 (2019) <https://doi.org/10.1088/1361-6587/ab03b5>

⁶⁸ Veranda M., et al Nucl. Fus. 60 016007 (2020) <https://iopscience.iop.org/article/10.1088/1741-4326/ab4863>

⁶⁹ Di Giannatale G., *Magnetic confinement properties of 3D equilibria for fusion plasmas: nonlinear MHD modelling and experimental comparisons*, Phd thesis in Fusion Science and Engineering (Università degli studi di Padova, Università degli studi di Napoli Federico II, Universidade de Lisboa) (2019-2020).

⁷⁰ Di Giannatale G., *et al.* Manuscript ready for submission (under RFX internal review process).

⁷¹ Enabling Research Project Proposal (2021-2023) “Addressing nonlinear transport using a new method based on Lagrangian Coherent Structures”. Theory & Modelling (CfP-FSD- AWP21-ENR-03) Turbulence, transport, confinement.

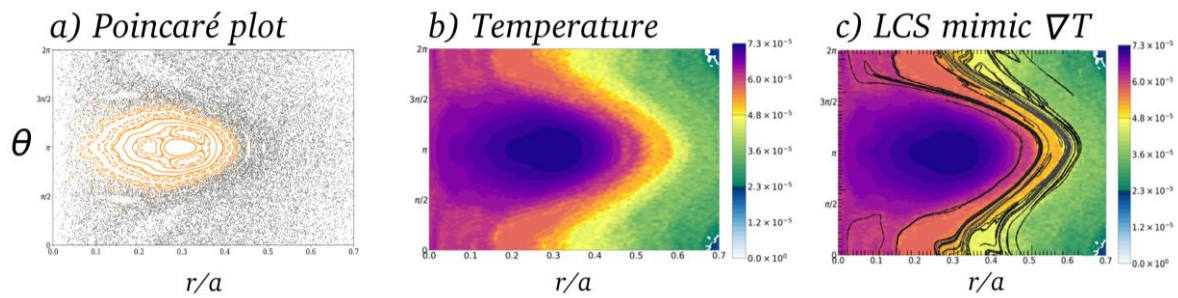


Fig. 3.15 MHD modelling shows that during the emergence of quasi-helical states, magnetic field lines stochasticity decreases (orange core of the Poincaré plot in panel a). The solution of the heat-transport equation at high-anisotropy with the Lagrangian algorithm (T3D) in panel b) reveals the presence of temperature gradient in the region of the Poincaré plot where a stochastic field is detected. The computation of the Lagrangian Coherent Structures of magnetic field lines reveals that they coincide with the temperature gradients detected by T3D.

3.6.3. *Use of machine learning tools in transport studies*

A preliminary assessment has been undertaken concerning the possibility to employ our basic -yet realistic- 3D nonlinear MHD modeling to train machine learning tools to address transport processes related to chaotic magnetic fields⁷². As a first step (in progress), we try to train a Neural Network to reconstruct internal magnetic fields from edge “measurements” using magnetic fields taken from our numerical simulations.

3.6.4. *Wave-particle energy transfer studies with Hamiltonian approach*

A basic physics study addressed recently in our group relates the process of wave-particle energy transfer adopting a Hamiltonian approach. It was shown that an irreversible energy transfer from a low frequency Alfvén wave to the particle gyration occurs, provided that the wave amplitude exceeds a threshold. The process represent a break-down of the adiabatic invariance of the magnetic moment, and the resulting net energy transfer to the particles is shown to be relevant to ion heating in the solar corona⁷³ and electron heating in the Earth magnetopause (work in progress). The background physical mechanism is very generic: it involves a break-down of the adiabatic invariant magnetic moment even under seemingly adiabatic conditions due to the existence of a pulsating separatrix in the phase-space of the system. Accordingly, it might be operative in several diverse scenarios, including fusion-relevant ones. Presently, we are exploring the possibility for the break-down of adiabatic

⁷² Cappello S. et al 28th IAEA FEC 2021 “Modeling of Basic Physics Issues in Toroidal Pinches and Tools for Performance Control” <https://conferences.iaea.org/event/214/contributions/17619/>

⁷³ Escande, Gondret, Sattin, Scientific Reports 9, 14274 (2019) <https://doi.org/10.1038/s41598-019-50820-x>

invariance to occur in Spherical Tokamaks in the presence of fast particles (i.e. beams ions or alpha particles).

3.6.5. ***Excitation of Alfvén eigenmodes by magnetic reconnection***

Concerning Alfvén waves in nonlinear 3D MHD simulations, as it was recently demonstrated for the RFP⁷⁴, the excitation of Alfvén eigenmodes by magnetic reconnection events is confirmed to occur in the simple visco-resistive modeling of circular tokamak configurations as well. In particular, the phenomenon is observed to be associated with plasmoids formation at high Lundquist number at the reconnecting $q=1$ surface in the tokamak core. The work is the subject of a PhD thesis in Fusion Science⁷⁵ (second year).

3.6.6. ***Simulation of disruption mitigation by shattered pellet injection***

Together with the modelling activities mainly related to RFP physics and the comparison with other magnetic configurations for fusion plasmas, a new activity specific to tokamaks started in 2018, with the use of the nonlinear MHD code JOREK for simulation of disruption mitigation by shattered pellet injection (SPI) in JET. The activity performed during 2020 relates the study of the dependency of the radiated energy upon the pellet composition, and, more in general, a sensitivity study upon SPI parameters (ablation and radiation models, number of shards, size and velocity distribution, Ne content, ...). A brief description of the results obtained so far can be found in the EUROfusion programme section 4.1.3.1.

3.7. ***Studies on RFP machine as Neutron Source and power generation***

The three-staged approach of a pilot Fusion-Fission Hybrid Reactor having a RFP as neutron source, proposed as alternative line respect to the more traditional solution with a Tokamak fusion reactor, has been further consolidated with studies aimed at identifying the optimum size of the minor radius with respect to performances (neutron production, wall loading and pulse duration)⁷⁶ for a continuously pulsed scheme⁷⁷, based on conservative scaling. On the one hand, for a given neutron production rate at a constant normalized density (n/n_e), a bigger minor radius implies a higher plasma current and a consequently a higher Volt-second consumption for the setting-up phase, implying a lower flat-top duration. On the other hand, at

⁷⁴ Kryzhanovskyy A. et al, poster presentation at EFTC (2019) <https://eftc2019.ugent.be/>. Paper in preparation

⁷⁵ Kryzhanovskyy A. XXXIV cohort, Phd thesis in Fusion Science and Engineering (Università di Padova - Ghent University) based at Consorzio RFX “*Alfvén waves excitation in toroidal fusion plasmas*”

⁷⁶ R. Piovan et al. “Status and Perspectives of a Reversed Field Pinch as a Pilot Neutron Source”, IEEE Trans. On Plasma Science, Volume: 48, Issue: 6, June 2020

⁷⁷ R. Piovan et al. “A continuous pulsed Reversed Field Pinch core for an ohmically heated hybrid reactor”, Fusion Eng. Des., vol. 136, pp. 1489–1493, 2018, doi: 10.1016/j.fusengdes.2018.05.040.

smaller minor radius, less plasma current is required to obtain the given neutron flux, with a corresponding reduction of Volt-seconds consumption; the smaller minor radius also implies a higher loop voltage, limiting again the flat-top duration. For a machine with $R=4\text{m}$ and neutron production to $19 \cdot 10^{18}$ n/s, this optimization would imply $a=0.8\text{m}$. These results are based on the assumption that RFX-mod2 will obtain improved performances, thanks to the machine enhancements presently underway, but would also require to consolidate RFP scaling at a higher plasma current than 2MA: To this end studies have been started in order to expand the present current limit of RFX-mod with an auxiliary magnetic energy storage⁷⁸. With a 125 MJ magnetic energy storage the RFX-mod2 maximum plasma current could be increased up to 2.6 MA.

4. EUROfusion Programme

4.1. ITER Physics Work Packages

4.1.1. Introduction

The Covid19 pandemic has caused the cancellation of almost all of the participations to the EUROfusion experiments. Nonetheless a significant amount of work has been done "at home" for the analysis of the experiments followed remotely, particularly on AUG, TCV and JET, or for more general tasks. JET has finally reached the full beam power capability and closely approached the target key parameters needed to justify the DT campaign foreseen in 2021. T only experiments have started, though there have been some delays in the NBI commissioning in Tritium, which will delay the beginning of JET Experimental Campaign C40 in 2021.

MAST completed its seven years upgrade programme with the first plasma of the renewed machine at the end of October. W7X has continued its shutdown in preparation of the experiments with actively cooled divertor and PFCs expected to start in the second half of 2022. JT-60-SA has started the preparation for the first plasma by cooling down the magnets. DTT has seen an increased number of studies on plasma scenarios, divertor configurations, diagnostics and the NBI system, while a structured organization was forming with RFX leading the groups of physics, divertor modeling and diagnostics integration. In the following the main activities related to the EUROfusion ITER physics and DTT are presented in some detail..

⁷⁸ F. Lunardon et al. "Feasibility study of RFX-mod2 performance improvement by additional magnetic energy storage", submitted for publication to Fusion Engineering and Design

4.1.2. MST1

4.1.2.1. Topic 06- Disruption prediction and avoidance

Within the high-level topic T06 during year 2020 the activity aimed at reconstructing the exact topology of the $m/n=2/1$ islands preceding a disruption, has continued. An obstacle in reconstructing these islands in detail is the presence of passive structures surrounding the plasma, such as the Vacuum Vessel (VV) and the Passive Stabilization Loop (PSL). These interact with the current produced by the tearing modes (TM), which possess frequencies in between 25 Hz and 10 kHz (1.7kHz in the case studied in ⁷⁹), and pollution in the $B\theta$ pick-up probe measurements has been already pointed out in the past⁸⁰. To this end, an original model of the surface current associated to each resonant surface has been developed and has been coupled with a magneto quasi-static (MQS) integral formulation. As a result, the eddy currents induced by an arbitrary linear combination of rotating TMs has been computed (direct problem), allowing for retrieving the real structure of each TM with periodicity $m=n$ (inverse problem). During year 2020 the direct problem has been solved⁸¹, while the inverse problem is work in progress for year 2021. An example of the result obtained is shown in Fig. 4.1: the magnetic field generated by a linear combination of two modes with periodicity 2/1 and 3/1, with no pollution, is plotted together with the fields generated by the TM together with VV plus

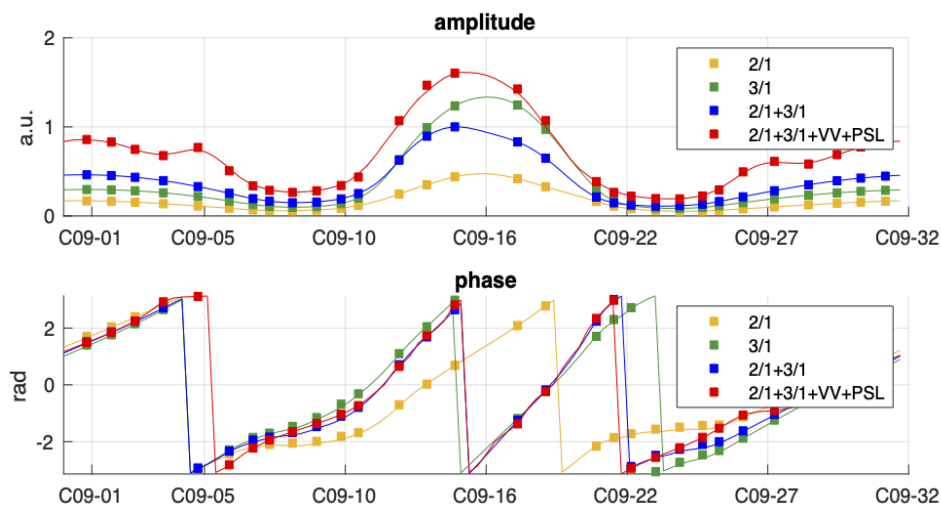


Fig. 4.1 comparison of the actual signals (red) at pick-up coils (C09-XX) w.r.t. the ideal case (blue) for a linear combination of two modes with periodicity $m/n=2/1$ and $3/1$

⁷⁹ G. Spizzo, R.B. White, M. Maraschek, V. Igochine, G. Granucci, and the AUG Team, “Nonlocal transport in toroidal plasma devices,” Nucl.Fusion, 59, 016019 (2019). <https://doi.org/10.1088/1741-4326/aaf07c>

⁸⁰ M. Schittenhelm and H. Zohm, “Analysis of coupled MHD modes with Mirnov probes in ASDEX Upgrade,” Nucl. Fusion 37,1255 (1997)

⁸¹ D.Voltolina, P. Bettini, R. Specogna, G. Spizzo, M. Maraschek and V.Igochine, *Proc. Nineteenth Biennial IEEE Conference on Electromagnetic Field Computation* (CEFC 2020, Pisa, November 16-18, 2020 Virtual Event) oral contribution WM O2, <https://www.cefc2020.org/technical-program/>

PSL. The effect of the VV tends to reinforce the actual field at the magnetic sensors positions w.r.t. the ideal case (field produced only by TMs), while the effect of the PSL tends to reduce the actual field behind it, and in the end the effect of the VV dominates over the PSL. These results have been recently submitted⁸². As a consequence, concerning the inverse problem of reconstructing the topology of the 2/1 island, one can expect the real size of the islands in pre-disruptive AUG discharges to be smaller than previously calculated on the basis of magnetic signals, thus maybe finally explaining a long-standing discrepancy between field-line tracing codes and ECE measurements in ASDEX Upgrade⁸³.

4.1.2.2. Topic 8 - Runaway electron beam physics and MGI in support of ITER SPI

Experiments on runaway electrons (RE) generation and mitigation have been performed during the year 2020 in AUG, TCV and COMPASS devices.

Most of the RE campaign in ASDEX Upgrade and TCV has been finalized to the study of runaways suppression by Massive Gas Injection (MGI) in plasmas with different equilibria (i.e. by varying I_p , $q(a)$, $B_T(a)$ etc); in addition, few shots have been dedicated to investigate the effect of externally applied 3D magnetic perturbations (MP) on RE beams in COMPASS.

A numerical test particle approach based on the Hamiltonian guiding center code ORBIT (relativistic version¹⁸⁴) has been used to interpret the data collected during ASDEX Upgrade experiments on RE mitigation executed in the past years. In agreement with the observed phenomenology, ORBIT simulations show that the configuration of the currents in the top/bottom arrays of error field coils which maximizes the plasma response to the applied perturbations is the one that most affects the high energy test electron trajectories in the edge region, thus leading to an enhancement of the energetic electron losses. This occurs both before and especially during the disruption, in the latter case taking into account the increased toroidal electric field associated to the fast plasma cooling. The same scheme could be applied also to analyze the experiments in COMPASS. Used in a predictive way, the numerical results suggest which coil configuration might further improve the RE mitigation.

Moreover, recently the guiding center code ORBIT has been installed at IPP Prague, in order to develop a reduced model of transport of runaway electrons in tokamaks, and to validate it over existing data in the COMPASS and RFX-mod devices (the latter operated as a circular tokamak). Reduced models are much faster than guiding centre codes in describing particle transport, while retaining the basic physics of the phenomenon. Moreover, the standard

⁸² P.Bettini, G.Spizzo, D.Voltolina, L.Marrelli, M.Maraschek, V.Igochine, R.Specogna, the ASDEX Upgrade Team, the EUROfusion MST1 team, submitted to IEEE Trans.on Magnetics (2020).

⁸³ J. P. Meskat, H. Zohm, et al., "Analysis of the structure of neoclassical tearing modes in ASDEX Upgrade," PPCF 43, 1325-1332 (2001).

⁸⁴ M. Gobbin et al Nucl. Fusion **57** (2017) 016014

approach for RE reduced transport models is diffusive: an Enabling Research project has been submitted⁸⁵, where an alternative, distinct approach based on a Montroll-Weiss subdiffusive equation is proposed, which could be further implemented in the EUROfusion standard software. The choice of the devices (COMPASS and RFX-mod) where to validate the model, is motivated by the necessity of knowing the perturbation spectrum quite in detail (in terms of poloidal and toroidal mode numbers m and n) and of possessing an ample database in terms of perturbation amplitudes (at least one full decade) and phases.

4.1.2.3. T09: Error Field Detection and Control

Spurious magnetic fields, known as error fields (EFs), are inevitably present in fusion devices and can be associated with either stationary non-symmetric electromagnetic sources (e.g. feedthroughs of the machine magnet system coils) or with transient phenomena inducing eddy currents with asymmetric geometrical features on passive structures of a specific machine.

The EUROfusion MST1 Work Package titled T09: *Error Field Detection and Control* aimed at characterizing intrinsic EFs in AUG (IPP, Garching, Germany) and in MAST-U (CCFE, Culham, UK) and delivering EF correction strategies. This study contributes in defining the EF correction for ITER, a key topic in the ITPA MHD, Disruptions and Control Topical Group.

In AUG, EF studies have been focused on low-torque ITER relevant regimes and in high-beta_N (β_N) plasma scenarios. The intrinsic EF, associated with PF coil feedthroughs, has been characterized by means of sophisticated EM CAFE⁸⁶ modelling. It is of paramount importance compensating such EF because it can cause locking of a ($m=2, n=1, 2/1$) mode, compromising the experimental target, and also leading to the premature end of the discharge. Two EF correction strategies have been derived from EM CAFE modelling, in vacuum approximation, and have been tested: the so called Virtual Shell and the Mode Control. Experiments showed that Mode Control approach is more effective than the Virtual Shell one in compensating the intrinsic EF, confirming RFX-mod tokamak and reversed-field pinch results. Besides this, the Mode Control approach which aims at reducing the $n=1$ component at $q=2$ only allows for the best achievements, the $n=1$ being the harmonics which mostly interferes with the plasma.

Fig. 4.2 shows the main result obtained in low-torque ITER relevant regime: by utilizing the EF correction current pattern highlighted in blue on the right panel, lower density can be achieved with respect to the reference plasma. This allows thus to explore a wider operation space in AUG, which was limited before by the triggering of a 2/1 locked mode.

⁸⁵ Enabling Research Project Proposal (2021-2023) "Development of a reduced, relativistic and subdiffusive model for runaway electron transport". Theory & Modelling (CfP-FSD- AWP21-ENR-03) subtopic 3.3 MHD, disruptions and fast particle physics.

⁸⁶ Bettini, P., et al, IEEE Trans. Magn., vol. 50, no. 2, Feb. 2014

To interpret the experimental results and to design future EF correction studies in AUG, the coupling between CAFE and MARS-F⁸⁷ codes has been developed, based on the equivalent surface current concept. This suite of codes has given promising results in terms of vacuum modeling of the external EF (Fig. 4.3), based on the AUG shot #36906. By calculating the plasma response to this EF as well, this method will allow tailoring of dedicated correction fields to be tested in future experiments. Preliminary work to apply the same procedure to MAST-U plasmas has been started, in preparation of 2020/2021 experimental campaigns.

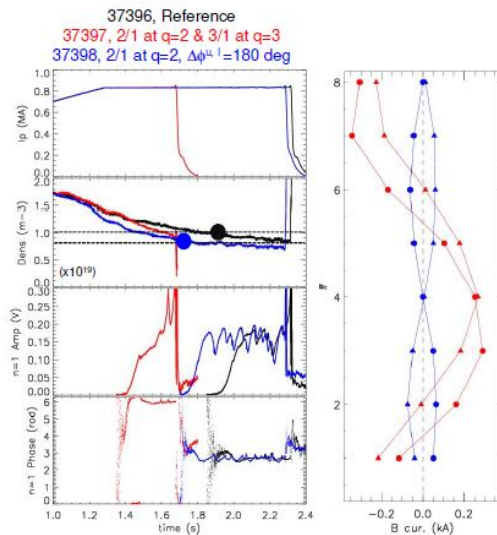


Fig. 4.2 Error Field correction in the low-torque ITER relevant regime.

EF correction has been tested in AUG also at high- β_N . Such experiments have been more challenging because the plasma scenario was not reproducible and a technical issue, i.e. inverted polarity in one error field correction coil, the BL5, has been encountered.

To optimize the plasma scenario, ECRH settings have been tuned for avoiding 3/2 and 2/1 NTMs, and EF correction based on the multi and single Mode Control approaches have been tested. It is worth mentioning that a straightforward comparison among high- β_N discharges cannot

be performed because the plasma, in which the multi Mode Control has been applied, had unwillingly inverted polarity in BL5-coil, which introduces an extra localized EF at this coil position. On the other hand, the plasma, in which the single Mode Control has been applied, had a 3/2 mode triggered while reaching the highest β_N values. Despite these caveats, by comparing the reference discharge with the plasma with single Mode Control applied, we can conclude that with EF correction β_N values around 3.2-3.3 have been achieved, while the reference case, without EF correction, has $\beta_N=3.0$. Besides this, the plasma rotation is also higher in the case with error field correction, as reported in Fig. 4.3.

T09 envisaged EF detection and correction studies also in the MAST-U device. Being the commissioning phase of this new experiment still ongoing, experiments have not been performed yet, but could be performed within the end of the year. The experimental plan has been finalized and foresees the characterization and the correction of the n=1 intrinsic EF only, being the shot budget limited to 15 shots. The compass scan technique will be applied by means of two coil sets: the ELM coils and the EF correction coils, placed internally and

⁸⁷ Liu, Y. Q., et al, Physics of Plasmas 7.9: 3681-3690, 2000

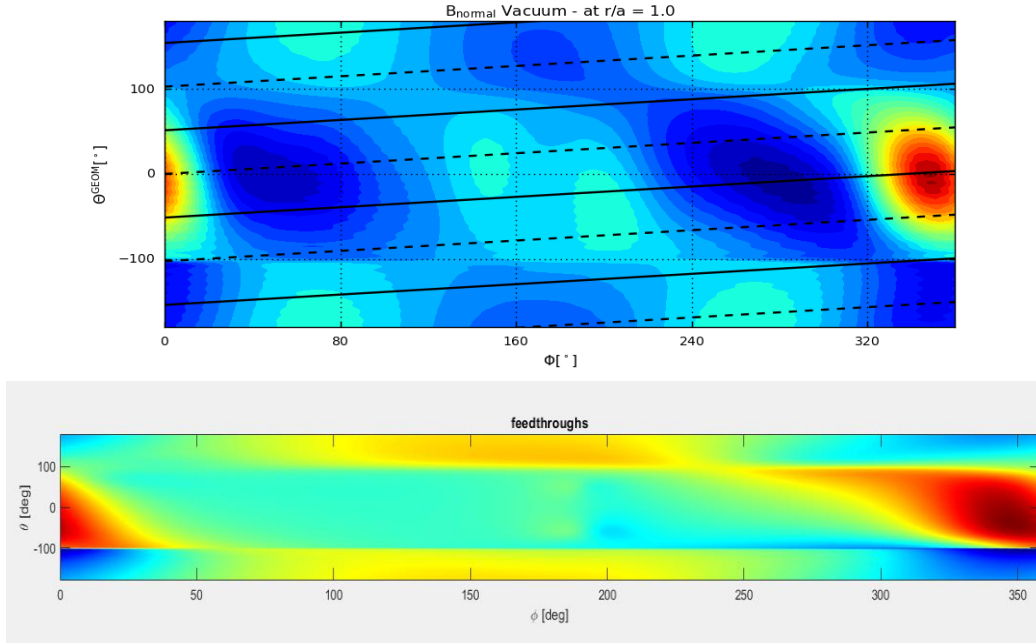


Fig. 4.3 (Top) Vacuum field calculated with MARS-F, approximated with a given set of toroidal Fourier harmonics. (Bottom) EF calculated with CAFE on the selected coupling surface

externally with respect to the vacuum vessel, respectively. Once magnetics data have been collected and analyzed, the EF correction strategy for $n=1$ EF minimization will be identified and ad-hoc experiments, aiming at testing the robustness and reliability of the EF correction, will be performed.

In preparation to MAST-U EF experiments, and, in particular, to assess effects on plasma configuration induced by EFs or external perturbations, a description of MAST-U was implemented for the VMEC code along with magnetic measurements for the V3FIT code. The combined use of VMEC and V3FIT will allow a plasma equilibrium computation from measurements. The present configuration does not include the full set of local probes so one cannot take full advantage of the 3D analysis, but it is useful for testing the results and consider a benchmark on a dry-run between modelled and measured data.

Fig. 4.5 shows magnetic measurements that were implemented in V3FIT: red crosses are local probes and blue lines are flux loops. The first wall and a plasma equilibrium are also shown.

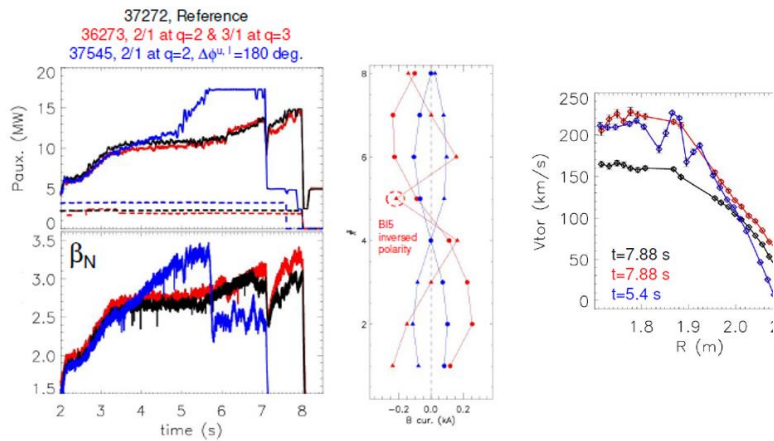


Fig. 4.4 Error Field correction at high-beta.

The next step will be to implement additional non-axisymmetric coils (ELM coils are already modelled for VMEC) and the full set of magnetic sensors as well as kinetic measurements⁸⁸⁸⁹⁹⁰⁹¹⁹².

4.1.2.4. Topic 11 Fast ion losses

The investigation on AUG NBI fast ion losses due to non-axisymmetric magnetic fields generated by Resonant Magnetic Perturbation (RMP) is being carried. The goal of the activity is to evaluate if fast ion losses generate a non-balanced radial current⁹³, which affects the radial electric field E_r ⁹⁴. The search for couples of AUG shots with similar densities (and therefore NBI deposition) but with RMP active in one case and off in the other is ongoing, with the identification of possible candidates. After the implementation in ASCOT⁹⁵ Monte Carlo code of the formula for the radial current due to fast ion losses, j_r , a benchmark between ASCOT 4 and 5 versions is now being performed.

4.1.2.5. Topic 13 TCV

Fixed boundary equilibrium analysis of shot #66046 at 0.65s were performed using IET code. The results in terms of plasma global quantities, flux surfaces and internal profiles were verified using RT-LIUQE/CHEASE (FBTE). Finally, the IET inverse reconstruction of coil currents was checked with the free-boundary FRIDA code.

4.1.2.6. Topic 16

In the framework of WP-MST1-Topic 16, investigation on AUG has concentrated on H-Mode shoulder formation. Shoulder formation has been achieved even in high P_{sep}/R condition whenever sufficiently high neutral pressure is observed. Shoulder formation has been checked

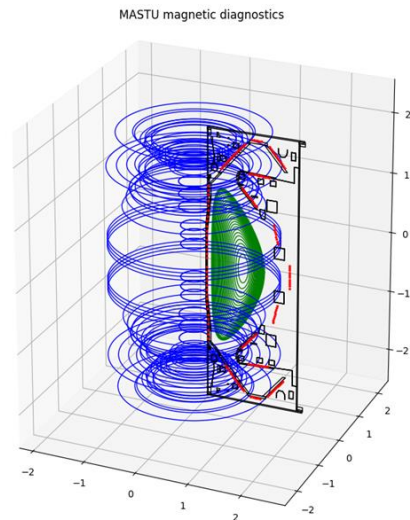


Fig. 4.5 V3FIT magnetic modelling with first MAST-U equilibrium calculation

⁸⁸ L. Pigatto et al, contribution at 47 EPS Conference

⁸⁹ M. Bonotto et al, contribution at 47 EPS Conference

⁹⁰ L. Piron et al, contribution at 47 EPS Conference

⁹¹ V. Igochine et al, contribution at 47 EPS Conference V. Igochine et al., Correction of small error fields at high βN in ASDEX Upgrade, paper in preparation

⁹² ITPA MHD, Disruptions and Control Meeting, 19-22 October 2020, MDC-19 Updates for ITER Error Field Correction Criteria, presented by J.-K. Park and N. C. Logan

⁹³ Heikkinen J.A. et al., "Neoclassical Radial Current Balance in Tokamaks and Transition to the H Mode", PRL 84.3 2000

⁹⁴ T.E. Stringer 1995 Nucl. Fusion 35 1008

⁹⁵ E. Hirvijoki, et al., Comput. Phys. Commun. 185 (2014) 1310–1321.

to build up with partial detachment of the outer strike-point, whenever this recycling condition is achieved through increased divertor fueling. On the other hand, power step experiments have revealed that once the shoulder is formed, plasma re-attachment through power increase does not bring back the upstream profile to the original shape. Key ingredient to the formation of the shoulder appears to be the neutral pressure at the midplane rather than the recycling state of the divertor and this has been proved by achieving high dissipative divertor, with strong detachment, through N₂ seeding, while keeping a low divertor fueling. In this experimental condition no upstream profiles flattening is observed, similarly to what seen in TCV in L-Mode, C-Mod and JET. Concerning filamentary transport, it has been noted that in H-mode condition with shoulder formation, strong variation of the filament dynamic occurs, with a general increase of the radial velocity of the filaments as inferred by the Thermal Helium Beam diagnostic, and also a variation of the filament frequency which nicely correlates with the midplane neutral pressure. In line with these observations whenever strong detachment is reached through N₂ seeding with low divertor fueling no sensible modification of the inter-ELM filament properties is observed.

A scenario for H-Mode shoulder formation has been obtained on TCV as well, through an increased upper triangularity and strong divertor fueling. As for AUG, strong neutral pressure is needed even though it has not been possible to assess if divertor or midplane neutral density plays the bigger role. On the other side, whenever the shoulder is formed, more skewed Probability Distribution Function on the ion saturation current at the wall is observed, suggesting an increase of the intermittent transport. Emphasis has been put as well in assessing the difference between baffled and unbaffled operation on TCV. With similar density at the separatrix and fueling level, density shoulder has not been observed in baffled scenarios, suggesting again a strong role played by the midplane neutral pressure in establishing flatter profile in the SOL. Numerical work is in progress to tackle this problem using turbulence codes with neutral interaction included.

4.1.3. **JET1**

4.1.3.1. **JOREK Modeling**

Jorek modelling of Shuttered Pellet Injection (SPI) into JET H-mode plasmas has been performed, with the main goal of providing support to the SPI experiments carried out on JET starting from 2019. After first tests with a pure Ne small pellet (4.5 mm diameter), a set of JOREK simulations with a mixed D₂/Ne medium pellet (8 mm diameter) has started. A scan in Ne content is ongoing, with the main goal of studying the increase of radiated energy with injected Ne atoms, looking in particular at a possible radiated energy saturation as observed in JET experiments. Another important task is the characterization of the radiation asymmetry,

mainly as a function of the toroidal angle. As in previous JOREK studies D. Hu et al, Nucl. Fusion 2018, in present simulations the thermal quench is observed to be triggered by the global magnetic field stochastization due to SPI-induced MHD modes (both "n=0 current contraction" and "helical cooling" mechanisms). A significant dependence on SPI parameters (ablation and radiation models, number of shards, size and velocity distribution, Ne content, ...) is also found. Synthetic diagnostics (Prad ...) have been introduced and validation against experimental data is ongoing.

4.1.3.2. TRANSP modeling

The main aim of the 2020 JET campaigns (C38B, C38C and C39) has been that of pursuing a neutron flux of 5×10^{16} n/s sustained for 5 seconds, with total input power larger than 36MW in preparation of the 2021 JET-DT2 campaign. Both interpretive and predictive TRANSP analysis have been carried out with TGLF as the transport model. The interpretive modelling, in support of the experimental campaigns, has been performed to assess the core plasma performance in high power, medium β_N (~1.9) baseline pulses and high β_N (~2.3) hybrid plasmas, identifying the transport channels that limit the fusion product, contributing to the preparation of the TT and DT following campaigns. The predictive studies have been carried out with the final scope of extrapolating the fusion output of the best performing baseline plasmas (in particular JPN96482 and JPN96994) to the DT operation, with 40 MW of input power, including realistic impurity mix, radiated power, and pedestal properties. The TGLF transport model has been tuned on a database of Deuterium baseline plasmas, reproducing the experimental kinetic profiles. The optimal settings have been then used to compute the DT plasma profiles at different input power. Sensitivity scan on rotation velocity and ICRF scheme have been also performed. The expected output of the DT baseline plasmas at 40 MW ranges from 13 MW to 18 MW. The main experiments and tasks involved in this studies are M18-01, M18-02, T17-07.

4.1.3.3. L-H transition studies

The work on L-H transition studies continued in 2020, within JET Task M18-14, whose aim is to investigate the physics of the existence of a minimum density for the L-H transition power in JET, and to evaluate the importance to the ion channel heating. In 2020, the power balance analysis of 3 different JET Deuterium, NBI-heated plasma datasets, having different divertor configurations, has been concluded. A dataset from 2019 JET D campaign has indeed been added, since core T_i measurements resulted available again. Each dataset contains 3 or 4 selected shots at different plasma densities, around the $n_{e,min}$ characterizing the L-H transition.

For each shot an interpretive transport simulation by JETTO⁹⁶ within JINTRAC has been run, using ASCOT5 to model the NBI-plasma interaction. The results of the power balance analysis show that, for these NBI-heated JET D discharges, the power coupled to the ions, $Q_{i,LH}$, is not linear with density at the L-H transition. JET experiments seem to confirm the theory elaborated for AUG NBI-heated plasmas⁹⁷, despite the differences in the heating schemes, with RF-heated discharges in AUG and C-mod, where the threshold $Q_{i,LH}$ has been shown to be linear with density⁹⁸. $Q_{i,LH}$ seems therefore not to be the key to explain the existence of a minimum L-H power threshold in density, for JET NBI plasmas. The model to estimate the L-H power threshold proposed recently by Bilato et al.⁹⁹ has been applied to JET data showing a good match with experimental data. These JET results have been presented in an invited talk at the AAPPS 2020 e-conference¹⁰⁰.

4.1.3.4. M18-01-M18-02-M18-07 W transport studies

The development of high performance “Hybrid” discharges in view of DT operations has been followed with an emphasis on the study of the role of W, which can profoundly influence the pulse evolution since the very beginning. Core-edge integrated simulations have been carried out by means of the COCONUT suite of codes that include JETTO for the plasma core and EDGE2D for the edge. ELM’s have been included in the simulations since they have an important role in expelling W from the pedestal region as well as enhancing the W source in the same time. The activity follows a long standing research (M13-25, M15-04 and M18-07 experiments) aimed at identifying ITER-like conditions in which W is expelled by the neoclassical-transport-dominated edge barrier, in which case the ELMs would reverse their effect and inject the W accumulated outside the pedestal. In Fig. 4.6 the W content in the plasma core is simulated along a gas scan and compared with experimental results. In the simulation the effect of gas puffing on the toroidal rotation is neglected. In fact, in M18-01 baseline experiments it has been shown that no gas puff conditions bring the plasma to very high rotation level, which tend to keep W in the peripheral volume, and to very high neutron rates. Actions have been taken in order to have the possibility to self-consistently compute in COCONUT the ELM triggering by coupling the edge stability code MISKA; a feature made available just at the end of December.

⁹⁶ Cenacchi G. and Taroni A. 1988 Rapporto ENEA RT/TIB(88)5

⁹⁷ F. Ryter et al. 2014 Nucl. Fusion 54 083003

⁹⁸ M. Schmidtmayr et al 2018 Nucl. Fusion 58 056003

⁹⁹ R. Bilato *et al* 2020 Nucl. Fusion **60** 124003

¹⁰⁰ P. Vincenzi et al., “Power balance analysis of JET-ILW L-H transition in Deuterium plasmas”, Invited talk, 4th Asia-Pacific Conference on Plasma Physics, 26-31Oct, 2020, Remote e-conference

4.1.3.5. M18-06 experiment: Impact of inner leg flux geometry on W influx

In the JET ILW experiment, the effects of the flux-expansion variation at the inner strike point location on the core W content and on the bulk radiation have been studied. The divertor geometries have been designed using the plasma equilibrium code CREATE-NL and experimentally achieved by a proper optimization of the divertor coils current in a few discharges with similar additional heating. Spectroscopic diagnostics were used to examine in both inter-ELM and intra-ELM phases the tungsten source from the divertor tiles, the W content and profile shape inside the plasma core and the total radiation. It has been found that there was not a strong impact of the flux expansion on the tungsten erosion at the strike point. A discharge with high flux compression has shown nonetheless a slight increase in core tungsten concentration, but this might also be the result of changes in ELMs frequency due to flux expansion variation. The effect on ELMs dynamics has been clearly observed making more difficult the analysis. Edge analysis has been performed with the SOLEDGE2D-EIRENE code excluding a significant variation of edge transport with flux expansion, pointing to an indirect effect on pumping efficiency and consequently on edge density effects.

4.1.3.6. M18-09: Prepare integrated RTC schemes for scenarios experiment

M18-09 experiment aimed at developing and testing real-time (RT) controllers for JET Deuterium-tritium (DT) operation which is planned in 2021 and at exploiting state space observer tools, such as RAPTOR, to monitor the plasma evolution. When operating JET in DT, each plasma discharge will in fact be a precious resource, being both T and neutron budgets limited. The main developed RT controllers for DT campaign are:

- isotope ratio controller, which will maintain the required 50:50 DT ratio needed to favor nuclear fusion processes;

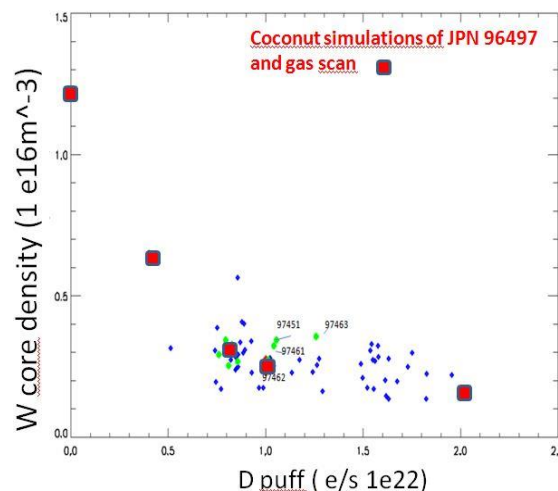


Fig. 4.6 Comparison between experiment and core edge integrated simulation of W core content in a puff scan of a hybrid discharge.

- the dud detector, which will terminate a discharge moving towards under-performing states;
- a series of improved RT controllers for detecting excessive radiation:
- brand-new detectors, also based on machine learning approaches, have been implemented for detecting off-normal events or pre-disruptive states in the new Plasma Event TRiggering and Alarms (PETRA) system.

The RAPTOR suite has been deployed into JET and will be used to identify control schemes, within RAPTOR capabilities, which could contribute to support the development of high performance plasma scenarios and to monitor the plasma behavior and possibly diagnostic faults. Outcomes: ¹⁰¹ ¹⁰² ¹⁰³ ¹⁰⁴¹⁰⁵

4.1.3.7. M18-41: Divertor geometry effect on detachment and SOL

On JET, analysis of data collected during the M18-41-2019 campaign continued. The spectroscopically derived average Outer Target temperature $\langle T_e \text{ OT} \rangle$ proved to be a key ingredient to describe the recycling state of the divertor. In a set of low- δ NBI heated plasmas, the different response of horizontal (HT) and vertical target (VT) to fueling, in term of separatrix density and pedestal properties, has been reconciled. Neutral line density has been inferred from spectroscopic means showing how different divertor configurations follow similar trends whenever considered in term of $\langle T_e \text{ OT} \rangle$. Finally, the far SOL e-folding length has been determined combining HRTS and Li-Be diagnostic: a progressive flattening is observed both in horizontal and vertical target whenever higher recycling condition is achieved and no sensible differences between HT and VT arises whenever the line density is considered as a function of $\langle T_e \text{ OT} \rangle$.

4.1.3.8. B18-19: Locked mode avoidance by the use of EFCCs system

B18-19 experiment aimed at identifying the intrinsic error fields (EF) in JET and at compensating it by means of error field correction coils (EFCCs). The compass scan technique has been applied to identify the $n=1$ EF. The first set of compass scan data has been acquired using EFCCs in $\phi=315^\circ$ configuration, suggesting that an intrinsic EF is present. To fully

¹⁰¹ L. Piron et al 2019 Fusion Engineering and Design 146 1364-1368

¹⁰² L. Piron et al Progress in preparing real-time control schemes for Deuterium-Tritium operation in JET submitted to Fusion Engineering and Design Journal

¹⁰³ - L. Piron et al Poster contribution titled Progress in preparing real-time control schemes for Deuterium-Tritium operation in JET at SOFT 2020 virtual edition - 31th Symposium on Fusion Technology, Virtual Edition, 20-25/09/2020

¹⁰⁴ C. Piron et al Development of the RAPTOR suite of codes towards real-time - reconstruction of JET discharges submitted to Fusion Engineering and Design Journal

¹⁰⁵ - C. Piron et al Poster contribution titled Development of the RAPTOR suite of codes towards real-time reconstruction of JET discharges at SOFT 2020 virtual edition - 31th Symposium on Fusion Technology, Virtual Edition, 20-25/09/2020.

characterize the EF more experimental time is needed. Dedicated experiments have been planned and are under discussion. By analyzing data collected so far, an interesting synergy among locked mode and Beta Alfvén Eigenmodes (BAEs) activity has been observed. Such MHD activity has been characterized considering various diagnostics and calculating the Alfvén continuum distortion associated with 3D $n=1$ perturbations. The main B18-19 experimental and modelling results will be presented at the forthcoming 47 EPS conference.

4.1.3.9. Pedestal analysis and isotope effect: GENE modeling

In the framework of task T17-05 the activity related to the study of the isotope effect on pedestal instabilities and turbulence has further proceeded. Two couples of D/H discharges characterized by the same stored energy and the same input power have been compared by artificially changing the main ion mass (D to H, and vice versa) so as to disentangle isotope from profile effects. The analysis has been carried out with the gyrokinetic code GENE focusing on the steep gradient region of the pedestal. The effort has tackled different levels of complexity, moving from linear to nonlinear simulations and from local to global domains. Local flux-tube simulations in the ETG range have revealed the absence of isotope mass dependence in the heat fluxes. On the contrary, global linear simulations have shown differences in the transport coefficient ratios at low wavenumbers, and a more complete view of the instabilities present in the pedestal with respect to local calculations. Finally, the first global nonlinear simulations show an anti-gyro-Bohm mass scaling of the ion/electron heat fluxes in qualitative agreement with the experiment.

4.1.3.10. Plasma equilibrium

The computation of plasma equilibria close to disruptions may require a non-axisymmetric approach. This issue was faced with two approaches: running EFIT with octant specific information and VMEC/V3FIT, respectively. The first approach has some issues since there is no real link among the equilibria computed for different octants. In this respect it was observed that differences in reconstructed equilibria are within uncertainties due to error bars in magnetic measurements. When using VMEC/V3FIT we have instead a full 3D description, but it was observed that the lack of a clear information on currents induced on passive structures has a non-negligible effect. This issue is indeed true also for the EFIT runs though in this case an axisymmetric model for passive structure is implemented and is being tested.

One aspect to note is the lack of internal measurements (e.g. temperature and density profiles) due to the small size of the plasma (for VDE) so the computation has to rely on magnetic measurements only and internal profiles are modelled with low order polynomials based on theoretical expectations.

4.1.4. *DTT*

Coordination of the physics activities has led to a first draft of the scientific program of the DTT experiment, which has been used to plan and launch the activities for 2021. In a similar way, coordination of the divertor physics studies, diagnostics integration and of the NBI design have prepared the path for related activities in 2021 and beyond.

4.1.4.1. *PEX/DTT Neutrals and impurities model and pumping in SN configuration*

- To define the requirements of the DTT divertor pumping system the plasma and neutral parameters in the divertor region in relevant plasma scenarios are to be evaluated. Plasma scenarios in terms of gas-puffing and particle flux from the core have been developed and then modeled with the SOLEDG2D-EIRENE edge code. Two full power scenarios have been developed for the DTT single null (SN) configuration high performance phase at 5.5 MA, corresponding to a low and high puffing Deuterium cases respectively. In both cases nitrogen and neon seeding were used to achieve heat fluxes and plasma temperature at the targets compatible with divertor heat flux removal and tungsten sputtering. It has been found that nitrogen seems more effective than neon to achieve deep detachment but this does not seem to affect neutral pressure. Plasma and neutrals evaluated parameters have been passed on to the Karlsruhe Institute of Technology (KIT) to compute neutral gas dynamics in the DTT sub-divertor.

4.1.4.2. *Neutrals and impurities model and pumping in DND configuration*

To compare the relative advantage of the Double Null Divertor configuration (DND) with respect to the Single Null Divertor (SND) it is necessary to consider also the requirements in terms of divertor pumping. Indeed in a DND fusion reactor the duplication of the pumping system in the upper part of the vessel affects both directly, due to the cost of the additional system, and indirectly, in terms of a reduced surface for the blanket and of reliability, due to the presence of additional components and vessel apertures. To this aim identical DND scenarios have been compared with respect to different pumping solutions. Two DND full power scenarios at medium and high density for Day 2 DTT at 5.5 MA have been analyzed, considering pumping from both divertors or from the bottom one only. Neon seeding was used to achieve heat fluxes and plasma temperature at the targets compatible with divertor heat flux removal and tungsten sputtering. Large D puffing was used to stress the pumping system. It has been found that pumping from bottom only provides an easier achievement of detachment than pumping from both divertors. The comparison with previous similar analysis performed for the SND configuration does not show an advantage of the DND in obtaining higher radiation fraction but further analysis is required to assess the effect of gas puffing

location. Plasma and neutrals parameters have been evaluated and passed on to KIT to compute neutral gas dynamics in the DTT sub-divertor region in both pumping cases.

4.1.4.3. Negative triangularity modeling

The possibility to experiment high power flux plasma scenarios in negative triangularity (NT) since the first operation period of DTT, without involving important modifications of the present design, but even proposing minor modification of the in vessel components and of the poloidal circuits, has been explored.

In this contest power exhaust modelling has been carried out to analyze the compatibility of negative triangularity equilibrium configurations and the proposed divertors and first wall.

The study of the performance of the divertors has been done in pure Deuterium at medium density ($n_{\text{sep}}=8 \cdot 10^{19} \text{ m}^{-3}$) and a power flowing to the SOL ($P_{\text{SOL}}=8 \text{ MW}$) slightly above the threshold for L-mode to H-mode transition in positive triangularity (PT). A preliminary assessment of the reference scenario at full power has been also done with neon seeding to radiate up to 90% of the power crossing the separatrix.

The most critical point of the modelling has been the selection of transport parameters. In PT case χ at the separatrix has been chosen to provide in the attached condition a heat flux fall-off length (λ_q) close to the one computed by the empiric scaling based on inter-ELM measurements, which predicts $\lambda_q \approx 1 \text{ mm}$; while for particle transport was chosen $D=\chi/3$. No scaling is presently available for the negative triangularity (NT) case, neither are available experimental evaluations of edge χ and D. For this reason χ and D were selected considering that in present experiments NT provides high confinement in L-mode discharges characterized by ELM-free and low amplitude edge transport barrier

The final results of the edge modeling were strongly affected by the higher transport parameters used for NT configuration: it has been found that the NT configuration detaches at all targets and also the heat fluxes are very small in NT. Instead the PT has been found attached with temperature higher than 20 eV. Modelling with neon seeding has confirmed pure Deuterium results in terms of an easier detachment of NT configuration and lower Z_{eff} at the separatrix for the same or higher radiation. In general the NT configuration has been found well compatible with proposed divertor and wall modifications.

The feasibility of testing NT configuration in DTT has been evaluated also in term of power load on the first wall in limiter configuration both in case of configuration setting-up, before transition to a diverted configuration, and in case of dedicated experiments at medium/high power. In terms of heat flux the configuration has been found compatible with the wall in a wide range of plasma heating (up to about 18 MW) but being a limiter attached configuration the situation has been found critical in terms of plasma temperature which was found always

very high. Due to the relatively high tungsten physical sputtering at high temperature, plasma contamination could be an issue for limiter operation but it could be solved by wall conditioning (boronisation) or by optimizing additional heating mix to avoid tungsten core accumulation.

4.1.4.4. DTT scenarios: METIS simulations

METIS¹⁰⁶ 0.5D transport code has been widely used for DTT design, both for plasma scenario studies and for the evaluation of the NBI design choices. The flat-top phase of the reference DTT SN, full power scenario, both for R=2.14m and R=2.19m, has been reproduced by METIS and validated against JINTRAC available simulations¹⁰⁷. This enabled, at first, the estimation of the NBI power deposition, current drive and fast ion losses (shine-through, first orbit losses) for different design options (e.g. including $E_{\text{NBI}}=400$ and 500 keV). The output of METIS has been used as input and for comparison in various other works within the DTT community (diagnostics, pellet injection, fast particle losses, neutronics etc.). A second part of the work regarded the simulation of the time evolution (at the moment, only ramp-up) of the reference SN, full power DTT plasma. CREATE plasma LCFS evolution has been used as input, keeping the reference flat-top plasma as the target. The goal of this activity was to develop a first estimate of the evolution of the main plasma parameters, and to check the feasibility of accessing the target flat-top scenario in terms of controllability (by $I_{i,3}$ and β_p values) and H-mode access. Different options have been evaluated, and a preliminary trajectory for auxiliary heating power waveforms has been proposed.

4.1.4.5. NNBI generated fast ions studies

Studies of fast-ion transport in DTT are ongoing: fast ions will be generated by the negative neutral beam (NNBI) system to be developed by Consorzio RFX¹⁰⁸ and fast ions interact with 3D fields, such as the toroidal field (TF) ripple. This type of studies is interlaced with the DTT engineering team, since calculating the impact of 3D magnetic structures on supra-thermal particle confinement is crucial for the efficient coupling of NNBI and minimization of the impact of energetic particle losses on the wall. Previous studies¹⁰⁸ had shown that with a DTT equilibrium with R=2.08 and maximum ripple of 0.22%, energy of the beam E=400 keV and injection angle (at the first wall) $\alpha_{inj} = 38^\circ 40'$ (tangency radius Rt=1.77m), collisionless losses of fast ions are globally 4%, consisting in 3.8% of prompt losses and 0.2% of ripple losses (trapped-precession resonant particles). Only 1% of deposited ions are born trapped.

¹⁰⁶ J.F. Artaud et al 2018 Nucl. Fusion 58 105001

¹⁰⁷ I Casiraghi, P Mantica et al. to be submitted

¹⁰⁸ P.Agostinetti, T.Bolzonella, M.Gobbin, P.Sonato, G.Spizzo, M.Vallar, and P.Vincenzi Fus.Eng.Design 146, 441-446 (2019) <https://doi.org/10.1016/j.fusengdes.2018.12.087>

During year 2020 these studies have been continued, using the new equilibrium with $R=2.19\text{m}$ which allows for a larger value of the safety factor $q_{95}\sim 3$. Initially, the birth positions of fast ions have been calculated with METIS and PENCIL¹⁰⁹. Then, more refined 3D initial distributions have been calculated with TRANSP simulations based on the scenario developed with the JINTRAC suite¹¹⁰. With the same energy $E=400\text{keV}$ and injection angle, results are promising, since they show vanishing prompt losses (0.03%) and 0.12% only of ripple losses. These results have been used by the engineering team for an improved version of the NNBI system, with energy 510keV and tangency radius $R_t=1.95\text{m}$. An assessment of fast ion losses with this new energy and geometry is ongoing work.

4.1.4.6. In-vessel non-axisymmetric coils studies

The installation of in-vessel non-axisymmetric coils is being considered for DTT since 2018. Similar systems are present in many present-day and forthcoming experiments, including ITER. Non-axisymmetric coils can serve multiple purposes, from securing the device operational space to real-time control and aiding scientific exploitation. Different geometries of active coils are being considered, constrained by in-vessel installation compatibility. An example is reported in Fig. 4.7. The vacuum spectra produced by these geometries have been calculated with both MARS-F (2D) and CARIDDI (3D) and characterized in terms of (n,m) Fourier harmonics. Plasma response studies can aid the design to maximize the effectiveness for specific purposes. A preliminary study has been carried out with the MARS-F code for two of the aforementioned coil configurations, focusing on the ELM control application¹¹¹. These results indicate that one of the two geometries could be more efficient in terms of produced X-point plasma displacement at given coil current (Fig. 4.8).

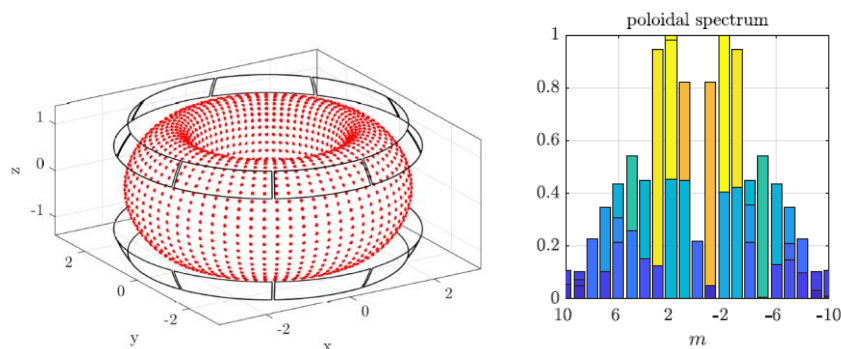


Fig. 4.7 (Left) Example of 2x9 up-down symmetric configuration for the DTT in-vessel coils (Right) Poloidal spectrum of $n=3$ perturbation

¹⁰⁹ G.Spizzo, M.Gobbin, I.Casiraghi, G.Granucci, P.Mantica, P.Vincenzi, G.Vlad Technical note DTT2020-378 <https://www.dtt-dms.enea.it/share/page/site/dtt/document-details?nodeRef=workspace://SpacesStore/fa0a6b92-f2d2-4689-b5d3-a7e0994587e6>

¹¹⁰ I.Casiraghi, P.Mantica, et al, submitted to Nucl.Fusion (2020).

¹¹¹ M. Baruzzo, et al, "MHD stability and Disruption studies in DTT", 4th Asia-Pacific Conference on Plasma Physics, 26-31Oct, 2020, Remote econference

4.1.4.7. Diagnostics Integration

A layout for a conspicuous set of diagnostics, not limited to the first operations, has been

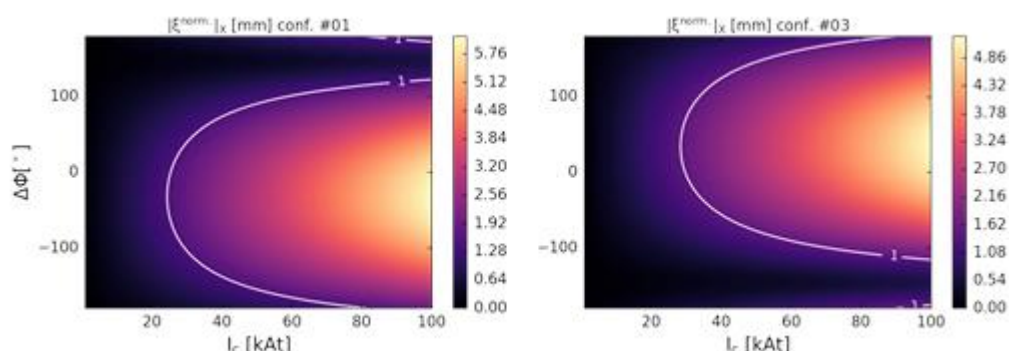


Fig. 4.8 Plasma displacement at x-point scanning coil phasing and feeding current. Configuration #01 shows slightly stronger effect at given current and optimal phase.

identified on the machine and for the necessities outside the torus hall (labs , direct access to Torus Hall), including systems for machine protection, real time control and physics exploitation. Needs for services inside and outside the Torus Hall (cooling water, electrical power, uninterruptible power supply etc.) have also been analyzed. The final integration of all of the systems is anticipated to be particularly challenging due to the large number of functions to be covered and the available space. A tangential port close to the NBI injector, which also makes use of a tangential access, has been suggested for specific diagnostics such as the LIDAR Thomson Scattering, the crystal spectrometer, tangential Bremsstrahlung and SXR 2D imaging. Several activities have been organized for 2021 in order to reach a Conceptual Design for several day-zero systems with particular regard to the in-vessel systems, and also for tasks of general interest in order to tackle problematic aspects such as hard radiation, EC stray, wall reflections, thermal excursions and mechanical vibrations during disruptions.

4.1.4.8. Interferometer-Polarimeter

Analysis of possible designs for both the vertical interferometer/polarimeter and for the tangential interferometer/polarimeter have been carried out. Possible ports/sectors have been indicated for each of the diagnostics mentioned above. For the vertical interferometer/polarimeter a study of the expected interferometric and polarimetric signals has been performed. Furthermore, new chord positions have been defined, by considering the DTT vacuum vessel space availability.

4.1.4.9. Active CXRS and MSE

Studies on the possibility to use the 500 keV, 10 MW power beam for diagnostic purposes have been carried out¹¹². If Motional Stark Effect (MSE) benefits from the large beam energy, which enhances the Doppler effect and therefore the possibility to separate passive and active spectra, for Charge eXchange Recombination Spectroscopy (CXRS) the situation is more complex as the CX cross sections for collision between D and typical impurities, such as Ne, decrease with energy. However the combination of larger penetration, favoured by higher beam energy, and reduced CX cross section does not seem to be particularly deleterious for the specific situation as shown in Fig. 4.9. Other aspects, however, require further thinking: namely the fact that the power beam at the moment does not seem to cross the magnetic axis ($\rho=0$), but rather points below and above it, and, second, the CXRS diagnostic would be limited to scenarios in which the beams are active.

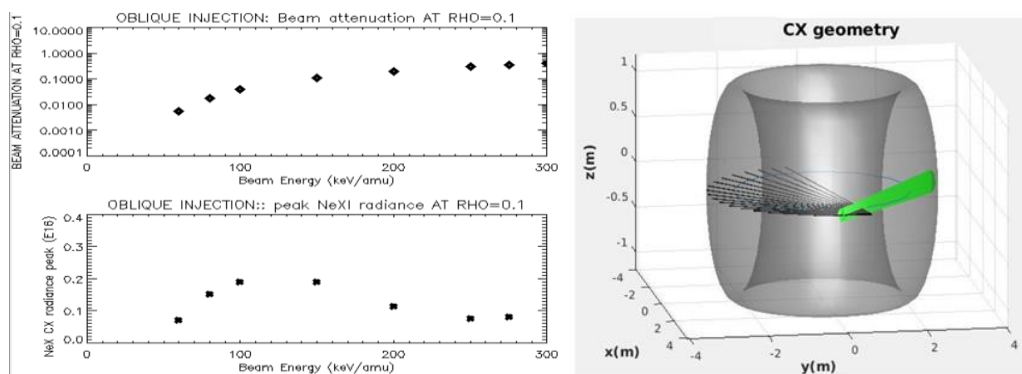


Fig. 4.9 Beam attenuation (top) and Ne CX emission at $\rho=0.1$ (bottom) as a function of the DTT beam energy. At 250 keV /amu the expected signal loss is only a fraction of the maximum expected from the plasma center. On the left the geometry of beam and optics.

4.1.4.10. Electrostatic sensors and thermocouple

A suite of electrostatic and calorimetric detectors embedded in the first wall and in the divertor to characterize the power losses has been conceived based on a series of available scenarios. The proposed layout foresees a distribution of poloidal arrays of sensors on divertor cassettes and first wall in three toroidal sectors. The system is thought as integrated into a wider set of diagnostics targeting the plasma edge, including a reciprocating probe and optical means to measure density, temperature, collective flows and turbulence properties.

4.1.4.11. NBI design activities

Regarding the activities on the design of the DTT NBI system, the conceptual design has been developed considering as main guidelines the maximization of flexibility, feasibility, RAMI and efficiency, and the minimization of cost and weight. The main components of the injector,

¹¹² with the contribution of M von Hellerman

shown in Fig. 4.10, are: a beam source (composed of an ion source and an accelerator), three beam line components (BLC, i.e. a neutralizer, a residual ion dump and a calorimeter), an absolute gate valve and a duct to connect the injector to the vacuum vessel. As for the NBIs of JT60 and LHD, a design with an air-insulated beam source is proposed, to reduce the vacuum volume, increase the source accessibility and avoid the need of a single large bushing to connect the Transmission Line to the vacuum vessel.

The two beam sources have been conceptually designed to accelerate 40 A of D^- (20 A each) to an energy of 510 keV. This is made by means of a set of grids biased at different potentials: a Plasma Grid (PG) operating at -510 kV, an Extraction Grid (EG) at -500 kV, a Hyperlens Grid (HG) also at -500 kV (attached to the downstream side of the EG), a first Acceleration Grid (AG1) at -333 kV, a second Acceleration Grid at -166 kV and a Grounded Grid (GG) at ground potential. In each of the two beam sources, all the grids are made of four copper segments to improve the beam aiming (each segment is in fact bent of about 1 degree with reference to the beam source axis) and thermal deformation (all the segments have a fixed constraint in the central part of each grid).

An extraction gap, about 6 mm long between PG and EG, has the function to extract the D^- ions from the plasma source and stop all the co-extracted electrons that are extracted together with the D^- . In fact, these electrons would generate excessive heat loads on the following grids if they were not stopped by the EG while they still have a low energy. To do this, an electrostatic potential of about 10 kV (varying in function of the density of the extracted D^- to obtain good beam optics) is applied between the two grids and the EG is equipped with permanent magnets that deflect the co-extracted electrons onto the EG surface. Maximizing D^- extraction while minimizing co-extracted electrons is one of the main critical issues for negative ion based NBIs. To do this, several methods are applied analogously to SPIDER, MITICA and ITER NBI: adopting an enhanced shape of the PG upstream surface (featuring

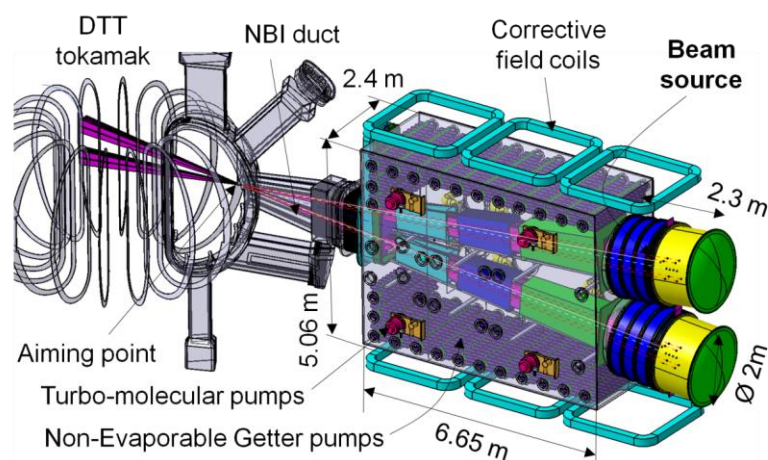


Fig. 4.10 Conceptual design of the beamline for DTT NBI

large chamfers with a 40° angle with reference to the beam axis); operating the PG at high temperature (about 150 °C); covering the PG with a mono-layer of Caesium, injected by dedicated Caesium ovens mounted on the ion source; applying a high current flow vertically through the PG (this generates a filter field in front of the PG).

After the extraction gap, there are three acceleration gaps with a thickness of about 100 mm and an applied potential of about 166 kV each. The D⁻ particles are accelerated passing through the apertures in each grid. Electrons, neutrals and positive particles are generated in the accelerator by stripping and charge-exchange reactions of the D⁻ particles with the background gas, that is mainly D₂. These particles, as well as the D⁻ having a large divergence (called halo fraction of the beam) are finally impinging on the grids and on the plasma source, generating high heat fluxes on this surfaces and other back-scattered particles. For this reason, all the grids and the plasma source components are equipped with high performance cooling systems able to avoid damages due to the extremely concentrated heat loads, and the density of the background gas in the accelerator is minimized by means of a high performance vacuum system mounted on vessel, composed by several NEG and turbo-molecular pumps. The pumping of the accelerator is enhanced by adding various holes on the flat part of the grid frames, so that the particles can flow to the pumped regions of the vessel. Each grid segment is mounted on a stainless steel support frame, that in turn is connected to its external flange (also made of stainless steel). The external flanges are separated by insulating rings made of Fiber Reinforced Plastic (FRP) having an external diameter of about 2 m and designed to hold the potential difference of about 166 kV between two adjacent flanges. In order to avoid discharges, the flanges are equipped with Electrostatic Screens and Triple Point Field Limiters on the vacuum side, and with Field Reducing Tubes on the air side. The accelerator grid segments represent a critical component as they have a rather complex design, with very small cooling channels, apertures for the negative ions and grooves for the embedded magnets. They can be manufactured by means of copper electrodeposition on a milled base plate made of pure copper. An alternative manufacturing process based on additive manufacturing is currently being investigated by means of a dedicated R&D program. Another critical R&D program is foreseen to develop and validate a manufacturing process for the FRP (fiber-reinforced polymer) rings of the accelerator. In fact, these rings are quite large (diameter of 2 m) and must fulfill various important functions, i.e. to maintain the electrical insulation between the acceleration stages and to support the beam source while being perfectly leak tight and having a vacuum compatible surface on the internal side.

In 2020, the pre-conceptual design of the DTT NBI power supplies has been developed. The NBI power supplies are composed of: Acceleration Grid Power Supply (AGPS, to feed the acceleration grids), Ion Source and Extraction Power Supply (ISEPS, to feed all the ion source

loads) and Ground Related Power Supply (GRPS, to feed the Residual Ion Dump and the correction coils to compensate the stray fields). The AGPS has to provide up to 500 kV on three acceleration stages (167 kV each), with an output current up to about 60 A. A specific requirement for this application is the capability to switch-off the voltage generation in some tens of μs in case of breakdown among the grids, to limit the energy delivered to the arc.

For the DTT AGPS, a scheme similar to ITER and MITICA has been conceived first. One step-down oil transformer feeds a 1-quadrant thyristor ac/dc rectifier system, which in turn feeds the dc-link at the input of 3 Neutral-Point-Clamped IGCT-based inverters, each connected at the output to the primary side of a step-up transformer. At secondary, the ac voltage is rectified by a 3-phase HV diode bridge, SF₆-insulated, producing 167 kVdc. The diode rectifiers are connected in series and also to the accelerating grids, through the inner conductors of the SF₆-insulated Transmission Line (TL). Upstream of the TL is connected the SF₆-insulated HV dc-filter. Downstream, the TL is connected to the accelerator through a SF₆-air bushing, carrying also the conductors at -500 kV for the ion source loads. Beside the ITER-like scheme, an innovative approach for the AGPS based on the Modular Multilevel Converter (MMC) technology has been considered, since it would provide a set of advantages. This topology is more and more widely adopted in HVDC power conversion stations, but it has never been selected for power supplies of high voltage accelerators. In rectifier each, arranged in air-insulated towers (1 per leg). Each rectifier feeds an acceleration step through the TL and the bushings. The arm of each rectifier is constituted by the series connection of tens of submodules (SM) and a filtering inductor to smooth the ac current ripple. Each SM contains a dc capacitor, which can be connected in series or bypassed in the branch by giving the proper commands to a set of IGBTs. The overall schemes of the two solutions are shown in Fig. 4.11. For both solutions, a tentative layout has been depicted; this is complicated by the need of reusing the existing buildings, at least partially. For the ITER/MITICA-like solution, the

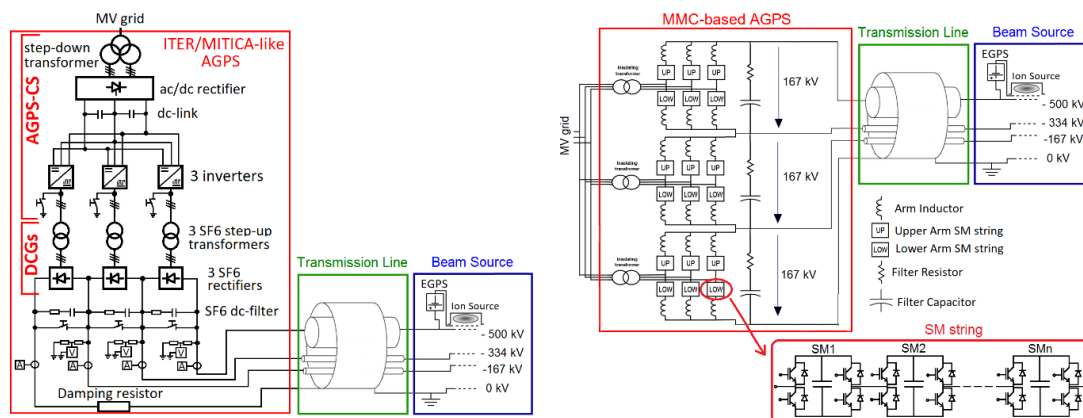


Fig. 4.11 Two possible schemes for the DTT NBI AGPS: ITER/MITICA-like (left) and MMC-based (right)

dimensions of the components have been derived from the MITICA installation. For the MMC-based solution, the dimensions of the towers and inductors have been calculated on the basis of specific studies. In this case, the air-SF₆ bushing would be placed in a new dedicated room, shorting very much the TL connecting the bushing to the NBI. In this way, the volume of SF₆ and the required storage tanks are much reduced. The MMC solution would provide also higher modularity, better control performances, higher efficiency and reduced charge transferred to the grids at breakdown. However, while the feasibility of the MITICA-like solution can be clearly inferred from the existing installations, for the second one further studies are necessary. Due to layout constraints, the step-up transformers would be connected to the conversion towers via HV cables, whose routing is complicated by their very large bending radius. Other concerns regard the compatibility with the available space and the overall cost. Detailed studies are in progress to verify how much is possible to reduce the number of static switches and the overall dimensions, preserving the capability to produce sufficient reverse voltage at grid breakdowns to quickly damp the arc current. These analyses will prosecute in 2021, together with optimizations of the control scheme and fault analyses, in support to the final choice among the two solutions.

Progress have been performed also on the conceptual design of ISEPS. In particular, while for the Extraction Grid Power Supply the Pulse Step Modulator topology adopted for ITER/MITICA NBIs seems again the best solution, for the Radio Frequency Power Supply (which feeds the RF drivers of the ion source) a different approach with respect to MITICA would be pursued. In fact, the experiments with SPIDER highlighted some important issues with tetrode-based self-oscillator technology, mostly due to the multiple resonant frequencies which appear when the self-oscillator is combined with the resonant load. These cause frequency flips during operation and prevent the oscillation at the ideal frequency in which the active power transfer would be maximized. The solid-state RF technology based on MOSFET amplifiers would provide much higher efficiencies (making possible air-cooled solutions), a working frequency settable by the operator and independent from the load and higher redundancy in case of fault. The limitations of this technology are under investigation, and further information will be collected from the procurement and testing of the new solid-state RF generators for SPIDER, planned in 2021.

In 2020, an important amount of work has been devoted also to the comprehension of the dielectric phenomena occurring on solid surfaces surrounded by insulating gas, in dc conditions. These studies apply in particular to the SF₆-insulated TL, but also to the SF₆-air bushings. A dedicated model, exploiting the combination of Matlab and Comsol, has been developed, implementing also optimization algorithms able to find the best parameters of the given geometry which minimize the electric field and the probability of discharge. For DTT, the

outcome of the model would be the optimization of the TL outer diameter, internal geometry and gas pressure, and the optimization of the bushing geometry, with clear impact on the building design and system reliability. This work will prosecute in 2021, hopefully including also the validation of the model on a real test bed.

4.1.5. **WPSA**

4.1.5.1. Modeling coordination

RFX has led the coordination of the whole Work Package modeling activity regarding the development of JT-60SA scenarios.

4.1.5.2. Fast Ions Simulations/ASCOT

ASCOT5 Monte Carlo code has been used for NBI fast ion simulations for JT-60SA plasma, scenario 4.2¹¹³. The aim of the work has been to generate a fast ion distribution function, both for N-NBI and P-NBI lines, that has been requested for fast ion stability studies. The work is still going on.

4.1.5.3. Equilibrium control and MHD studies

JT-60SA is an upcoming device which will start operating in early 2021 and is designed to provide important insight for ITER and DEMO, in particular when dealing with steady-state plasmas and Advanced Tokamak scenarios. With tokamak construction completed in March 2020, JT-60SA is going through an Integrated Commissioning phase which will culminate in the first plasma in early 2021. Within the WPSA framework, EU teams started interfacing with local QST ones. In particular Consorzio RFX is actively participating in the topics of “plasma equilibrium & control” and “magnetics & MHD”. With on-site participation postponed to 2021, off-site work has started for the preparation of a disruption database to be applied since the early plasma phases. A preliminary set of measurable quantities has been identified, taking into account the limited information that will be available at the time of the first plasma. This exercise can be considered important both for future disruption studies on JT-60SA and as a test for disruption identification/classification with limited sets of diagnostics.

Progress has been made in modeling of global MHD stability in scenarios for Initial Research Phase I and II, towards full integration of magnetic feedback with passive stabilization of Resistive Wall Modes in high β scenarios. In particular the $n=1$ RWM, which is first triggered by increasing pressure, is found to be strongly damped by resonance with trapped particle bounce motion with strong plasma flow. This could lead to a weakly unstable or marginally

¹¹³ see https://users.euro-fusion.org/iterphysicswiki/index.php/Research_Plan

stable mode, which can be controlled by magnetic feedback. The CarMa-D model is applied to JT-60SA for self-consistent integration of these effects. Preliminary results show good match between MARS-K and CarMa-D¹¹⁴ results for the $n=1$ mode with axisymmetric. The $n=1$ growth rate is reduced in drift-kinetic modeling, with respect to a purely fluid MHD formulation, by two orders of magnitude. This brings the growth rate to values compatible with typical RWM regimes ($\gamma\tau_w \sim 1$). Furthermore, ideal MHD stability calculations with MARS-F

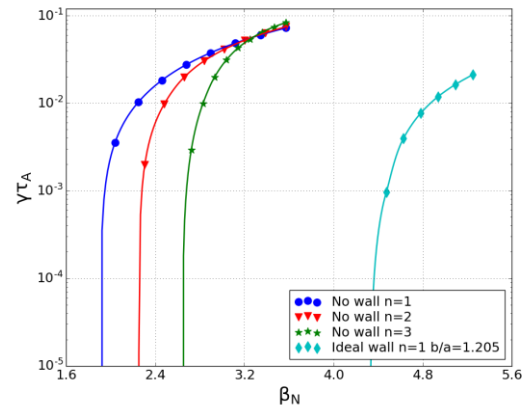


Fig. 4.12 Normalized growth rate of the ideal kink for $n=1,2,3$. Diamonds on the right (cyan) show the ideal-wall limit for $n=1$

indicate that the $n=2$ and $n=3$ modes will also be unstable in the target plasma. Interestingly enough, the $n=2$ mode is triggered at higher β with respect to $n=1$, but grows then with stronger growth rate. Ongoing work is dedicated to drift-kinetic stability of $n>1$ modes and coupling to magnetic feedback with the CarMa-D model mentioned above.

4.1.5.4. METIS-EGENE code coupling (Abate)

Preliminary tests of EGENE code on scenario 4.1¹¹³ were performed for all static equilibria of PID document with an agreement within 1% for global equilibrium quantities. EGENE was then used for designing the start of flat top (SOF) static equilibrium of scenario 4.2. The inputs were selected following three approaches: by scaling quantities from SOF of scenario 4.1, by using global quantities (β_p , I_i) from METIS and by using internal profiles (p' , ff') from METIS. The consistency in computing global equilibrium quantities was confirmed; different plasma shapes were obtained with different plasma current density profiles. Since no reference plasma boundary exists for scenario 4.2, the reference was given by plasma shape parameters (k, δ) in the research plan. Furthermore, the METIS-EGENE weak coupling was defined and used to produce new scenario snapshots for scenario 4.2. The equilibrium time instants chosen for the weak coupling were given by METIS simulation. The weak coupling procedure is described in Fig. 4.14 and the results were compared in terms of β_p and I_i against METIS outputs. Considering the time instants before NBI heating activation, the EGENE results agree

¹¹⁴ M. Bonotto et al, 2020 Plasma Phys. Control. Fusion **62** 045016

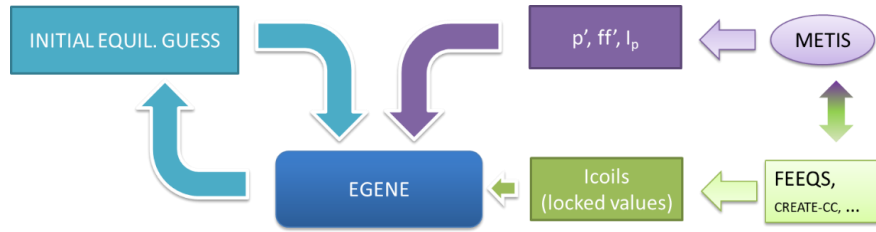


Fig. 4.14 EGENE-METIS weak coupling scheme.

with the METIS ones (Fig. 4.13); on the other hand, when NBIs are turned on a disagreement is present. This could be related to differences in the plasma shapes. A reference plasma shape would be useful to provide a more meaningful benchmark. The strong coupling scheme has also been run for Scenario 4.2, but problems arise around 7.5s where a sudden increase of poloidal beta is registered, and plasma moves toward the external wall.

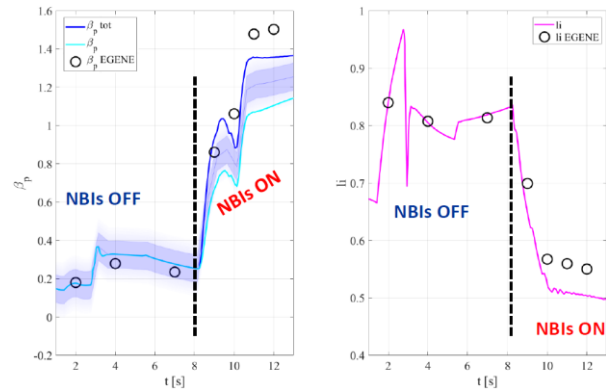


Fig. 4.13 EGENE-METIS weak coupling results for scenario 4.2.

4.1.5.5. VUV divertor spectrometer

The design of the VUV divertor spectrometer sponsored by EUROfusion and to be mounted on JT60-SA in October 2022 is now mature for the procurement phase. The instrument is based on the spectrometer that has been in use on Textor, with refurbished gratings detectors and pumps, an optical relays based on two toroidal mirrors per channel and an alignment system with possibility of remote adjustments (Fig. 4.15).

Additional features have been introduced in order to allow remote adjustment and verification of the alignment and also to maintain the temperature of the relays mirrors inserted into the cryostat at a temperature that avoids vapors condensations on the reflecting surface. Manufacturing of custom toroidal gratings has encountered unexpected difficulties due to changes in the internal organization of the major European producers of those special optical components. Related delays should be absorbed in the assembly and test phases, originally conceived particularly long to

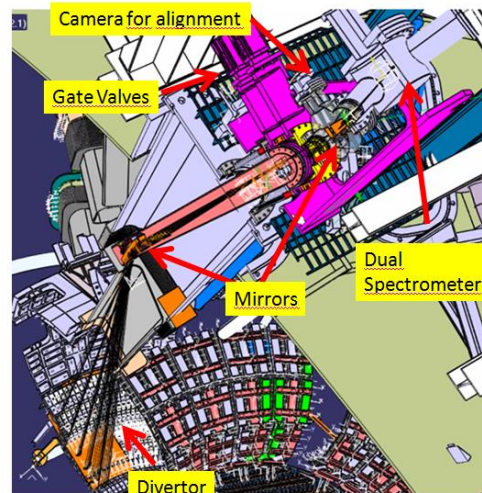


Fig. 4.15 Current design of the VUV spectrometer for JT60-SA

compensate for possible setbacks. Simulation of the expected spectra have also started, to be presented at the next EPS conference

4.1.5.6. Thomson Scattering

Within the collaboration between EU and QST-Japan for the procurement of components for the JT-60SA experiment, Consorzio RFX is leading the EU contribution to the design of the core and edge Thomson scattering diagnostics and the in-kind procurement of five subsystems: the collection optics with their mechanical structure and the laser of edge TS system, the fibers and polychromators for both core and edge TS systems.^{115,116} The project team comprises the Romanian Institute of Atomic Physics (IAP) and the Institute of Applied Physics IFAC-CNR.

In 2020 most procurements have started, after completion of the design phase. Procurements of fibers and polychromators are managed by F4E, where CRFX is in charge of the technical supervision: radiation hard fibers are manufactured by Molex and first delivery to QST is ready for shipment; the 100 polychromators are developed by the Italian company G.N.R. which has just started the contract and is in the design phase. Collection optics are procured directly by CRFX: after a competitive design phase between two companies, the contract has been awarded to Officina Stellare, which is also finalizing the design by early 2021. The mechanical structure of the collection optics is provided by IAP and CRFX is mainly addressing the integration and interfaces issues. The laser for the edge system is also procured by CRFX: the tendering phase has started with the Russian supplier which has already built the custom Nd:YAG laser for the RFX Thomson scattering.

4.1.6. WPS1

4.1.6.1. Thomson Scattering

In 2020 the collaboration with the Thomson scattering team of W7-X was continued by contributing to the preparation of dual-angle Thomson scattering experiments, planned for the next W7-X campaign. We have contributed by carrying out a detailed analysis of the expected performances of this technique, that in W7-X will be implemented by reflecting back the laser beam in a two-pass configuration and measuring the scattering signals from the return beam in addition to the forward one. The results of these simulations indicated that 1) the technique can improve the accuracy of Te and ne measurements, in average by a factor 1.5 and even more in some measurement positions; 2) by performing a statistical analysis of the dual-angle scattering data it is possible to implement continuous, online monitoring of the spectral

¹¹⁵ R.Pasqualotto et al., Journal of Instrumentation 15, C01011 (2020)

¹¹⁶ H.Tojo, Review of Scientific Instruments, submitted

sensitivity of the polychromator channels. This dual-angle technique is analogous to the dual-laser Thomson scattering technique, foreseen for the future campaigns of W7-X.

4.1.6.2. Filamentary structures

For the study of electrostatic and magnetic properties of filaments characterizing the edge region of the stellarator experiment W7-X¹¹⁷, a specifically designed insertable probe head¹¹⁸¹¹⁹ was constructed within the framework of EUROfusion WP.S1 work package in collaboration between Consorzio RFX, IPP Greifswald and FZJ Julich. The probe head, named High Resolution Probe (HRP), was conceived to be installed on the mid-plane multi-purpose fast reciprocating manipulator on W7-X. The design development, the R&D studies and the applied solutions for the sensors embedded in the probe head required particular attention. Specifically, the presence of 140 GHz ECRH plasma environment represents one of the main challenges for reliable magnetic fluctuation measurements.

First measurements were performed during the W7-X experimental campaign OP1.2b, where in particular the probe was exploring different magnetic configurations. The respective features of the electromagnetic turbulence are compared.

Both electrostatic and magnetic fluctuation signals were measured, including the direct measurement of parallel current density fluctuations. However a reduced amount of measurements were available at once on MPM during the OP1.2b experimental campaign, so that the HRP probe was not yet fully exploited. The first results provided: consistent modifications of edge parameters during iota-tuning experiments¹²⁰ and example evidence of

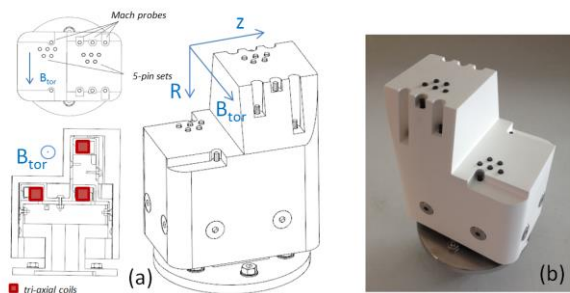


Fig. 4.16 Schematic sensor layout within the probe head (a); HRP probe head final assembly (b) [35].

the presence of current carrying filaments in the edge region. Equilibrium magnetic field profiles measurements are encouraging.

The study of those phenomena in W7-X stellarator is of particular interest as the electromagnetic features of filaments are expected to become more relevant with the increase of the local plasma beta. Given

the limited number of signals and programs available in the previous experimental campaign,

¹¹⁷ M Spolaore, et al. S1-B.13 -T002-D005: WP18.S1.B6.D5: Commissioning report high-resolution probe (ENEARFX) IDM reference: <https://idm.euro-fusion.org/?uid=2MMRYU&version=v1.1>

¹¹⁸ Agostinetti, Piero, et al. "Design of a high resolution probe head for electromagnetic turbulence investigations in W7-X." IEEE Transactions on Plasma Science 46.5 (2018): 1306-1311

¹¹⁹ Spolaore, M., et al. Journal of Instrumentation 14.09 (2019): C09035.

¹²⁰ S. Lazerson et al. Nucl. Fusion 59 (2019) 126004

further developments are envisaged for the next OP2 experimental campaign in W7-X. More details are reported in the final report 2020 for EUROfusion¹²¹.

4.1.7. **WPISA**

WPISA activity in 2020 has been devoted to the development of new features of for Data Backend in the ITER Integrated Modelling & Analysis Suite (IMAS). IMAS relies on a database abstraction that is implemented in different media, among which memory mapped data structures and MDSplus pulse files. In particular, development carried out in 2020 has been targeted to improving data access performance.

4.1.8. **Further collaborations. Plasma equilibrium and 3D em code integration**

This work is being carried on within the F4E OPE0951 to couple the 3D equilibrium code VMEC with the 3D electromagnetic code Cariddi in order to develop a code able to take into account the plasma response to 3D fields produced by eddy currents induced on the machine passive structure. The coupling procedure was designed and implemented in a flow diagram using an external framework to assess numerical issue. The first tests were done both considering a plasma with circular cross-sections as well as a case for ITER.

The analysis was successful for the single time instant, but the time evolution showed some issues due to the fact that it was based on the Virtual Casing Principle which required the control surface to be a flux surface. Since this cannot be due to the fact that the control surface has to be defined as fixed (in order to compute comping matrices once for all) it was decided to modify the algorithm providing as input to the matrix computation the vector potential (instead of the magnetic field) still keeping as output the magnetic field as required by VMEC.

The general flow diagram is still valid and does not require any change. We are now in the process of computing the new coupling matrices for the ITER case in order to start a new test phase which will be carried out in 2021.

4.2. **PPPT Projects**

4.2.1. **WPHCD – Heating and Current Drive systems**

The injection of high energy neutral beams is one of the main tools to heat the DEMO plasma up to fusion conditions. A conceptual design of the Neutral Beam Injector (NBI) for the DEMO fusion reactor is currently being developed by Consorzio RFX in collaboration with other European research institutes. High injector efficiency and RAMI (Reliability, Availability,

¹²¹ M. Spolaore, et al. Final Report on S1-WP19-20.X.2.B-T001-D002: Analysis HR probe in OP1 (2020) (ENEA-RFX) IDM reference: <https://idm.euro-fusion.org/?uid=2P4MR5&version=v1.2>

Maintainability and Inspectability), which are fundamental requirements for the success of DEMO, must be taken into special consideration for the DEMO NBI.

A novel design of the beam source for the DEMO NBI is being developed featuring multiple sub-sources, following a modular design concept, capable of increasing the reliability and availability of the DEMO NBI. During 2020, the DEMO NBI conceptual design has been discussed with the interested working groups of EUROfusion, working on the main related issues (physics, integration, breeding blanket, remote maintenance, neutronics). Moreover, a Final Design Review meeting has been organized in June 2020, which has given a feedback on the proposed design solutions.

In this framework, a strong collaboration between EUROfusion WPHCD and WPTFV working groups has been set up in order to evaluate the heat loads on the NBI system of DEMO, with a particular focus on the NBI duct. By means of an integrated suite of models developed in the COMSOL environment, all the relevant phenomena of the beam from the accelerator exit to the first wall were simulated in collaboration with KIT, by evaluating the particle trajectories in presence of electric and magnetic fields and at the same time the reactions (stripping, neutralization, re-ionization) due to the interaction of the fast particles with the background gas. The main results are the heat loads on neutralizer, Residual Ion Dump (RID) and duct.

In the DEMO NBI context, a collaboration program was started with INFN Padova regarding the possible application of additive manufacturing to the DEMO NBI. The use of three copper powders with different granulometry was tested for the laser powder bed fusion process. The results show that the manufacturability of the powder with the finer particle size distribution was better. The parts produced with this powder had higher densities, which led to higher mechanical and thermal properties. With the correct scan strategy, it was also possible to improve the lateral surface roughness (from 12 μm to 3 μm). The influence of the height of printing on the mechanical and thermal properties of the copper alloy CuCrZr was also investigated.

Photoneutralization is regarded as one of the most interesting alternatives to stripping neutralizers in NBI systems. R&D activity on photoneutralization at Consorzio RFX involves the construction and test of a non-resonant cavity for second laser harmonic trapping, fed by a pulsed Nd-Yag laser RING concept

In 2020, the activity on photoneutralization addressed the construction of a new RING mockup, featuring high reflectivity mirrors and an improved mechanical stability, the numerical analysis of beam propagation through a misaligned RING cavity and building up a diagnostic system for thermal induced mirror deformations.

4.2.2. **WPFTV - Tritium, Fuelling and Vacuum Pumping Systems**

The activities carried out during 2020 on the WPTFV framework were aimed at finalising the experimental characterisation of the large Non-Evaporable Getter pump mockup. After the getter poisoning occurred in 2019, which was found to be due to insulating materials of thermocouple cables, we developed a strategy for the experimental activities, consisting in two approaches. A fast-track approach, finalised at obtaining regeneration data and pumping speed stability after many regeneration, was carried out on the basis of the existing NEG cartridges that had lost permanently part of their pumping capability (down to 13 m³/s from the 25 m³/s demonstrated after the initial activation): after replacement of the thermocouple cables, the mockup was repeatedly loaded with Hydrogen and regenerated (heating at temperature greater than 550°C), demonstrating a very good repeatability of results and a slight increase of its performance after repeated regeneration. After the aforementioned tests, the mockup pump was sent back to SAES company and cleaned and refurbished by replacing the conductors with copper cables protected with alumina-based tubes and beads (instead of Kapton-insulated cables). In parallel, new NEG cartridges were prepared for replacing the poisoned ones; the cost was covered by SAES, and only 17 cartridges out of the original 34 were replaced. The second approach, finalised at obtaining accurate data on clean cartridges and optimised materials could start at that point: during the second part of the year, 16 sorption and regeneration tests were carried out, covering pressures between 6 mPa and 100 mPa, gas loads up to 11 Torr L/g, and sorptions at various temperatures between room temperature and 180°C, highlighting a rather stable pumping speed over time; the pumping speed ranged between 17 m³/s and 12 m³/s depending on the conditions (in general, it was higher with higher sorption temperature, and higher for lower pressures). The repeatability was excellent and the measured pumping speed was in line with the initial results obtained the previous year before poisoning (having half the cartridges). Numerical models showed that the pumping speed at the cartridges was about 12% higher, clarifying the “packing” effect of many cartridgeges one close to the other: in this sense, the experimental data needed for a design based on NEG cartridges is now available, and can be scaled to any geometry via numerical modelling. The experimental tests in TIMO will continue next year, focusing on Deuterium performances (up to now, a reduction by a factor $\sqrt{m_{H_2}/m_{D_2}}$ was found when operating Deuterium) and on the regeneration duration.

4.2.3. **WPBoP - Balance of Plant**

4.2.3.1. **PES – Plant Electrical System**

The primary objectives of the PES are to provide the electrical power to all DEMO plant loads with the characteristic required according to their functions and requirements and to deliver to

the Power Transmission Grid (PTG) the power produced by the electrical generator minus the power to be recirculated.

The CRFX work in the first months of 2020 was mainly concentrated in further identifying the most critical aspects related to the development of the conceptual design in the next Framework Program FP9 and in the preparation of a relevant plan to tackle them in FP9¹²². Fig. 4.17 shows a simplified block scheme of the PES, with the indications of the main issues identified so far.

Then, the work was concentrated in summarizing the R&D and design work on the PES done in the DEMO pre-conceptual phase in FP8, in view of the Design Reviews.

In the role of coordination of the PES project, CRFX led the preparation of the documents of the PES Project Management Plan, Project Definition Dossier and Project justification Dossier to be presented at the PES Design Review in June and at the Design Review of the whole DEMO design (called G1) in November. The panel gave a positive judgement, saying that *“was impressed by the very high technical quality of the performed analyses and the professionalism of the presented reports”*.

The most significant part of the CRFX R&D and design work in 2020 is related to the completion of a preliminary ITER-like design of the CPS system to identify possible issues, found very challenging in terms of peaks of active power and reactive power demand, and to the exploration of alternative technologies. The studies on the new Magnetic Energy Storage

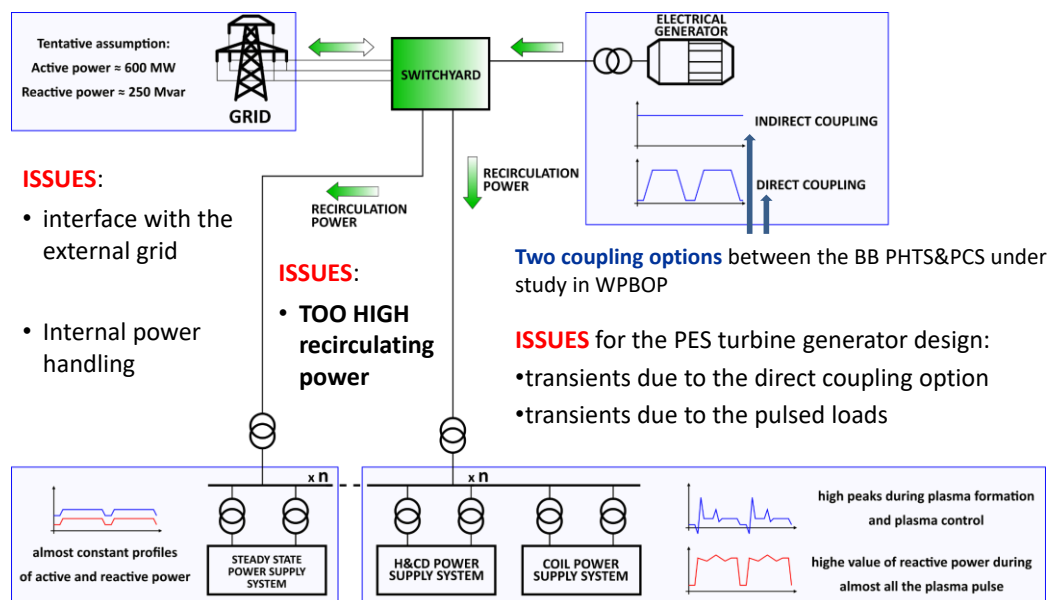


Fig. 4.17 Simplified block scheme of the EU DEMO Plant Electrical System with indication of the main open issues

¹²² E.Gaio et al., The EU DEMO Plant Electrical System: Issues and perspective, Fus Eng and Design 156 (2020) 111728; <https://doi.org/10.1016/j.fusengdes.2020.111728>

and Transfer system, already started in 2019 proceeded in 2020; the results showed that potentially the MEST could smartly solve both the issues related to high power peaks and huge reactive power demand associated to the adoption of the traditional design solution based on thyristor converters. The work, presented at ISFNT conference in 2019, was published this year¹²³, then the study on this topic was concentrated on the control section.

Also the R&D on Voltage Source Converters continued in 2020 both on cascade topology with Active Front End, which could be suitable for PF coils. In addition, the application of Modular Multilevel Converters for the HV Power Supply (PS) system of H&CD was further explored. The results of the study for Acceleration grid PS of Neutral Beam Injectors was presented at the SOFT Conference and the paper was submitted to Fusion Engineering Design.

4.2.3.2. Thermal-Hydraulic Design of Demo PHTS, BoP and Auxiliaries

The European DEMO, the nearest-term fusion reactor with the aim to generate several hundred MWs of net electricity, will operate with a closed tritium fuel-cycle (achieving the tritium self-sufficiency) and will qualify technological solutions for a Fusion Power Plant. DEMO will be operated as a steady state electricity source, although the near term conservative operation will be pulsed to cope with physics and technology limits; in particular, pulses with length of 2 hours will be interrupted by dwells of 10 minutes. The heat exhaust in the fusion power plant will involve the first wall with the breeding blanket, the divertor and the vacuum vessel. The design of these components for EU DEMO is not yet finalized, but configurations and operation parameters have been identified. Different Breeding Blanket (BB) concepts are under investigation and two of them, relying on different coolants and breeding technologies, are considered for the EU DEMO baseline design: the Helium Cooled Pebble Bed BB (HCPB) and the Water Cooled Lithium Lead BB (WCLL).

Preliminary thermo-mechanical designs of the main heat exchangers and steam generator components were finalized during the 2020, in particular for the intermediate heat exchanger helium/molten salt of the HCPB concept and for the steam generator of the WCLL concept. FEM analyses were carried out to verify the sizing and identify the local discontinuities needed to satisfy the requirements in the most stressed regions. Stresses resulting from analyses were verified applying Section III of ASME Boiler and Pressure Vessel Code (Rules for Construction of Nuclear Facility). The main results were published within the paper¹²⁴:

¹²³ F. Lunardon, et al., The MEST, a new magnetic energy storage and transfer system: application studies to the European DEMO, Fus Eng and Design, <https://doi.org/10.1016/j.fusengdes.2020.111666>

¹²⁴ M. Zaupa, M. Dalla Palma, A. Del Nevo, I. Moscato, A. Tarallo, L. Barucca, Preliminary Thermo-Mechanical Design of the Once Through Steam Generator and Molten Salt Intermediate Heat Exchanger for EU DEMO, IEEE Transactions on Plasma Science PP(99):1-7, 2020, DOI: 10.1109/TPS.2020.2972058

The selection of the BB type is a key factor for the development of the whole DEMO plant including the Balance of Plant (BoP) system and, in particular, its sub-systems having the responsibility to remove thermal power generated by the plasma, its conversion in mechanical and finally electrical energy.

During 2020 a new flexible code to simulate power plant conversion systems was developed with Matlab aiming to investigate possible concept designs of the DEMO BoP systems accommodating two different BB: in the largest part of the Tokamak the Driver Blanket and in the remaining part the Advanced Blanket. The code allows to carry out thermal cycle analyses both for design/off design scenarios. Available energy and exergy streams were analyzed in order to optimize the power production by minimizing the internal irreversibility for a combined fusion reactor made of WCLL as Driver BB and HCPB as Advanced BB. Different scenarios were investigated:

- the HCPB power is entirely used to store thermal energy;
- only a portion of the HCPB power is deviated to the energy storage system;
- the HCPB power is supposed to be used to over-heat the steam downstream the WCLL steam generator.

4.2.4. *WPMAG – Magnet System: Quench Protection Circuit Studies*

The design and tech. R&D of Fast Discharge Units of Superconducting (SC) coil was moved within the scope of the PES; the 2020 task was limited to study the interface aspects between the MAG and PES WPs and to collect and analyse the requirements for the CPS main converters and FDUs in order to assess the inputs for the development of the CPS conceptual design in the next FP9 phase. This task with this scope will be maintained in the next years.

4.3. *Socio Economic Studies (SES) and DEMO*

4.3.1. *Fusion power plant assessment studies*

The FRESCO code has been used for further assessments of the economics of a fusion power plant. The resulting investment cost was used in the economic characterization of the technology in energy scenarios studies.

4.3.2. *The role of fusion in long term energy scenarios*

The resources allocated on the EUROfusion Work Package on Socio Economic Studies encompass both project management and research activities.

Consorzio RFX worked on the development of new global energy scenarios, based on the 2019 results and specifically aimed at exploring the effects of the limited fusion material availability on fusion penetration in a future decarbonized energy system. Fusion capacity is

assumed to increase by 12% per year in the most conservative scenario, mainly due to the limited tritium availability for the start-up of new power plants. In that case, to meet the most ambitious climate goals (scenario Harmony, global temperature increase <math><2^{\circ}\text{C}</math>), fusion electricity covers ~2% of the global electricity demand that corresponds to around 150 power plants, 1GWe size, in 2100. In a more optimistic scenario, where a faster fusion deployment is assumed, namely the same as that experienced by nuclear fission in the '70s, the share of fusion electricity increases up to 8% (Fig. 4.18).

The Harmony scenarios delineate alternative pathways towards the achievement of the Paris Agreement Goal that include the full-renewable option as well. Although equally feasible from a modeling perspective, different power system configurations and management correspond to each option to ensure the security of electricity supply. On this regard, Consorzio RFX, in collaboration with ENEA and the Joint Research Centre (JRC), further developed the studies on the analysis of the dispatch model of a European power system based on the SES Harmony scenarios. The results show that global energy models generally underestimate the need of flexible capacity in full-renewable scenarios. The still ongoing analyses have been focussed on the identification of the causes unserved power events, happening even in scenarios with enhanced power grid connections, and possible mitigation strategies.

Consorzio RFX contributed to the enhancement of the ETM model¹²⁵ and to the analysis of the socioeconomic effects of fusion deployment through the Multi Regional Input-Output methodology¹²⁶

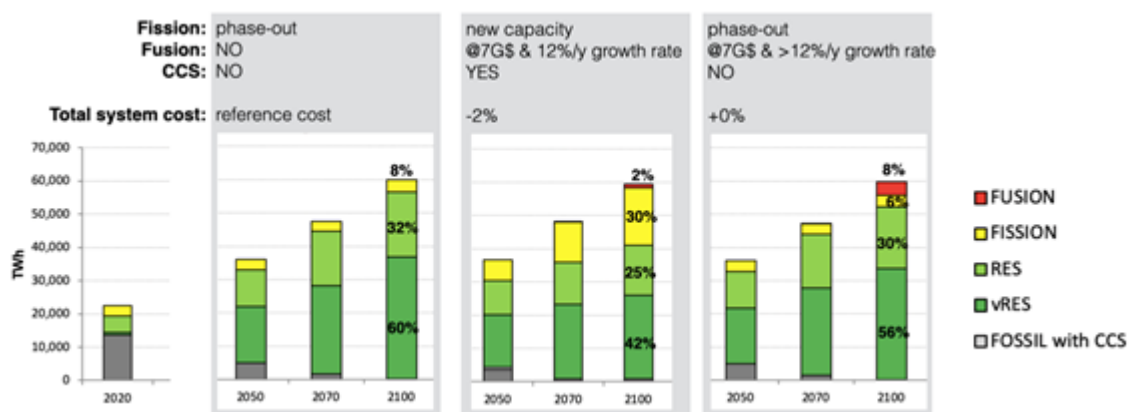


Fig. 4.18 : Fusion penetration in Harmony scenarios with a deployment rate equal or higher than 12%, compared to a 100% renewable scenario

125 Lerede, D.; Bustreo, C.; Gracceva, F.; Lechón, Y.; Savoldi, L. Analysis of the Effects of Electrification of the Road Transport Sector on the Possible Penetration of Nuclear Fusion in the Long-Term European Energy Mix. *Energies* 2020, 13(14), 3634; <https://doi.org/10.3390/en13143634>

126 Santacruz Banacloche, Ana R. Gamarra, Yolanda Lechon, Chiara Bustreo, R.83. Socioeconomic and environmental impacts of bringing the sun to earth: A sustainability analysis of a fusion power plant deployment, *Energy* 209, (2020), 118460; <https://doi.org/10.1016/j.energy.2020.118460>

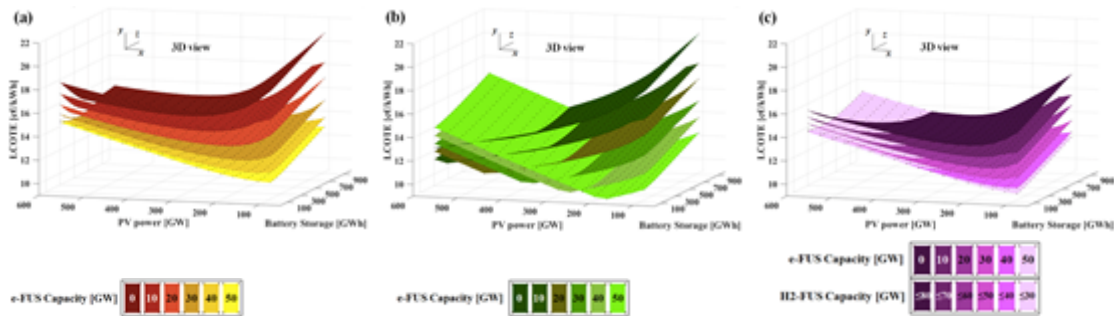


Fig. 4.19 : LCOTE surfaces of No-H2 (a), RES-H2 (b), Fus-H2 (c) scenarios. The No-H2 scenarios depict the case where the shift to hydrogen use does not happen. In the RES-H2, H2 is produced by excess electricity and then used to generate dispatchable power through fuel cells. In the FUS-H2 scenario an additional fleet of fusion reactors is assumed to produce the amount of H2 necessary to cover the whole yearly residual demand once converted into electricity.

Furthermore, an alternative possible application of nuclear fusion beside electricity generation, namely Hydrogen production, was explored with the COMESE code (*COsto MEdio del Sistema Elettrico*). The study, presented at the 31st Symposium on Fusion Technology (SOFT2020) assesses the reliability of alternative carbon-free Italian power system configurations, representative of a potential future solar-based energy system. Base-load capacity such as nuclear fusion power is assumed to be available and conventional dispatchable energy from biogas OCGT or electricity from Hydrogen cover the residual demand. Hydrogen can be generated either from excess renewable generation or from fusion electricity. Results shows that the average cost of electricity is lower when nuclear fusion is part of the electricity generation mix. The lower cost of electricity is achieved when nuclear fusion power plants deliver electricity to the grid and Hydrogen is produced by excess generation rather than by dedicated fusion power stations.

4.4. Education and Training

In the framework of the doctorate programme in “Fusion Science and Engineering” (FSE) jointly run by the Universities of Padua (UNIPD) and Gent (UGENT), fifteen PhD students have been enrolled in the last three academic years:

- Academic year 2017/18 (XXXIII cycle): four
- Academic year 2018/19 (XXXIV cycle): four
- Academic year 2019/20 (XXXV cycle): seven¹²⁷

In 2020 three PhD students of the XXXIII cycle have completed their 3-years research programs and have been admitted to the PhD thesis defense (to be held early 2021); one has

¹²⁷ One student has withdrawn in 2020 from the program because of personal reasons.

postponed his thesis defence by 12 months because of tight experimental limitations in 2020 due to COVID-19 pandemic.

In the stream of the successful experience in coordinating the Lisbon-Munich-Padua (LMP) international doctoral network and the joint doctoral program with UGENT, starting from this academic year (2020/21), the doctorate programme in FSE is jointly run by UNIPD and the Università di Napoli “Federico II” (UNINA), with the support of a large network of national and international universities and research laboratories. In this new framework, eight PhD students have been enrolled on October 1st: six positions with scholarships funded by UNIPD (2), UNINA (3), ENI (1) and two positions reserved to Consorzio RFX’s employees.

Overall, in 2020 more than twenty PhD students have been operating at Consorzio RFX and partners’ premises (only remotely during COVID-19 pandemic specific restrictions), under the tutoring of members of the PhD Academic Council and Consorzio RFX’s researchers.

4.5. Communication and outreach

The 2020 communication and outreach activity was affected by COVID-19 pandemic, as the restrictions on social distancing prevented in-person events, forcing to steer the program into virtual and remote outreach activities. As with any change, this entailed benefits and drawbacks. Socially distancing and face masks have forced to better focus on the contents and taught us how to use digital tools to our advantage.

Despite the COVID-19 restrictions, on 10 March 2020, the event “La Scienza in diretta” could take place in person in the RFX experimental hall, on the occasion of the International Woman Day celebration, in collaboration with the CNR Padua Research Area and with the participation of Mrs. Luisella Pavan Woolfe, Director of the European Council Office in Venice. The event was aimed at enticing young female students towards higher science and technology studies, inspired by the storytelling of female researchers of Consorzio RFX. The event was streamed on the Consorzio RFX YouTube channel and viewed by more than 5000 students.

During the following lockdown period, with the increase in public request for on-demand science information, associated with a strong need for on-line learning, the communication activity of Consorzio RFX focused on the realization of a thematic video clip campaign, which resulted in a set of 3-minute video courses streamed on RFX socials and YouTube channels. The audience response was also positive.

Last but not least, the 2020 European Researchers’ Night event: Consorzio RFX participated to the HORIZON 2020 call in partnership with 4 CNR institutes of the CNR Research Area in Padua in the framework of the MeetMeTonight 2020 Project, taking place in various major Italian cities and aimed at realizing a special opportunity of meeting and interaction between

the public and the world of research. The initial date in September was postponed on November 27 2020, with a live broadcast from 17.00 pm to 22 pm: 5 hours of interviews and video clips live streamed on Facebook, YouTube and CNR Live TV channel directly from the NBTf premises. The funds obtained with the participation to the European call fully covered the costs both for video clip pre-production and technical and logistics support.

Social-media communication activity was reinforced. The activity for the revamping of the Consorzio RFX website was completed; the new website will be published in January 2021.

5. Broader Approach

5.1. Contribution to the JT-60SA Power Supply Combination Tests

In 2020 Consorzio RFX continued the voluntary contribution to the Power Supply (PS) Combination Tests of JT-60 SA with particular attention to the Quench Protection Circuits, procured by CRFX, on behalf of CNR. Along the year, CRFX contributed in analyzing issues encountered during the tests, together with QST, F4E and the QPC Supplier.

5.2. Power supplies for in-vessel sector coils for RWM control

The RWM power supply system is devoted to feed the 18 in-vessel sector coils of JT-60SA, aimed at controlling a set of plasma instabilities called Resistive Wall Modes (RWM). The dynamic requirements are very stringent, beyond the standard industrial performances: bandwidth of 3 kHz and latency between output voltage and reference lower than 50 μ s. This is why a new technology, based on hybrid Si-SiC IGBTs (Isolated Gate Bipolar Transistors), has been proposed. In 2015 the Agreement of Collaboration and the Procurement Arrangement for the full system were signed. The contract for the procurement of the RWM-PS was awarded to the company E.E.I. Equipaggiamenti Elettronici Industriali, Vicenza (Italy) on March, 2016. On the basis of the positive results of the Factory Routine and Integrated Tests, in 2018 QST, F4E and Consorzio RFX gave green light to E.E.I. to proceed with the shipment. The container containing the RW-PS components departed from Genova, Italy on July 2018 and arrived at Yokohama port in Sept., 2018. At the joint inspection, only case n. 3 showed some little damages; however, all the original shock and tilt detectors were un-tripped, thus the shipment has been transferred to Naka Site via road transportation, under QST responsibility. At Site, upon opening of the case number 3, it was discovered that the content (the cabinet PCC-B, corresponding to half of the conversion system) sustained severe damages. Therefore, QST and E.E.I. opened a claim to their respective transportation companies, and with the packaging company (for E.E.I.). The cause of the damages were never discovered, thus the Italian insurance company proposed a partial reimbursement of 55% of the request; for the same reasons, Japanese Insurance company offer no

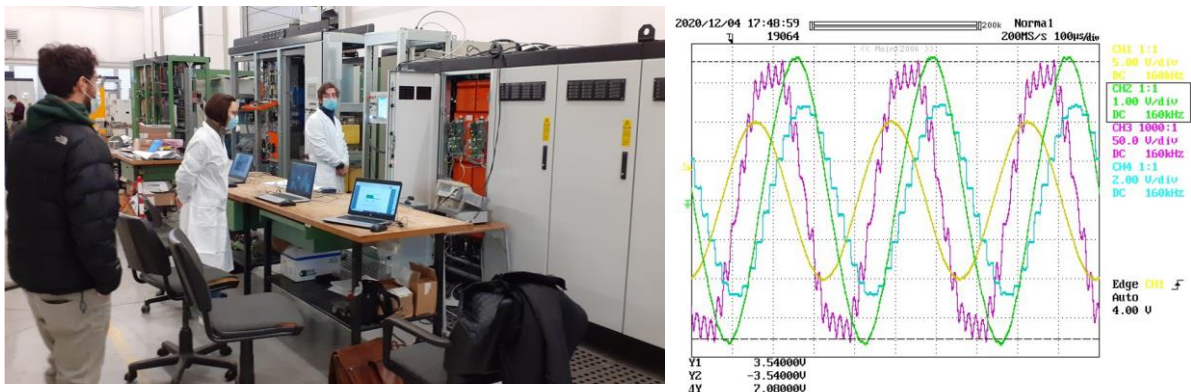


Fig. 5.1 Official Factory Tests at E.E.I. premises, witnessed by Consorzio RFX (in person), QST and F4E (remotely connected). Right: experimental result for inverter n. 10, with 300 Apk, 3 kHz current reference (in yellow, 30 A/V). In green: output current (60 A/V). In purple: output voltage (1 V/V). In cyan: output current acquired by control board (45 A/V).

reimbursement at all. The reimbursement offer was then further reduced to 45% due to delays in the disposal procedures of the damaged cubicle by QST. Nevertheless, E.E.I. accepted the partial reimbursement to manufacture and test the new cubicle, even if in face of losses, but without the duty of the packing and transportation to Japan. The reimbursement was received in Dec. 2019 and in Jan. 2020 E.E.I. started the purchasing of the materials and then the manufacturing. The new PCC-B has been completed in Nov. 2020, and the Factory Routine Tests have been performed between Nov. and Dec. as planned, supervised by Consorzio RFX (see Fig. 5.1). The official Factory Tests have been carried out on Dec. 15, witnessed by QST, F4E and Consorzio RFX, with full success. E.E.I. issued the Factory Test Report, reviewed by the partners, thus green light to the closure of the contract is given, being the packaging and transportation of the new reconstructed cubicles under F4E and QST responsibility.

6. Industrial and non-fusion related collaborations

6.1. Design of Vacuum Interrupters with the Voltage Holding Prediction Model (VHPM)

The main outcome of the research, supported by Siemens AG-Berlin, was the identification of an optimum for the values of the m , W_0 , α , β and γ , which are the physical parameters of Voltage Holding Predictive Model. Fig. 6.1 shows the prediction results for tubes rated for 36 kV, AMF type, comparing two set of parameter: the first, derived from dc - long gap configurations (Pilan-Kojima PK set); the second derived from the breakdown model by Slivkov, evolution of the Cranberg breakdown model (Cranberg-Slivkov CS set).

Further investigation have been carried out in order to improve the prediction capability, correcting the effect of the delay between the voltage collapse and the actual breakdown

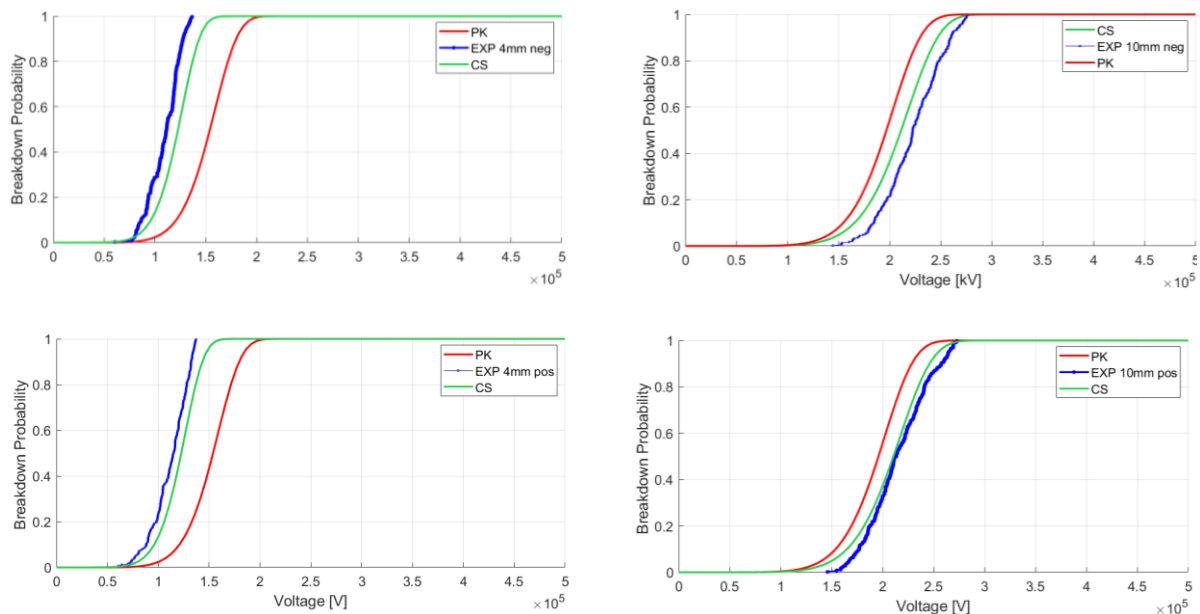


Fig. 6.1 Comparison of the PK and CS parameter sets, for 4 and 10 mm electrode gaps (left-right) and both negative and positive polarity (top-bottom). It is evident the better prediction performance of the simulation made using the CS values (green line)

initiation. This delay is hard to be measured, and it has been estimated in a range between 50 and 350 ns. The analysis of the results is still ongoing.

Finally, the energy dissipated in the arc during the breakdown has been measured for the first time, in order to see if the apparent wearing of tube VSG36 (floating screen) at long gap (15 mm) appears also if the grounded screen tube VSA12050, when subjected to the same arc energy. This last tube didn't show any deconditioning at the same arc energy and shorter gap but showed a lower hold off voltage for 15mm gap keeping constant the arc energy of the previous case. So the reason of the voltage holding degradation at long gap for the tube VSG36 likely is related to surface degradation and/or interaction with the floating screen (main difference between the two kinds of tube). Conversely, the lower voltage for the VSA12050 likely is due to the geometry which presents a gap between the side surface of the electrodes and the screen shorter than the gap between the electrodes. The application of the VHPM to the latter tube is foreseen, in order to confirm if the reduction of the breakdown voltage is determined by the geometry of the tube, whereas for the former the model did not predict any voltage degradation due to the geometry.

6.2. Biomedical plasma applications

The activity on biomedical plasma applications has proceeded despite the limitations due to the Covid-19 pandemics, although some activities had to be postponed, in particular fast camera measurements of streamer development and the start of the clinical study on dermatological applications.

A new location for performing activities related to the development and testing of atmospheric pressure plasma sources has been identified on the university Industrial Engineering Department premises. This laboratory has been equipped with instrumentation and tools, including a 3D printer, and is now operational, although it is not autonomous, but hosted within a space shared with other research groups. The 3D printer in particular has been found to be an extremely useful tool for producing parts of the plasma sources, avoiding delays related to workshop activity, and allowing fast prototyping and optimization.

An Arduino-based gas mixer has been developed, assembled and tested, with the aim of starting an activity on the optimization of the chemical and biological effects of the plasma sources by adding known fractions of oxygen, nitrogen or other gases to the main helium or argon flow. The mixer is now operational, and allows to mix a main gas flow with a minority one, with high precision and reproducibility. Preliminary spectroscopic measurements with helium-argon mixtures have been performed, within a bachelor's degree thesis work, indicating that even the simple mixture of two noble gases allows the possibility of achieving different results in terms of chemical species produced (derived from ambient air).

From the point of view of biological effects, a new collaboration has been set up with a veterinary medicine department of the university, aimed at investigating the effect of the RF source on the eye. The work has just started, and will profit from an existing protocol on cornea conservation and treatment, allowing ex-vivo experiments.

A study on the antiviral properties of the available sources has been started, in collaboration with the Department of Molecular Medicine of the University, as the capability of inactivating viruses has become a very relevant topic. Preliminary results show that indeed it is possible to inactivate viruses deposited on surfaces with a good efficacy and limited exposure time.

Finally, a new method for the production of atmospheric pressure plasmas, based in the helical resonator concept, has been studied. Following a critical examination of the available literature, a set of measurements has been performed, within the context of another bachelor's degree thesis. This has led to the production of the prototype of a new version of the RF indirect plasma source, based on this new concept, which was found to be much better coupled to the power supply than the previous one, and could be operated with just one tenth of the previous input power. Such a good performance, made possible by the fact that the dissipation over the voltage-raising inductor was eliminated, opens up the possibility of easily raising the RF frequency, possibly exploring domains where gas ionization can occur at lower voltage and thus with lower power. This will allow in the future to develop a very compact design, which could be exploited in case occasions for the development of an industrial prototype materialize.

7. Publications

The 2020 scientific production of Consorzio RFX has been affected by the Covid-19 pandemic, since most of the conferences scheduled in the first half of the year have been canceled or postponed (such as the EPS Conference postponed to 2021), whereas in the second half of the year, most were held in a virtual way.

To date, the list of publications 2020 with authors of Consorzio RFX ¹²⁸ includes:

- 97 papers with co-authors of Consorzio RFX published in International Journals,
- 57 of the above submitted by a Consorzio RFX first author;
- 63 participations of Consorzio RFX researchers to National and International Workshops and Conferences,
- 53 of the above with a submitting / first author of Consorzio RFX, 9 of which were invited talks and 1 was an oral presentation.

The share among the different main disciplines in which Consorzio RFX has published in this year is shown on Fig. 7.1 where a comparison with the last twenty years is also shown.

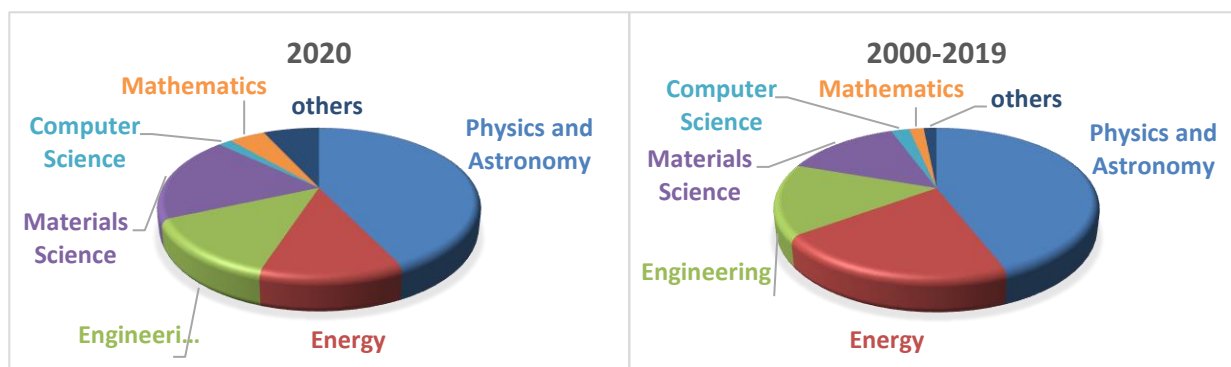


Fig. 7.1 Sharing of disciplines in which Consorzio RFX has published in 2020 compared with the sharing in the last 20 years.

¹²⁸ Attached document Consorzio RFX Publication List 2020